

A perspective on nanoscale pattern formation at surfaces by ion-beam irradiation



Cite as: J. Appl. Phys. 128, 180902 (2020); doi: 10.1063/5.0021308

Submitted: 9 July 2020 · Accepted: 17 October 2020 ·

Published Online: 9 November 2020



R. Cuerno^{1,a)} and J.-S. Kim^{2,3,a)}

AFFILIATIONS

¹ Departamento de Matemáticas and Grupo Interdisciplinar de Sistemas Complejos (GISC), Universidad Carlos III de Madrid, 28911 Leganés, Spain

² Department of Physics, Sook-Myung Women's University, Seoul 04310, South Korea

³ Institute of Advanced Materials and Systems, Sook-Myung Women's University, Seoul 04310, South Korea

a)Authors to whom correspondence should be addressed: cuerno@math.uc3m.es and jskim@sm.ac.kr

ABSTRACT

The formation of periodic patterns on the surfaces of many solid materials undergoing ion-beam irradiation has long been known. The advent of high resolution characterization techniques elucidated the nanoscopic traits of this self-organization process, enabling a wide range of applications for the nanostructures thus produced, from optoelectronic to biomedical. Meanwhile, full theoretical understanding of the technique has been challenged by its multiscale nature, whereby the external perturbation implemented by the ion beam acts at a much slower rate (typically, one ion arrives per square-nm every second) than the microscopic processes, like collision cascades and material transport, which try to relax such external perturbations (collision cascades or surface diffusion attempts usually relax after a few picoseconds). Here, we present a Perspective on the main developments that have led to the current understanding of nanoscale pattern formation at surfaces by ion-beam irradiation, from the points of view of experiments, applications, and theory, and offer an outlook on future steps that may eventually facilitate full harnessing of such a versatile avenue to materials nanostructuring.

Published under license by AIP Publishing. <https://doi.org/10.1063/5.0021308>

I. INTRODUCTION

In 1962, Navez *et al.*¹ reported the nanoscale ripple patterns that spontaneously form on glass substrates irradiated by a beam of ionized air. The geometry of such surprising arrangements of nanostructures was expected to depend on experimental conditions and thus to enable the engineering of surface topographies at small scales. Indeed, almost 40 years later, nanodot patterns were found to also form,² provided the ion beam is incident near normal to the surface, with the original ripple patterns emerging under oblique incidence of the ion beam. Subsequent studies have demonstrated that this so-called ion-beam sputtering (IBS) method of structuring solid surfaces at the nanoscale is applicable to most solid materials, ranging from metals to semiconductors, and from organic to inorganic materials, which makes IBS a rather versatile tool.^{3–5} Moreover, IBS is a low-cost, easily scalable technology that fabricates patterns on wide areas in a single process, and has long drawn attention due to its potential applications in industry. Indeed, N. Taniguchi, who defined the concept of *nanotechnology*

in 1974, already pointed to IBS as a key technique for this, at the time nascent field.⁶ From the perspective of basic science, IBS has also drawn the attention of the research communities interested in the mechanisms behind spontaneous pattern formation and self-organization.⁷

However, the development of surface nanopatterning by IBS as we know it today dates back mostly to the late eighties of the last century. Two seminal contributions boosted the research in the field. *First*, in 1988, Bradley and Harper (BH) laid the theoretical framework for the pattern formation process that takes place in IBS.⁸ According to the BH theory, and as is generally the case for many self-organization processes far from equilibrium,⁷ during IBS, the pattern forms on the surface as a result of the competition between two counteracting effects. On the one hand, the incident ion beam erodes valleys faster than ridges according to Sigmund's theory of ion sputtering (see Sec. II B),^{9,10} which causes a morphological instability amplifying local height differences. On the other hand, the surface tries to reduce its free

energy via mass transportation. In the original BH model, following the classic description of thermally activated surface diffusion by Herring and Mullins,^{11–13} a surface mass current is driven by the gradient of the surface energy that is assumed proportional to the surface curvature, locally smoothening surface features.

Second, it was not until the late eighties that high-resolution nano probes became widely available, such as scanning probe microscopy (SPM),^{14–18} or grazing incidence small angle x-ray scattering (GISAXS)¹⁹ due to the then burgeoning third generation synchrotron facilities. SPM, especially scanning force microscopy, has enabled the detailed three-dimensional (3D) characterization of the morphology and topography of IBS patterned surfaces close to atomic resolution, while GISAXS has allowed the real-time investigation of the pattern dynamics during IBS.

After the BH theory was proposed, there have been many significant developments from the theoretical and from the experimental points of view. Thus, the original BH model implements a linear approximation whereby the vertical velocity at which the height of a point on the target surface changes is assumed proportional to small height deviations from a uniform, flat shape. This approximation was later relaxed to take into account the fact that the erosion rate depends non-linearly on the local surface inclination.^{20,21} Moreover, the net current of the material subject to transport on the surface was later found to include additional contributions from different physical origins, such as ion-induced mass redistribution/displacement²² and/or stress-induced, surface-confined viscous flow,^{23,24} and, in general, requires detailed modeling of its own, to be then coupled to the time evolution of the surface height.²⁵ More microscopic models have also developed. In particular, the ion–surface interaction has been described with improved space resolution via molecular dynamics (MD) simulations, elucidating the detailed way in which the IBS surface instability originates not solely from erosion, as predicted by Sigmund,¹⁰ but also from ion-induced mass displacement at the surface.^{26,27} Due to the rapidly growing computing power, MD^{28,29} and kinetic Monte Carlo (kMC) simulations,^{30,31} as well as hybrid simulation³² combining both, have increasingly contributed to the elucidation of the pattern formation process from the atomistic point of view.

With respect to experiments, in 1999, Fascko *et al.*² crucially reported IBS production of highly ordered nanodot patterns showing quantum confinement effects, thus demonstrating IBS as a promising nanotechnology as seminally suggested by Taniguchi.⁶ The role of metal codeposition in the pattern formation then became a central issue for a decade or more, since metallic impurities can dramatically improve the order in the pattern and also produce patterns composed of basic motifs other than periodic ripples or dots.^{33–39} A quest for defect-free pattern formation has been also consistently pursued, being particularly fruitful in the case of IBS of compound semiconductors at temperatures beyond the recrystallization temperature.⁴⁰ Further, the capabilities of unconventional irradiation setups to fabricate novel patterns have been also actively investigated, and has also served as a test bed for the examination of the theoretical predictions.⁴¹

More recently, similar breakthroughs are becoming naturally less frequent in the context of IBS surface nanopatterning, which indicates the maturity of the field and the difficulty of the remaining open problems. These, on the other hand, still warrant the

attention of experimental and theoretical researchers for their basic and applied interest. Hence, we feel that it is high time to reflect on previous achievements and assess problems which are still open in the field, as well as to prospect for future research directions.

We start this Perspective article with a brief survey on the key issues which have been dealt with up to the recent past with respect to both experiments and applications and theoretical aspects of IBS surface nanopatterning, which are addressed in Secs. II A and II B, respectively. Then, we assess the current status of open problems which we consider important, again providing perspectives on these from the points of view of experiments and applications (Sec. III A), and also from the theoretical and computational viewpoints (Sec. III B). For definiteness, we restrict the discussion to the patterns formed by low energy ($E_{\text{ion}} \leq 10 \text{ keV}$), broad ion beams, albeit with occasional mention of results at higher energies. Actually, to lighten up the presentation somewhat while keeping a clear focus on the main issues discussed, this article is not intended as an comprehensive review, either. For additional detailed reviews with diverse emphasis, the reader is referred to publications in specialized journals and books,^{3–5,42–48} as well as to journal special issues which have been specifically devoted to this topic,^{5,49} some of them quite recently.

II. ESTABLISHED RESULTS

A. Experiments and applications

As mentioned above, in 1999, Fascko and collaborators reported the production of a hexagonally ordered pattern of nanodots on a GaSb surface by near-normal irradiation of a 420 eV Ar⁺ ion beam,² see Fig. 1(a) for a SEM image. The height–height correlation function in Fig. 1(b) shows that the order of the dots extends over several periods on the substrate plane, this pattern setting the standard for the length-scale and order of the surface nanopatterns achievable by IBS. Moreover, the photoluminescence spectrum from the dots produced showed a blue shift from that of bulk GaSb, as shown in Fig. 1(c), indicative of quantum confinement effects. This work demonstrated quite eloquently that IBS could be promisingly employed as an efficient nanotechnology for device-oriented applications, and drew an explosive attention, largely expanding the community of practitioners of the field. However, as will be explained in some detail in what follows, elucidating the main mechanisms responsible for the formation of such a well-ordered pattern has taken near 15 more years (with some aspects remaining under scrutiny), partly related with the fact that the substrate material is not monoatomic.

1. Clean monoelemental semiconductors

In order to introduce the basic experimental facts about the formation of surface nanopatterns by IBS, it is probably best if we start by the simplest, paradigmatic case of IBS of monoelemental semiconductors. In general, this class of targets is simpler to study because they become amorphous upon low-energy ion bombardment,⁵⁰ thus obviating complexities that originate for crystalline surfaces from the instability caused by so-called Ehrlich–Schwoebel (ES) barriers to surface diffusion,^{51–53} although we will also address these later. Among semiconductor targets, a large majority of the

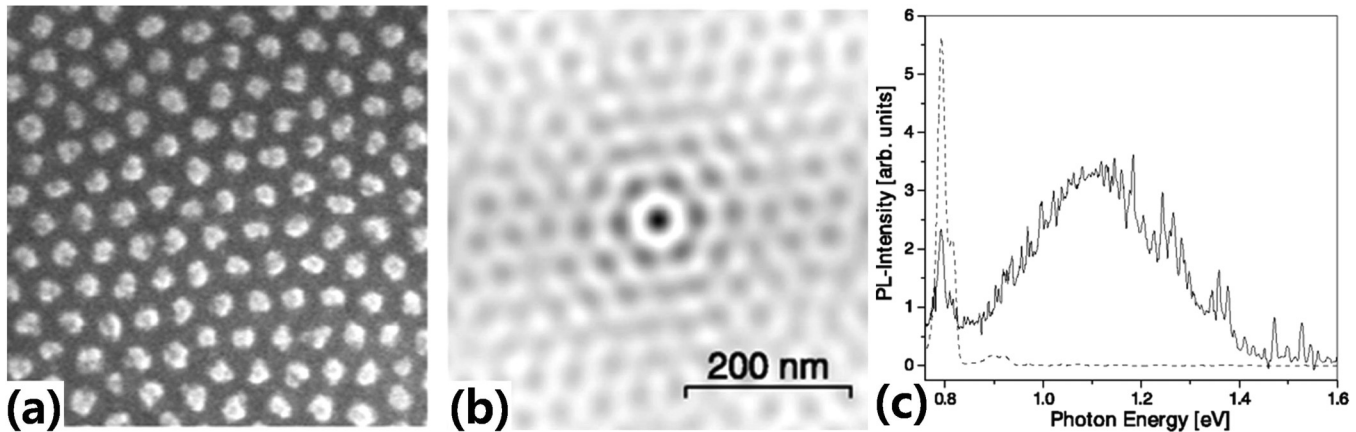


FIG. 1. (a) The extract of a SEM image and (b) the corresponding two-dimensional autocorrelation reveal the regularity of the hexagonal ordering (extending over more than six periods) of a nanodot pattern produced by IBS of a GaSb film on an AlSb substrate.² (c) The low-temperature (15 K) photoluminescence (PL) spectrum (in arbitrary units) of the GaSb dots shows a broad, weak spectrum. The solid line is the PL of the dots scaled up by a factor of 50 relative to the GaSb bulk spectrum, drawn as a dashed line. Reproduced with permission from Fasko *et al.*, Science **285**, 1551 (1999).² Copyright 1999 American Association for the Advancement of Science.

works in this context employ Si,⁴⁶ but analogous results are obtained for many other choices.⁴ Similarly, we will be mostly discussing experiments using Ar⁺ ions, but analogous results are obtained for, e.g., heavier noble gas species.⁴⁶

In view of the complexity and diversity of the processes engaged in IBS, a simplified approach is to study the pattern formation process in the early-time regime in which the surface

topography deviates slightly from the initially flat profile. It is in this regime that (linear) approximations in the surface height as, e.g., the classic BH theory are expected to apply. The main qualitative behavior for IBS of clean Si is summarized in the left panel of Fig. 2, which shows a morphological diagram obtained in terms of two readily accessible experimental parameters, namely, the polar incidence angle of the Ar⁺ ion beam, θ , and the ion energy E_{ion} .

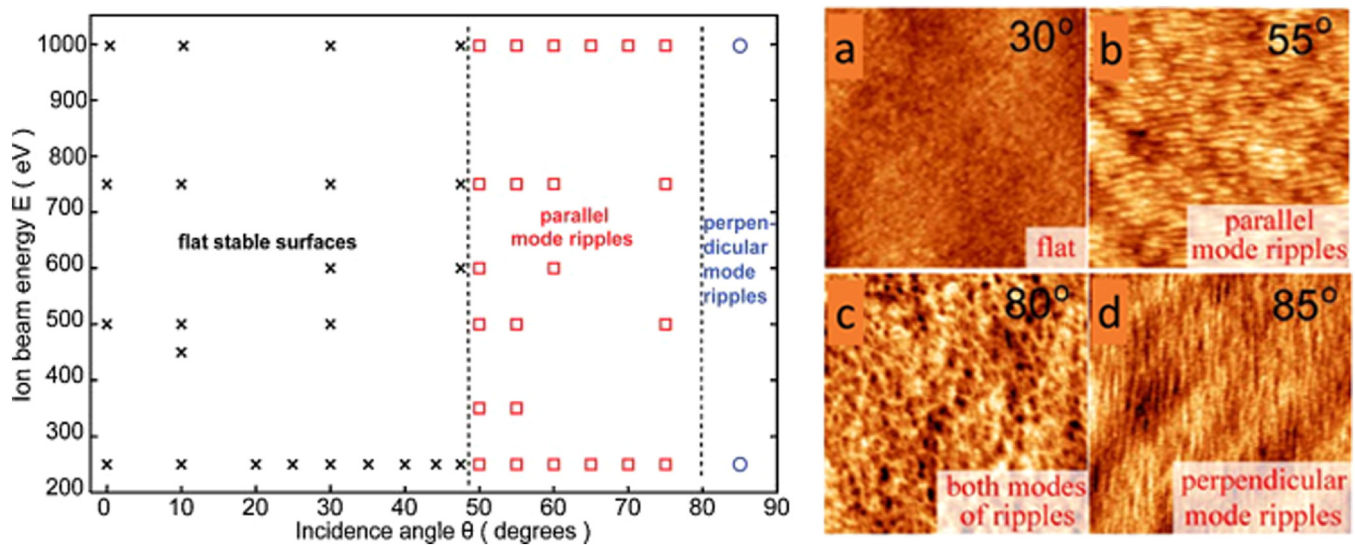


FIG. 2. Left panel: Morphological diagram for pattern formation of Ar⁺ IBS of Si(001), in the linear regime of surface dynamics, in terms of the ion incidence angle and energy. Experiments are nominally at room temperature, fluence is $3.8 \times 10^{18} \text{ cm}^{-2}$ for flat stable surfaces, and $3.2 \times 10^{17} \text{ cm}^{-2}$ for parallel and perpendicular mode ripples at $\theta \geq 50^\circ$. Reproduced with permission from Madi *et al.*, Appl. Surf. Sci. **258**, 4112 (2012).⁵⁴ Copyright 2012 Elsevier. Right panel: $1 \times 1 \mu\text{m}^2$ AFM top-views for 250 eV for θ as indicated. In all panels, the projected ion beam runs vertically bottom to top and the z-range is 2 nm. Reproduced with permission from C. S. Madi, Ph.D. thesis (Harvard University, 2011).⁵⁵ Copyright 2011 C. S. Madi.

Remarkably, for $\theta \leq 48^\circ = \theta_c$, the morphologies observed under IBS are “flat” (i.e., non-patterned) as shown in Fig. 2(a) in the right panel, contradicting a prediction from the classic BH theory that flat surfaces are unstable to pattern formation for any incidence angle, including normal incidence ($\theta = 0^\circ$). For $\theta > \theta_c$, ripples do form with wave vector parallel to the projection of the ion beam direction as in Fig. 2(b) (so-called parallel ripples, as those reported in the seminal observations by Navez and co-workers), an orientation which rotates by 90° (inducing perpendicular ripples) at even higher angles as found in Fig. 2(d), as actually described by BH. The morphological transition that takes place at $\theta = \theta_c$ is characterized by a diverging (ripple) wavelength,^{54,56–59} being termed type II in the pattern formation terminology, in analogy to a continuous or second-order equilibrium phase transition in which the correlation length diverges.⁷

Note that the experimental results summarized in Fig. 2 were performed almost 25 years after BH’s theory was published. Today, we know that the existence of metallic contaminants in many experiments is responsible for thus delaying the clarification of the morphological behavior of clean monoelemental targets under IBS;⁴⁶ we will come back to this crucial issue later. At any rate, the basic structure of this morphological diagram is now regarded as quite generic for IBS of semiconductors, and other materials that are or become amorphous under IBS,⁵⁰ and has also been assessed in the medium energy range up to $E_{\text{ion}} \approx 100$ keV, see, e.g., cases for Si and Ge in Refs. 60 and 61, and references therein. And while some properties (like the value of θ_c) are known to depend on, e.g., ion/target combination,^{31,59,62} some other are expected to be universal,⁵⁹ like the type of divergence of the ripple wavelength for $\theta \simeq \theta_c$. On the other hand, and as noted, the occurrence of a non-zero value for the critical angle cannot be accounted for in the classic BH description of Sigmund’s sputtering instability competing with temperature-activated surface diffusion, and is discussed in some detail in Sec. II B. Currently, at a microscopic level it is considered to be induced by the ion beam via the local rearrangement of material.^{22,27,62,63} Mesoscopically,^{24,59,64,65} it can be seen to be a consequence of the relaxation of the residual stress induced by the irradiation in the amorphized topmost surface layer via surface-confined viscous flow.^{23,66}

Additional experimental studies of the static^{54,56,57} and dynamic aspects⁶⁹ of ripple formation on Si have further clarified the physical origin of the morphological instability in IBS. As generic for pattern-forming systems,⁷ this can be done in the early-time linear regime, studied by Madi and co-workers by employing GISAXS.⁶⁹ Specifically, they measure the diffuse scattering intensity during IBS as shown in Fig. 3(a), which is proportional to the height structure factor, $|h(\mathbf{q}, t)|^2$. Here, $h(\mathbf{r}, t)$ denotes the target surface height above point $\mathbf{r} = (x, y)$ on the substrate plane at time t , and $h(\mathbf{q}, t)$ denotes its space Fourier transform, with \mathbf{q} being the wave vector. Close to the instability onset (in the present case, for $\theta \simeq \theta_c$), one generically expects⁷ $|h(\mathbf{q}, t)|^2 \propto e^{2\omega(\mathbf{q})t}$, where the wave-vector dependent amplification factor $\omega(\mathbf{q})$ is the so-called linear dispersion relation.⁷ By fitting the temporal evolution of the diffuse intensity for each \mathbf{q} as shown in Fig. 3(b), the full θ -dependent behavior of $\omega(\mathbf{q})$ can be obtained, see Fig. 3(c). More precisely, data in Fig. 3(c) are for the real part of the linear dispersion relation, $R(\mathbf{q}) = \text{Re}[\omega(\mathbf{q})]$, which is the one characterizing the

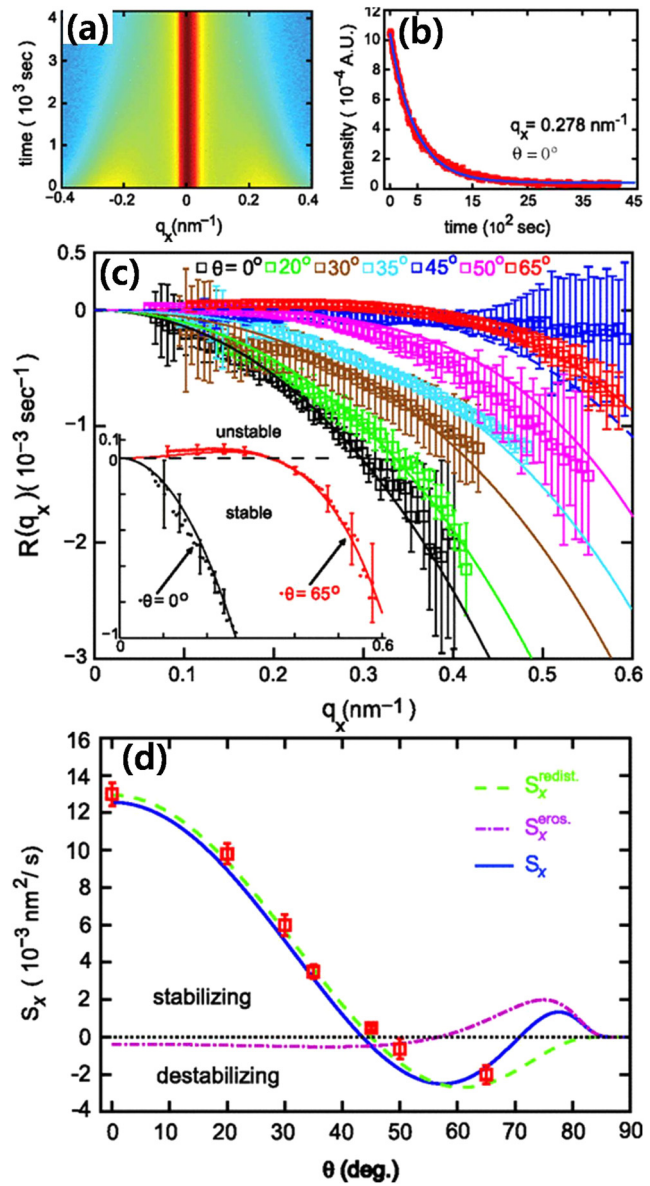


FIG. 3. (a)–(b) Time-resolved GISAXS for normal incidence IBS of Si. (a) A sample with initial rippled topography obtained at $\theta = 65^\circ$ is smoothed by normal incidence IBS. (b) Exponential decay due to a negative amplification rate value, $R(q_x) = 0.278 \text{ nm}^{-1}$. (c) Measured linear dispersion relation $R(q_x)$ for several ion beam incidence angles. The curves are fits to Eq. (1), with fixed $B = 0.011 \text{ nm}^4/\text{s}$ (obtained from fits excluding data at $\theta = 45^\circ$), and changing S_x for each value of θ . The dashed blue line represents the theoretical dispersion relation at $\theta = 45^\circ$ for $B = 0.011 \text{ nm}^4/\text{s}$ and allowing the quadratic coefficient $S_x(45^\circ)$ to vary freely. The inset shows the 65° and 0° linear dispersion relations, with (without) an unstable Fourier mode band for $\theta = 65^\circ$ ($\theta = 0^\circ$). (d) Angle dependence of the best-fit (symbols) and theoretical estimates (lines) for $S_x(\theta)$ and $S_x^{\text{eros}}(\theta) + S_x^{\text{redist}}(\theta)$, with $S_x^{\text{eros}}(\theta)$ ($S_x^{\text{redist}}(\theta)$) including a parameter-free (one-parameter) Yamamura correction^{67,68} to the BH⁸ (CV²²) value. Reproduced with permission from Madi et al., Phys. Rev. Lett. **106**, 66101 (2011).⁶⁹ Copyright 2011 American Physical Society.

growth of the surface amplitude. The conclusion of the analysis is that the experimental data agree with the polynomial form⁶⁹

$$R(\mathbf{q}) = -S_x q_x^2 - S_y q_y^2 - B(q_x^2 + q_y^2)^2, \quad (1)$$

where $S_y, B > 0$ and the sign of S_x depend on θ , being positive for $\theta < \theta_c^{\text{exp}} \simeq 48^\circ$ and negative for $\theta \geq \theta_c^{\text{exp}}$. Hence, in the former case all Fourier modes of the height decay with time leading to a flat surface while, in the latter case, those modes $h(\mathbf{q}, t)$ with \mathbf{q} in the finite band making $R(\mathbf{q}) > 0$ increase in amplitude, the one maximizing $R(\mathbf{q})$ at $\mathbf{q} = \mathbf{q}_*$ growing the fastest, and inducing the ripple wavelength value $\ell_* = 2\pi/|\mathbf{q}_*|$.

As readily verified by Fourier transform, if the surface height obeys the evolution equation

$$h_t = S_x h_{xx} + S_y h_{yy} - B \nabla^4 h, \quad (2)$$

where subindices denote partial derivatives, then $R(\mathbf{q})$ is given precisely by Eq. (1). Let us note that, strictly speaking, the height equation considered in Ref. 69 was not the deterministic Eq. (2) but, rather, a variant of it which includes an additional noise term on the right hand side, an issue to which we will come back in Sec. III B. Importantly, Eq. (2) is linear in the substrate height h . And indeed, it happens to have the precise same form as the BH model.⁸ However, the interpretation of the coefficients $S_{x,y}$ and B is crucially different. Here, $S_{x,y} = S_{x,y}^{\text{erosion}} + S_{x,y}^{\text{redist}}$ includes two contributions.^{69,70} On the one hand, S_x^{erosion} represents sputtering as in the classic BH theory. Theoretical estimates discussed in Sec. II B indicate that this coefficient remains negative [see Fig. 3(d)] for θ well above θ_c^{exp} , inducing an instability: the local velocity is more negative at a local surface minimum, which erodes faster than a maximum, and local height differences are amplified. On the other hand, S_x^{redist} is given by the Carter-Vishnyakov (CV) model,²² according to which the ion-beam induces local mass rearrangement in a θ -dependent fashion, such that, as borne-out from theoretical refinements of this model discussed in Sec. II B, S_x^{redist} remains positive for $\theta \lesssim \theta_c^{\text{exp}}$, see Fig. 3(d). Fitting the dispersion relation for each incidence angle in Fig. 3(c) by the theoretical dispersion in Eq. (1) gives the best-fit S_x data as shown in Fig. 3(d). Note in this last figure that ion-induced mass rearrangement dominates over sputtering not only in stabilizing the surface for $\theta < \theta_c^{\text{exp}}$ as originally predicted by CV,²² but also in destabilizing the surface for $48^\circ \lesssim \theta \lesssim 70^\circ$. Hence, the destabilizing physical mechanism controlling ripple formation is not sputtering as assumed in the classic BH theory, but mass rearrangement, and only for large enough θ . Moreover, the stabilizing mechanism counteracting it [implemented by the term with parameter B in Eq. (2)] is not thermally activated surface diffusion as classically assumed,⁸ either, but rather surface-confined viscous flow.^{23,66} Later on, more microscopic modeling of mass rearrangement,^{27,31,62,63,69,71} mentioned in Sec. II B, has allowed to assess in further detail the significantly destabilizing role of the ion-induced mass displacement mechanism. Moreover, comparison of the above and further experimental observations, such as the energy dependence of the ripple wavelength,^{58,59} with continuum descriptions,^{24,58,59,64,65,72,73} have validated the mesoscopic view of the pattern formation process as

relaxation via viscous flow of the residual stress induced in the topmost irradiated layer by the ion irradiation, see also Sec. II B. Indeed, IBS near or below the sputtering-threshold energy (hence, with a negligible sputtering yield) has been seen to still produce similar ripple patterns on various other clean substrates such as mica, Ge(100), GaAs(100), and Si.^{29,74–76} In the most general case, one naturally expects all discussed physical mechanisms to participate to some extent in the detailed dynamics of surfaces subject to IBS.⁷⁷

Linear approximations like those behind an interface model as represented by Eq. (2) also succeed in describing additional surface properties which are beyond ripple production and amplification, like ripple transport on the target plane at a precise velocity. A number of detailed experimental observations exist on, e.g., Si or different glasses,^{78–83} see Ref. 4 for further references. Similar to the case of the morphological instability, again different physical processes like sputtering and surface-confined viscous flow compete nontrivially to control features like the (upstream vs downstream) orientation of the ripple transport with respect to the ion beam incidence.^{73,82,84,85}

Finally, for large enough fluence, nonlinear effects become non-negligible. In particular, they are responsible for the saturation of the surface to a steady state with a finite amplitude or roughness. Beyond that, they are also associated with nontrivial behaviors also exemplified by IBS of amorphizable materials, such as wavelength coarsening (i.e., an increase of the ripple wavelength with irradiation time) at low^{86–88} and medium energies,⁸⁹ formation of highly disordered terraced morphologies with saw-tooth profiles^{80,90–95} (also reported at medium ion energies^{96,97}), and even surface kinetic roughening, again both for low^{14,98–101} and medium^{96,102} ion energies. Further details on the current understanding of linear and nonlinear properties can be found in Sec. II B on theory and simulations.

2. Metallic surfaces: Two regimes

Metals keep their crystalline structure under IBS due to the high efficiency of diffusion,⁵³ while semiconductors, if not kept at elevated temperatures during IBS, become amorphous.⁵⁰ For metallic surfaces, moreover, a key factor which can control material transport at the surface by diffusion is the so-called Ehrlich-Schwoebel (ES) effect.^{51–53,104} This is the existence of an extra barrier to surface diffusion due to the fact that, when crossing a step edge, an adatom passes through an area with a low number of nearest neighbors. Thus, the ES barrier hinders the diffusion of adatoms (advacancies) down (up) a step edge, and increases the density of the adatoms (advacancies) on the upper (lower) terrace bordered by the step. Then, the probability to form mounds (pits) on the upper (lower) terrace increases, making the surface roughen, signaling a morphological instability (ES instability from now on) on the surface. The ES barrier at kink sites also biases the corner-rounding diffusion of adspecies, which influences the edge orientation of the surface structures, as well as the coarsening and roughening kinetics of the surface structures. Such effects of the ES barriers have been intensively studied in the context of epitaxial thin film growth.^{53,104}

In metals, the morphological evolution of the irradiated surface is determined both by sputter erosion and by the diffusion

of the adspecies (adatoms and vacancies) created by the sputtering process. The strong influence of the crystallinity of the metallic surface under IBS divides experimental sputter conditions into two different regimes, a so-called diffusive regime and an erosive regime.^{3,4,44}

At elevated temperatures and/or relatively low ion fluxes, thermal diffusion of the adspecies dominates over surface erosion, with respect to the pattern formation process. The adspecies diffuse along high symmetry directions under the influence of ES barriers, and the pattern follows the crystallographic symmetry of the surface, irrespective of the ion beam direction. For example, Fig. 4(a) shows a ripple pattern formed on Ag(110), an anisotropic surface. Even though the ion beam impinges under normal incidence, the anisotropic diffusion of the adspecies on the surface produces an anisotropic pattern of ripples elongated along the $\langle 1\bar{1}0 \rangle$ high-symmetry direction.¹⁰⁵

Under the erosive regime, e.g., for a high ion flux and/or low surface temperature, the anisotropic surface erosion and mass displacement induced by the ion beam play the dominant roles in the pattern formation process, overriding surface diffusion associated with the crystallinity. Figure 4(b) shows a ripple pattern formed by a 1 keV Ne^+ ion beam impinging at a grazing angle on Ag(001) at $T = 180$ K, under such an erosive regime. As seen in the figure, now the direction of the ripple ridges follows the surface-projected ion-beam direction, irrespective of the surface crystalline symmetry on the square-symmetric Ag(001).³ Again, the erosive scenario for IBS of metals has been also found at much higher energies, see an example in the case of Ti targets implanted with Au^+ at 100 MeV, corresponding to the erosive regime.¹⁰⁶

Still within the erosive regime, the order of the pattern depends on the direction of the incident ion beam with respect to the crystalline direction. For example, if an Ar^+ ion beam is incident along the high symmetric $[110]$ direction of Au(001) at a grazing angle $\theta = 78^\circ$, then, a well-ordered ripple pattern forms.¹⁰³ The better the ion beam is aligned along the high-symmetric $\langle 110 \rangle$ direction, the higher the order of the ripple pattern is achieved, i.e., the uninterrupted length of the ripple ridge increases, as shown in Fig. 4(c). This indicates that, even in the erosive regime, the diffusion of the adatoms still contributes to the pattern formation with a varying degree of relevance, depending on how much the azimuthal angle of the incident ion beam deviates from the high-symmetric, close-packed directions.

3. Reverse epitaxy

Above the recrystallization temperature at which the damage caused by IBS is efficiently healed, semiconductors also remain crystalline during IBS. Thus, ES barriers become crucial for the pattern formation also for these materials, unless the temperature is so extremely high that the ES barrier is easily overcome as well. If the substrate temperature is tuned making adatoms swiftly diffuse and stick to nearby step edges, while vacancies are not that mobile, the vacancies become the dominant adspecies. Moreover, IBS inherently produces more vacancies than adatoms, since it permanently removes some of the sputtered atoms from the substrate while the matching vacancies remain in the substrate.¹⁰⁷ Then, vacancy diffusion becomes the rate-limiting process and determines the evolution of the surface morphology.¹⁰⁴ Ou *et al.*¹⁰⁷ name

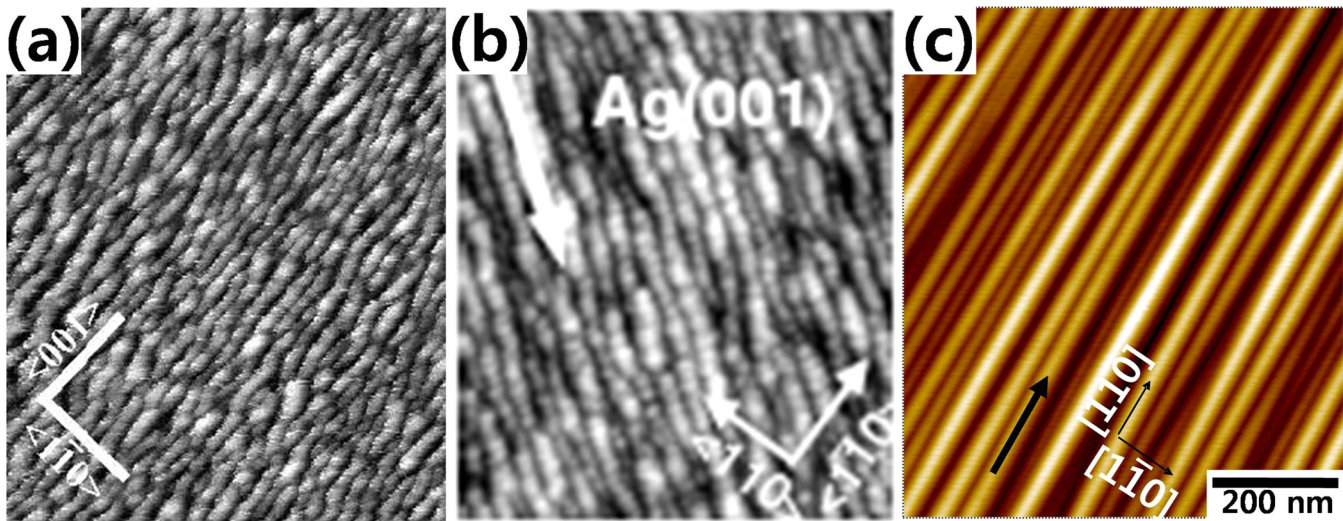


FIG. 4. (a) $400 \times 400 \text{ nm}^2$ image of a ripple pattern obtained by 1 keV Ar^+ IBS of Ag(110) under normal incidence at $T = 230$ K, in the diffusive regime. (b) $180 \times 180 \text{ nm}^2$ image of an Ag(001) substrate eroded with an oblique ($\theta = 70^\circ$) 1 keV Ne^+ ion beam at $T = 180$ K, in the erosive regime. The arrow shows the projection of the ion beam on the target plane. The thin white bars in both panels indicate crystallographic directions. Panels (a) and (b) are reproduced with permission from Valbusa *et al.*, J. Phys.: Condens. Matter **14**, 8153 (2002).³ Copyright 2002 Institute of Physics. (c) $750 \times 750 \text{ nm}^2$ image of a ripple pattern on Au(001) sputtered at $\theta = 72^\circ$ by 2 keV Ar^+ at room temperature in the erosive regime. The surface-projected ion-beam direction indicated by the black arrow lies along the $\langle 110 \rangle$ direction. Reproduced with permission from Kim *et al.*, Nanotechnol. **22**, 285301 (2011).¹⁰³ Copyright 2011 Institute of Physics.

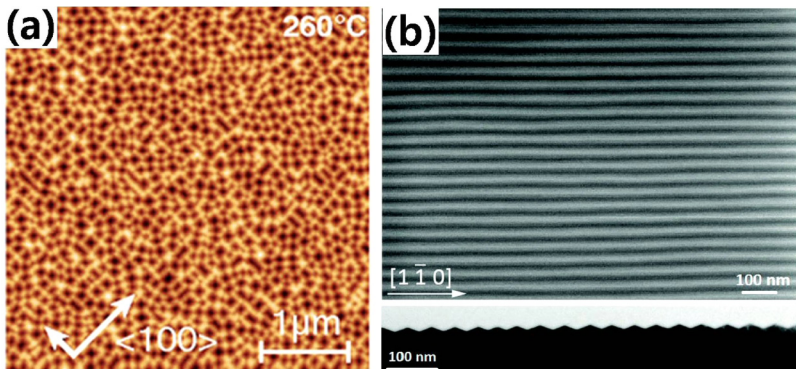


FIG. 5. (a) AFM height image of Ge(100) after 1 keV Ar^+ irradiation for an ion fluence of $3 \times 10^{18} \text{ cm}^2$ at $T = 260^\circ\text{C}$. The $\langle 100 \rangle$ crystal directions are marked by arrows and $\Delta z = 38 \text{ nm}$. Reproduced with permission from Ou *et al.*, Phys. Rev. Lett. 111, 016101 (2013).¹⁰⁷ Copyright 2013 American Physical Society. (b) Regular nanowire patterns produced on GaAs(001) by low-energy IBS. (Top) SEM image of highly ordered nanogroove patterns formed on surfaces aligned along the $[1\bar{1}0]$ direction after 1 keV Ar^+ irradiation under normal incidence for 130 min at $T = 410^\circ\text{C}$. (Bottom) Cross-sectional TEM image of the nanogroove pattern. Reproduced with permission from Ou *et al.*, Nanoscale 7, 18928 (2015).¹⁰⁸ Copyright 2015 The Royal Society of Chemistry.

reverse epitaxy the pattern formation process induced by the vacancy diffusion above the recrystallization temperature, since in their experiments inverse pyramids form by IBS normal to the square-symmetric Ge(100) for temperatures $260^\circ\text{C} \leq T \leq 350^\circ\text{C}$ as shown in Fig. 5(a). These inverse pyramids form because vacancies cannot move to the upper layer due to the ES barrier that prevails at the step edge for such intermediate temperatures. Likewise, IBS normal to a twofold symmetric surface such as GaAs(001), in which the (4×2) surface reconstruction makes the $[1\bar{1}0]$ and $[\bar{1}10]$ directions inequivalent, produces a faceted ripple pattern featuring notably high order, see Fig. 5(b).^{40,108} The crest of the ripples run along $[\bar{1}10]$, the easy diffusion direction, while the diffusion along $[\bar{1}10]$ or across the step edge is hindered by the ES barrier, which causes the surface instability.

4. Binary targets

At the time of its initial publication, the dot pattern shown in Fig. 1 defied theoretical knowledge in a number of aspects. Thus, being linear and operating within morphologically unstable conditions, the BH theory predicts unbounded amplitude growth, while the observed dots reached a finite steady-state amplitude, albeit with a high aspect ratio. But even more remarkably, the space ordering of the pattern was quite high, beyond description by either the BH model or the nonlinear extensions of it which were available at the time,^{20,21,109} see Sec. II B. While some attempts were made at explaining these hexagonal ordering properties via global¹¹⁰ or local²⁵ redeposition of the eroded material, understanding its physical origin remained a challenge. Indeed, as shown by Shenoy, Chan, and Chason,¹¹¹ for compound surfaces like those studied in Ref. 2, one needs to crucially take into account the chemical heterogeneity in the target atomic species inducing different rates of erosion (differential sputtering), as well as different surface diffusivities. A kinetic phase separation takes place in the topmost surface layer of the target due to such differential sputtering and ion-induced transport, in such a way that the element with the higher sputter yield sits preferentially at the pattern peaks; this effect couples then nontrivially with, e.g., the BH instability,^{111–113} see Sec. II B for further details. For the case of GaSb targets, an alternative mechanism for dot (actually, cone) formation has actually been proposed, that is based on a purely chemical (in contrast

with kinetic) origin of the compositional instability:^{114,115} thus, Ga would spontaneously segregate on the surface and act as a mask against erosion. Although the competition between the two mechanisms has been debated,^{116,117} consensus exists on the need of atomic heterogeneity on the target for the production of highly ordered patterns by IBS. Such high-quality patterns can be fabricated by IBS on stationary targets and also on rotating binary semiconductors such as InP,^{34,118} GaAs,^{117,118} InSb,¹¹⁸ and InAs.¹¹⁸ Moreover, similar patterns are also produced on binary targets for ion energies up to the medium energy range $E_{\text{ion}} \simeq 100 \text{ keV}$.¹¹⁹ The order of the dot patterns on binary compounds depends more sensitively on experimental parameters like the ion species¹¹⁷ and the substrate temperature,¹²⁰ than in the case of elemental semiconductors, such as Si and Ge. Indeed, such a highly ordered pattern as the one shown in Fig. 1(a) needs fine tuning of the experimental conditions.

5. Impurities

Elemental semiconductors, especially Si, have drawn enormous attention due to their industrial applications. Dot patterns formed on Si by a 1.2 keV Ar^+ ion beam were first reported in 2001,³³ to be followed by a number of additional experimental observations, as surveyed, e.g., in Refs. 4, 43, and 46. As for ripple patterns, a representative example is shown in Figs. 6(a) and 6(b), which corresponds to a nearly perfect pattern formed on Si by IBS with 1.2 keV Kr^+ ions impinging under $\theta = 15^\circ$ inclination with respect to the surface normal. The reproducibility of patterns like this one was a central issue for some time, and was resolved by concluding that the patterns suffered from an inadvertent codeposition of metallic impurities during the IBS experiment.³⁵ Figure 6(c) shows the surface of Si sputtered normal to the surface (i.e., for $\theta = 0^\circ$) by a 1.0 keV Ar^+ beam, resulting in the lack of pattern formation. In contrast, if Mo atoms are codeposited during IBS under otherwise the same sputter condition, a nanodot pattern does develop as shown in Fig. 6(d). Experimentally, a minimum (threshold) impurity concentration is required to induce nanodot pattern formation via impurity codeposition by IBS.¹²¹

The systematic study of the effects of impurity codeposition on the pattern formation was enabled by the use of various methods to intentionally seed the target with impurities. For instance, Hofsäss and Zhang³⁷ conceived an experimental set up

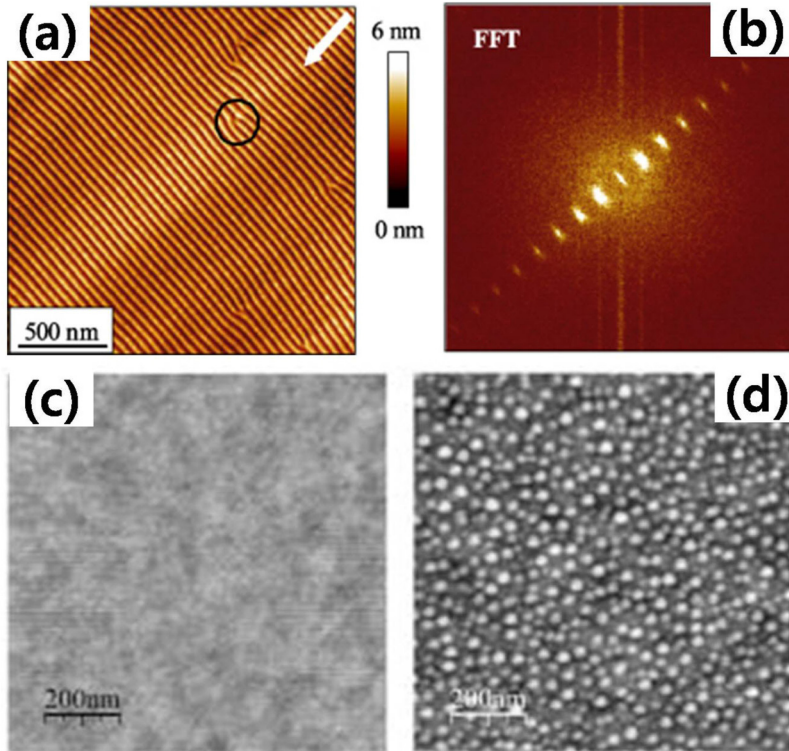


FIG. 6. (a) Surface topography of a Si target after Kr^+ IBS with $E_{\text{ion}} = 1.2 \text{ keV}$, $\theta = 15^\circ$, and ion fluence $1.3 \times 10^{19} \text{ cm}^{-2}$. The solid circle in (a) indicates an existing defect between otherwise highly ordered ripples. (b) Absolute value of the 2D Fourier transform of the image in (a). Both images are reproduced with permission from Ziberi *et al.*, *J. Phys.: Condens. Matter* **21**, 224003 (2009).³⁹ Copyright 2009 Institute of Physics. (c), (d) AFM images of the samples sputtered at 1000 eV (c) without Mo seeding, and (d) with Mo seeding. Reproduced with permission from Ozaydin *et al.*, *Appl. Phys. Lett.* **87**, 163104 (2005).³⁵ Copyright 2005 AIP Publishing LLC.

(termed surfactant sputtering) allowing the continuous variation of the impurity flux and incidence angle over the substrate, as sketched in Fig. 7(a). This approach emphasizes the key role of the metallic impurities in the pattern formation process. Figure 7(b) shows the different patterns produced on Si surfaces with the use of Ag (upper topography) and Pt (lower topography) impurities during IBS with 5 keV Xe^+ ions. Surfactant sputtering has been widely practiced with different codeposited metals and geometries,^{122–127} with the general conclusion that impurities need to form silicides near the surface for pattern formation to occur as shown in Figs. 7(c) and 7(d).

Note that alternative experimental setups exist, such as the use of suitable metallic masks on top of the semiconductor target, which also enable tailoring the surface morphology via the selective incorporation of impurities. Such methods have been employed to control the type of pattern obtained in terms of the experimental conditions. For example, see Fig. 8 for a case in which the basic motif which repeats itself periodically to make the pattern is either a dot or a hole, depending on the ion current density,^{38,46,129} or, alternatively, depending on the chemical species of the impurities.¹²⁸ Interestingly, qualitatively very similar results can be obtained at intermediate ion energies ($E_{\text{ion}} \approx 50 \text{ keV}$).^{130,131}

In the experimental systems mentioned, silicide formation is believed to be a necessary condition for the formation of a pattern when conditions (e.g., an incidence angle θ below threshold) would otherwise lead to the formation of unstructured surfaces. Hence, patterns ensue for, e.g., Ag, Pt,³⁷ Fe, Ni, Mo, or W impurities,¹³² all of which produce silicides, see a survey of additional works, e.g., in

Ref. 46. Still, cases are also known in which patterns are produced in the absence of silicide formation. An example is due to Moon and co-workers,¹³² who observed that Au deposition during IBS produces the ripple patterns shown in Fig. 9. In this case, Au does not form any stable silicide, while the sputter yields of Au and Si are virtually identical under the given sputter condition. Nevertheless, ripples form due to kinetic effects.¹³⁴ Since the eroded Au is constantly replenished by the deposited Au, the effective sputter yield of Au can be considered lower than Si, this heterogeneity in the sputtering rate allows for a surface instability.⁴ Additional experimental features of this experiment nonetheless remain to be elucidated, such as the change in the orientation of the ripples observed in Fig. 9.

6. Unconventional formats

One of the major concerns with respect to surface nanostructuring by IBS is the high density of defects quite frequently displayed by the ensuing patterns, a common trait of this self-assembly process that often limits the applications of the structures produced. There have been various attempts to improve the quality of the spatial order in IBS-induced patterns, and they have in common implementing IBS routines using experimental setups which depart from the conventional ones discussed thus far. Overall, such innovative setups have enriched the diversity of pattern motifs which can be produced, and have also enabled a deeper understanding of the mechanisms of pattern formation by IBS.

A first approach is to employ directed self-assembly, in which IBS is performed on a well-defined template fabricated by other

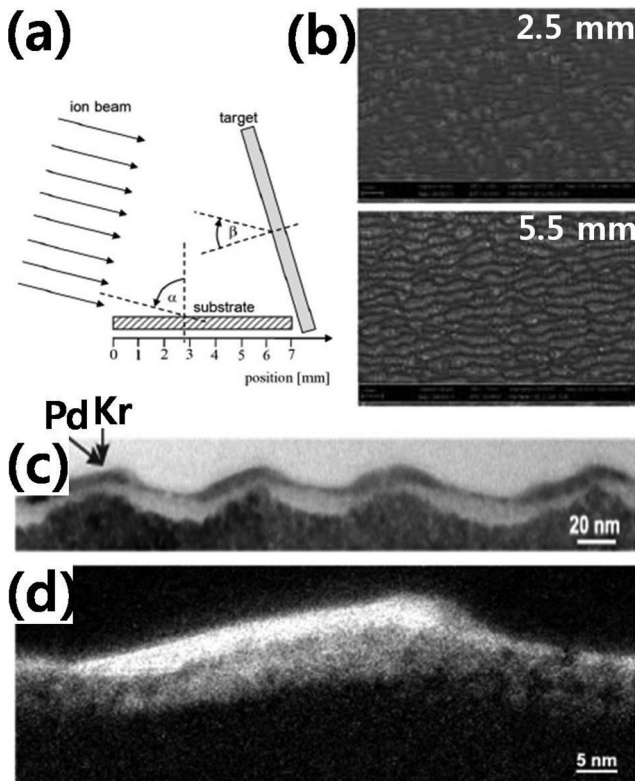


FIG. 7. (a) Schematic experimental setup used for surfactant sputtering. (b) SEM pictures of Si surfaces eroded with 5 keV Xe^+ with silicide-forming surfactants like Ag (top row) and Pt (bottom row). (c) Cross-sectional TEM image of a Kr^+ -irradiated sample subject to simultaneous Pd co-evaporation, with relative flux $\Phi_{Pd}/\Phi_{Kr} = 0.8$, and (d) energy-filtered TEM image showing the ensuing Pd distribution. Panels (a) and (b) are reproduced with permission from Höfsäss *et al.*, *Appl. Phys. A* **92**, 517 (2008).³⁷ Copyright 2008 Springer Nature. Panels (c) and (d) are reproduced with permission from Engler *et al.*, *Nanotechnology* **25**, 115303 (2014).¹²² Copyright 2014 Institute of Physics.

means such as lithography, which act at a larger spatial scale than that of the motifs formed by IBS. This is done, for instance, by Cuenat *et al.*,¹³⁵ who fabricated a stripe pattern on a Si(001) substrate, with 430 nm-wide valley bottom. Then, the ion beam was irradiated along the long axis of the valleys, with ripples developing preferentially along that direction, as shown in Fig. 10(a). Although the ripples in the valleys are not perfect, their alignment is better than for ripples produced on a template-free terrace, proving the successful effect of the pre-patterned structures in guiding subsequent ripple formation.

Sequential ion beam sputtering (SIBS) can alternatively be employed to direct self assembly without the need to resort to top-down techniques like lithography. For instance, Kim *et al.* produced^{103,137,138} an initial ripple pattern on Au(001) by 2 keV Ar^+ IBS at $\theta = 78^\circ$. Then, this rippled surface is sputtered by the Ar^+ beam at normal incidence. The initial ripples direct the growth of dots along the previous ripple ridges as shown in Fig. 10(b). This fully bottom-up directed self-assembly process produces a

hierarchical pattern combining 1D ripples and 0D dots, termed *nanobeads*. Such a nontrivial pattern can be further used as a touchstone to identify the mechanism best reproducing the observed pattern, supporting specific nonlinear effects that need to be included in the continuum description of the system via evolution equations like Eq. (2) and its generalizations,^{103,137,138} see Sec. II B. Moreover, it demonstrates the role of the space correlations which may exist in the initial surface prior to IBS treatment, which have been exploited experimentally to understand, e.g., interrupted¹³⁹ or reverse¹⁴⁰ coarsening at low and medium ion energies, respectively.

A different implementation of SIBS is provided in Ref. 136, where the order in a Si ripple pattern is improved by performing SIBS along different azimuthal directions. Thus, a ripple pattern was first induced by Ar^+ IBS of Si at $\theta = 65^\circ$ as shown in Fig. 10(c). In a subsequent step, the substrate was rotated in azimuth by 90° , after which the ripple-patterned surface was further irradiated at $\theta = 85^\circ$, so that the ion beam now runs along the ridges of the previously formed ripples. Notable improvement of the order of the ripple pattern was indeed achieved, as shown in Fig. 10(d).

IBS of rotating substrates has long been practiced in the context of depth profiling under the name of Zalar rotation.¹⁴¹ By this method, the sputtered surface reduces the surface roughness, and depth resolution improves. With respect to pattern formation, Frost *et al.*³⁴ led the production of nanodot patterns on rotating substrates by performing 500 eV Ar^+ IBS of InP. Under the same oblique-incidence sputter condition, but with stationary substrates, no periodic surface structure formed. Many experimental works have followed, devoted to different substrates, such as GaSb,¹¹⁸ InSb,¹¹⁸ InAs,¹¹⁸ Si,^{142,143} and highly oriented pyrolytic graphite (HOPG).¹⁴⁴ Note that well-ordered patterns form only on compound semiconductors. Theoretical^{143,145–147} and computational approaches^{148,149} have attempted to elucidate the pattern formation mechanism, since descriptions based on the classic BH model fail to fully elucidate the observed surface dynamics.³⁴ The current consensus is that the compound nature of the targets needs to be taken into account, this being regarded as a particular instance of IBS of binary semiconductor systems, see Sec. II B for further discussion.

Additional unconventional IBS formats (see Sec. III A below for some very recent ones) include the simultaneous use of multiple ion beams.¹⁵⁰ This was theoretically proposed with the expectation that various interference patterns might be thus produced in solid phase.^{151,152} Experimentally, dual ion beam sputtering was performed on Au(001).¹⁵³ In contrast to the theoretical prediction, the observed pattern is governed by that ion beam which causes the strongest instability, being sensitively vulnerable to uncontrollable errors in experimental parameters.

Besides, a situation in which the beam has a controlled, non-negligible divergence could arguably be considered as another instance of multiple ion beams. Ziberi *et al.*¹⁵⁴ have addressed the role of the ion-beam divergence for Si irradiated by 2 keV Xe^+ , finding that a change in the incidence angle by 1° drastically transforms the pattern from rotated ripples to a square dot arrangement, although a word of caution is required, since these results may be also affected by inadvertent impurity codeposition. From this experimental observation, the ion-beam divergence was suggested to influence pattern formation, as inferred from the gradual change of the pattern with the increase of the beam divergence.¹⁵⁴ A continuum

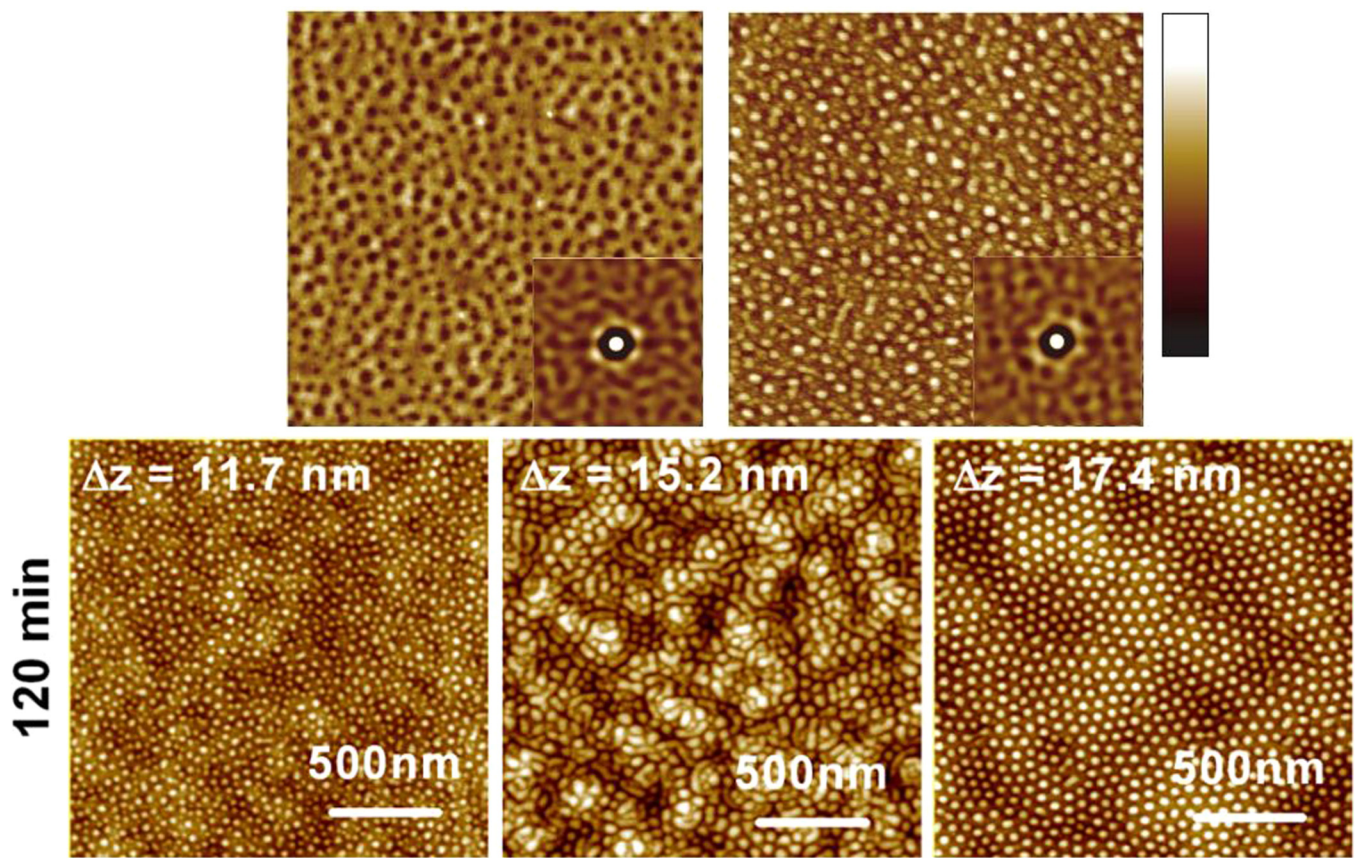


FIG. 8. Upper row: $1 \times 1 \mu\text{m}^2$ AFM images for Si(001) irradiated under normal incidence by 1 keV Ar^+ ions for a fixed ion fluence, using $J = 105 \mu\text{A cm}^{-2}$ (nanohole pattern, left panel) and $J = 260 \mu\text{A cm}^{-2}$ (nanodot pattern, right panel). The vertical scale represents the [0.6–5] nm interval and the insets show the corresponding auto-correlation functions. Reproduced with permission from Sánchez-García *et al.*, Nanotechnology, **19**, 355306 (2008).³⁸ Copyright 2008 Institute of Physics. Lower row: $2 \times 2 \mu\text{m}^2$ AFM images showing Si(100) surfaces subject to IBS at $\theta = 0^\circ$, with metal co-deposition from a mask of diameter d and impurity species as indicated: $d = 14 \mu\text{m}$, Fe (left panel); $d = 12 \mu\text{m}$, Fe (center panel); $d = 12 \mu\text{m}$, Mo (right panel). The vertical range Δz is indicated for each image. Reproduced with permission from Redondo-Cubero *et al.*, Nanotechnology, **25**, 415301 (2014).¹²⁸ Copyright 2014 Institute of Physics.

model taking the beam divergence into account was later proposed,¹⁵⁵ which predicts the surface stability and the ripple orientation to be affected by the beam divergence. Additional kMC simulations find that, specifically, the latter enhances surface diffusion.¹⁵⁵ Both the experimental and the theoretical studies suggest that the beam divergence may be an additional parameter to be considered in designing the experimental conditions and interpreting the results. The beam divergence is, however, not easy to control, while no further relevant studies have been reported in this connection, to the authors' knowledge. As a result, no unambiguous correlation seems available between the beam divergence and specific pattern properties. Further systematic studies along these lines seem highly desirable.

Finally, the possibility to subject the nanostructures to some kind of after-treatment is also worth mentioning, since this can also be employed as a further method for the modification and/or improvement of the surface structures produced by IBS. As examples, we can mention the manipulation of the size of previously

IBS-formed pores on a Si_3N_4 membrane by suitably tuning the substrate temperature during irradiation.¹⁵⁶ Also, the features of pre-patterned nanostructures, like holes, can be further sharpened quite steeply by IBS, in a process which is understood in terms of the dynamics of shock waves around the hole edge.^{157–159} Although the aforementioned after-treatments do not deal with the nanopatterns but, rather, with isolated nanostructures, they can still be adopted in order to “nanosculpt” the motif of the patterns formed by IBS. From this point of view, SIBS can also be viewed as a “nanosculpting” technique.^{41,150}

7. Applications

The nanopatterns formed by IBS have been used for various applications as they are, or as ordered templates. Since the wavelengths of the ripple patterns are around 50 nm, which belongs to the UV range, ripple patterns have been often employed for optical

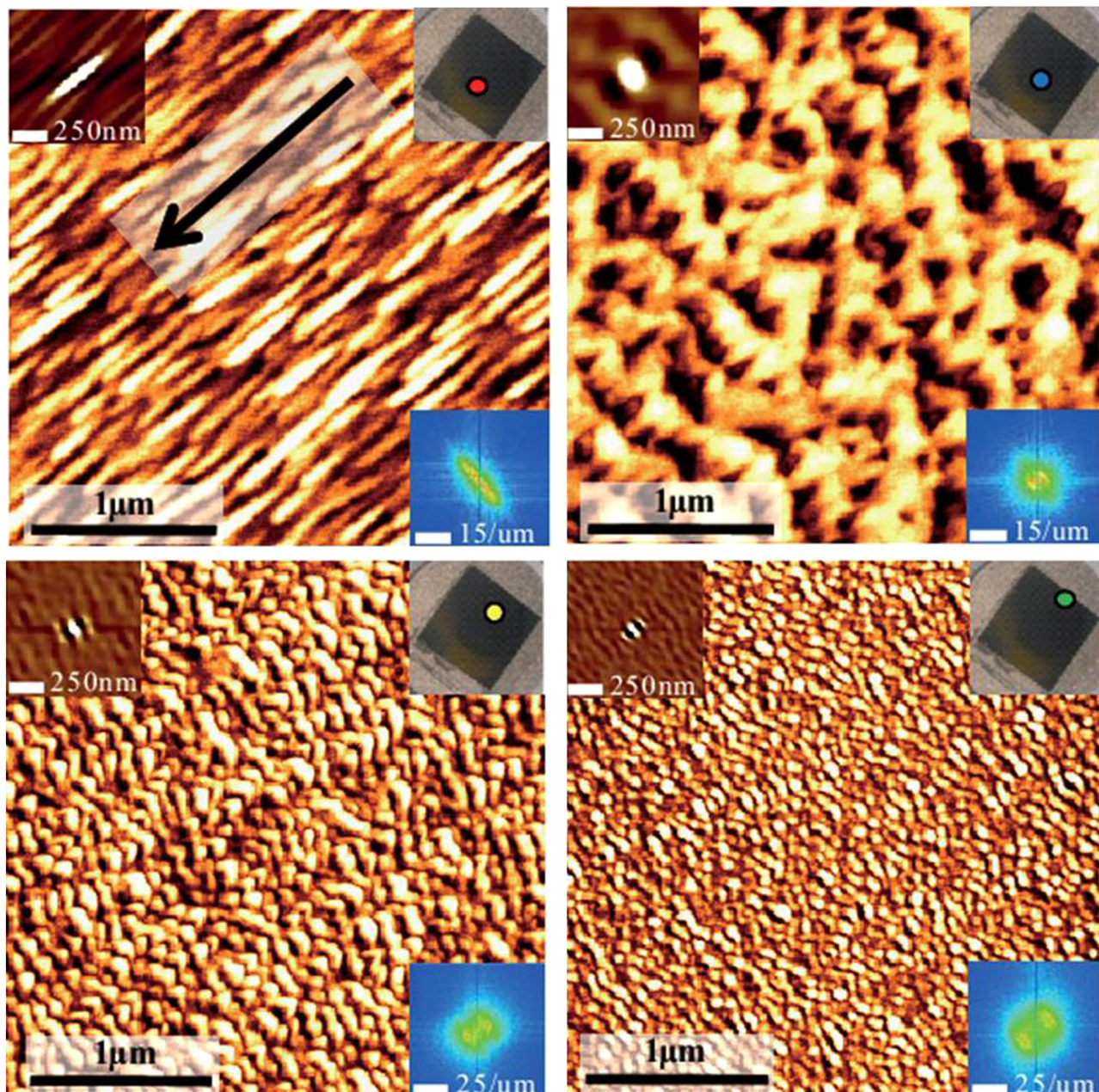


FIG. 9. Patterns on Si substrates formed by 2 keV Ar^+ IBS with (non-silicide forming) Au co-deposition. The Au flux decreases clockwise from the top, left image, in which the arrow indicates the projection of the ion beam direction on the surface, common to the four images. Top-left and bottom-right insets in each image show the corresponding 2D autocorrelation and Fourier transform magnitude, respectively, while the top-right inset indicates the position on the target where the AFM image is taken. Reproduced with permission from Moon *et al.*, Phys. Rev. B **93**, 115430 (2016).^[32] Copyright 2016 American Physical Society.

and plasmonic applications. A ripple-patterned substrate decorated by a metallic film shows an optical reflectance that is anisotropic^[160] and sensitive to the polarization direction of the incident light.^[161] On the other hand, the deposition of zinc tin oxide on ripple-

patterned Si shows a significant reduction of the reflectance, which can be used for broadband antireflection coatings.^[162]

Recently, reverse epitaxy has proved its capability to fabricate a template for optical gratings even in the wafer scale. Remarkably,

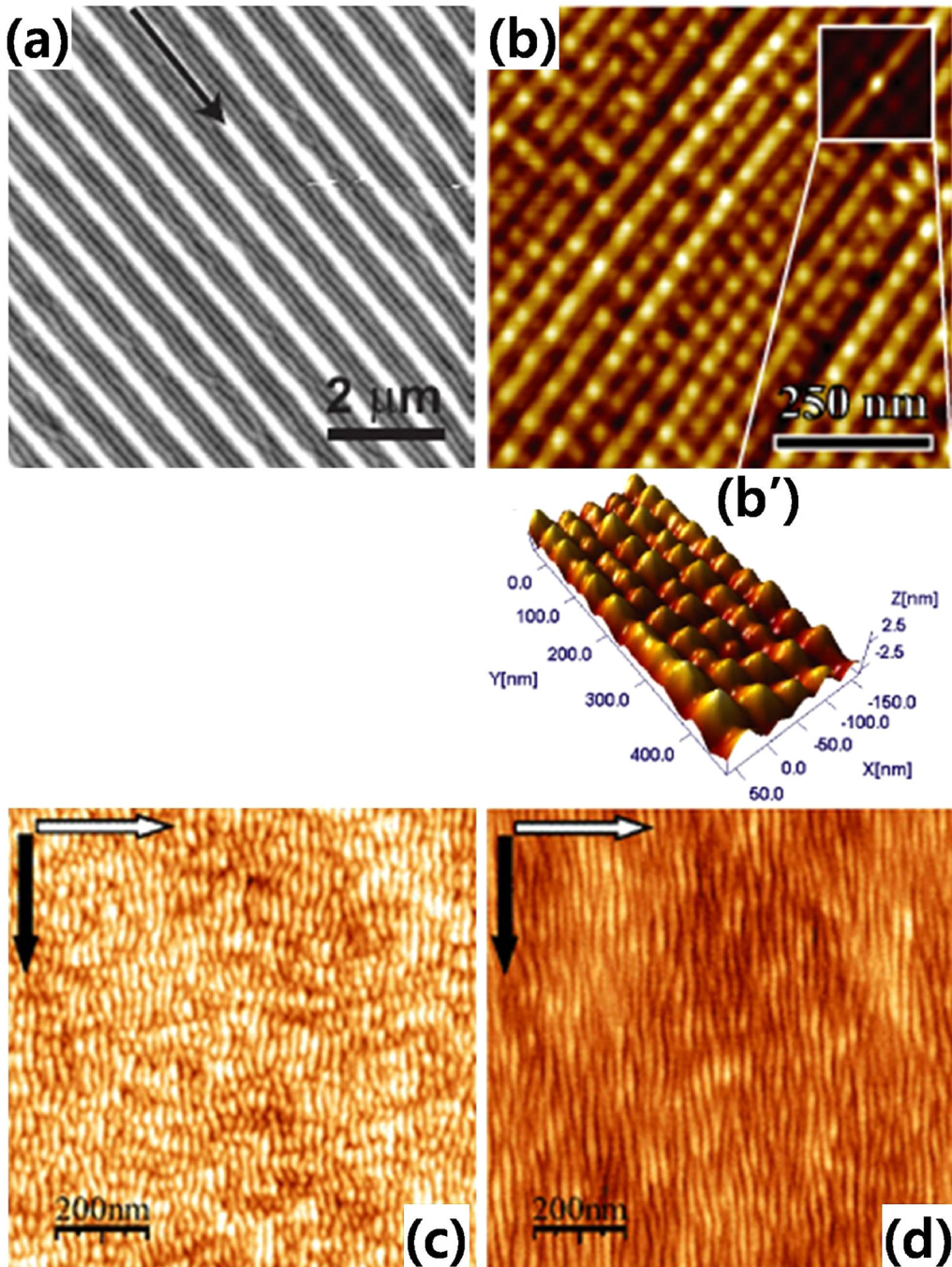


FIG. 10. (a) Sputter-ripple morphologies on Si(001). The arrow indicates the projection of the ion beam. Self-organized ripples form on a lithographically defined template with 430 nm width. Reproduced with permission from Cuenat *et al.*, *Adv. Mater.* **17**, 2845 (2005).¹³⁵ Copyright 2005 Wiley-VCH. (b) AFM image of the surface morphology produced by 1 keV Ar⁺ IBS normal to an initially rippled Au surface, after a fluence of 1781 ions nm⁻². (b) 3D magnified image of the ordered nanobead pattern shown in (b). Reproduced with permission from Kim *et al.*, *Nanotechnology* **22**, 285301 (2011).¹⁰³ Copyright 2011 Institute of Physics. (c) AFM image of the ripple pattern created on Si in a first IBS step and (d) after subsequent grazing-incidence IBS after a fluence of 1.610 ions cm⁻². The white (black) arrow represents the substrate projection of the ion beam in the first (second) irradiation step. Panels (c) and (d) are reproduced with permission from Keller *et al.*, *Phys. Rev. B* **82**, 155444 (2010).¹³⁶ Copyright 2010 American Physical Society.

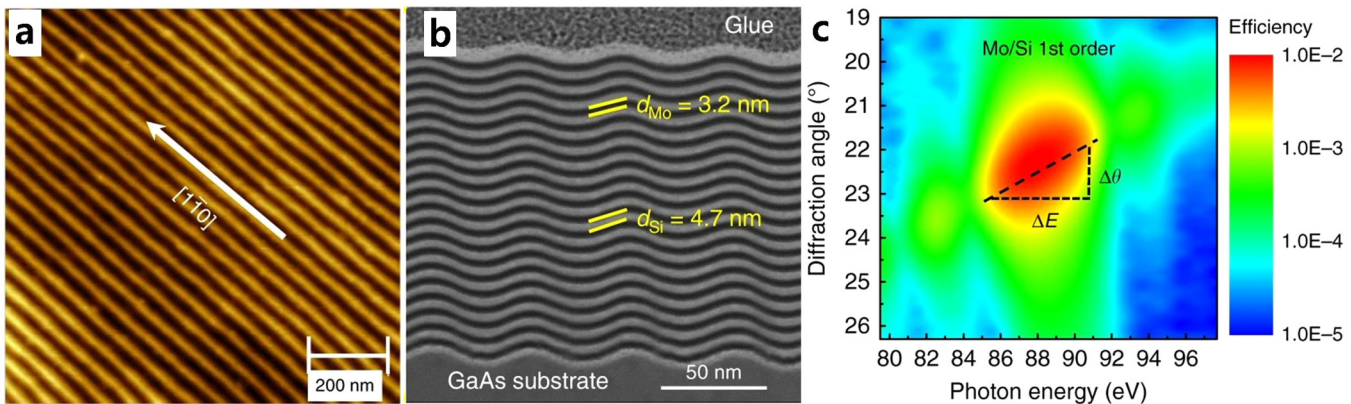


FIG. 11. (a) GaAs substrate with a nanogroove density approximately of $20\,000 \text{ lines mm}^{-1}$ that is induced by reverse epitaxy. (b) Alternating layers of Mo and Si are deposited on the GaAs grating to enhance its reflectivity. (c) Unprecedentedly-high dispersive power of light in the EUV range is demonstrated by the multilayer blazed nanograting. Reproduced with permission from Huang *et al.*, Nat. Comm. **10**, 2437 (2019).⁴⁰ Copyright 2019 Springer Nature.

the line density of the grating that can be produced is about four times larger than those achieved by conventional methods such as mechanical ruling, laser interference lithography, or e-beam lithography.⁴⁰ Such a high line density with a ripple wavelength below 50 nm is requested to achieve high angular dispersion of light, especially for extreme ultraviolet (EUV) and soft x-ray radiation. Figure 11(a) shows the diffraction grating formed on GaAs(100) by reverse epitaxy. The wavelength of the ripple pattern is around 50 nm, equivalent to a nanogroove density of 20 000 lines per mm. In order to increase the reflectivity, alternating layers of Mo and Si are deposited on the grating as shown in Fig. 11(b). Figure 11(c) shows the first-order diffraction angle and the energy of light for EUV light illumination of this multilayer blazed grating. Using θ

for the angle showing the maximum intensity for each light energy E , the energy dispersive power of the grating $\Delta\theta/\Delta E$ is determined to be approximately $0.21^\circ/\text{eV}$. Such a $\Delta\theta/\Delta E$ is consistent with the prediction of the grating equation and roughly 4.5 times larger than that for the grating with the currently available maximum groove density, approximately 5000 lines per mm.¹⁶³

For plasmonic applications, ordered Ag or Au nanostructures have been grown on ripple patterns.^{161,164–166} For an example on ordered ripples produced by IBS over large areas on PDMS substrates, see Fig. 12(a). The localized surface plasmon resonance (LSPR) frequency is tunable from the infrared to the visible range by controlling the ripple wavelength and the width of the Au nanowires grown over the ripples, as shown in Fig. 12(b).¹⁶⁶ Such

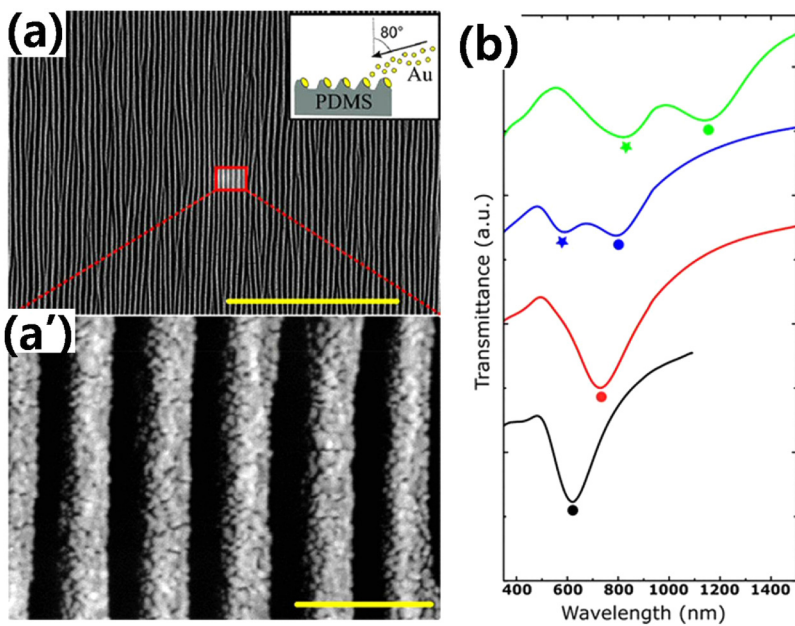


FIG. 12. (a) SEM image of a 10 nm-thick Au film deposited at grazing incidence on a rippled PDMS substrate. The deposition geometry is sketched in the inset: the Au flux is perpendicular to the long ripple axis and is at 80° with respect to the substrate normal. The yellow scale bar corresponds to $10 \mu\text{m}$. (a') Zoom-in of the image shown in (a) in which the polycrystalline structure of the Au wires is visible. The yellow scale bar corresponds to 500 nm. (b) Optical extinction spectra of light polarized orthogonal to the ripple edges, for samples A (black curve), B (red curve), C (blue curve), and D (green curve). The circles identify the position of the dipolar localized surface plasmon resonance, while the stars identify the multipolar resonance. Reproduced with permission from Barelli *et al.*, ACS Appl. Polym. Mater. **1**, 1334 (2019).¹⁶⁶ Copyright 2019 American Chemical Society.

tailored surface can be used for surface enhanced Raman spectroscopy (SERS) for probing a wide energy range of surface excitations. We note that the pattern forms on the pre-stretched substrate that is bombarded by an air plasma. The pattern formation is attributed to a modified elastic modulus in the skin layer as compared with that of the bulk. Both the pattern formation mechanism and the μm pattern wavelength differ in principle from most of those dealt with in this Perspective, although see Sec. III B. We still consider this example as a natural extension of IBS pattern formation, which has also been pursued in the community.

IBS nano-patterned substrates also find applications to solar cells,^{167,168} for which enhancing the conversion efficiency of light energy to electrical energy is the key concern. For that purpose, a nano-rippled glass substrate is employed, onto which Si and Ag thin films are subsequently grown, reproducing the pattern of the glass substrate as sketched in Fig. 13(a). The Si film is the active medium where light absorption occurs, while the Ag film acts as the reflector which confines light in the solar cell. The patterned glass substrate enhances the haze transmission of the incoming solar light via diffuse scattering at its rugged surface, and reflection at the interface with the Ag film also produces the haze as illustrated in Fig. 13(a). Thereby, the path length of light in the active medium is increased, and the conversion efficiency is expected to increase. Indeed, the nano-patterned glass substrate enhances the haze transmission as shown in Fig. 13(b), and thus the angle-integrated light absorption ΔA increases as compared with the widely used Asahi-U glass, see Fig. 13(a). In the figure, zone 2 of the glass substrate is rougher than zone 1, Asahi-U glass being much smoother than both zones.

The magnetic anisotropy of thin magnetic films can be modified by the ripple patterns formed by IBS due to both the uniaxial in-plane anisotropy, via the shape anisotropy, and the anisotropic proliferation of the steps.¹⁶⁹ The kink sites can also contribute to the uniaxial anisotropy.¹⁷⁰ The growth of antiferromagnetic multilayers on an IBS-structured substrate leads to an enhanced magnetic coupling between the layers.¹⁷¹

Considering the high density of local defects generated by IBS, many such patterned surfaces are studied in search of catalytic applications. For instance, Ag surfaces structured by IBS were shown to promote O_2 dissociation, while flat surfaces remain inactive.^{172,173} Such a catalytic activity was associated with the kink and vacancy sites created by IBS.

It has also been demonstrated that Si nanoripple patterns can preferentially align DNA nanotubes along the ripple ridges, as shown in Fig. 14.¹⁷⁴ This allows the wafer-scale fabrication of ordered arrays of functional DNA-based nanowires, which is a prerequisite for DNA-based nanoelectronics and sensors. Similarly, ripple-patterned surfaces can also direct the growth direction of biomaterials, such as osteoblast-like cells.¹⁷⁵ The possibility to tune the ripple wavelength with ion energy allows for the production of surface patterns with typical scales up in the micrometer scale, with potential for biointegration.¹⁰⁶

Also, fluid wettability properties at surfaces can be controlled by nanopatterning surfaces by means of IBS. The wettability of elemental Si surfaces subject to medium-energy IBS also changes from being hydrophilic to hydrophobic as the fluence of 60 keV Ar^+ ion increases.¹⁷⁶ This is because amorphized Si surfaces have a lower surface free energy than crystalline ones. Upon the formation

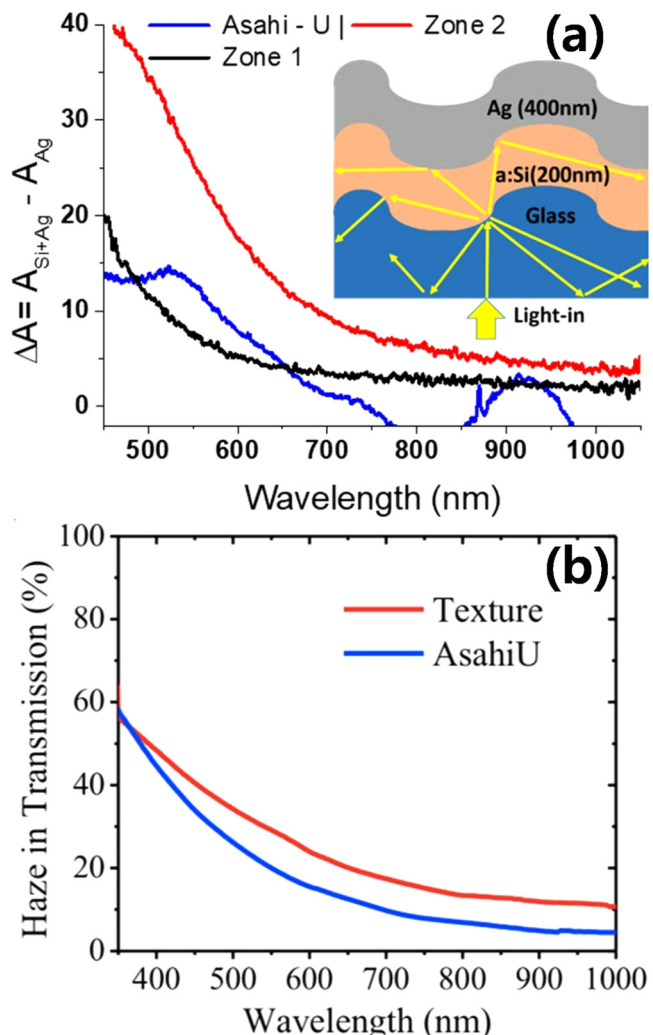


FIG. 13. (a) Angle-integrated absorption ΔA of a silicon thin film absorber capped by an Ag back-reflector on Asahi-U glass (blue line) and on zone 1 (black line) and on zone 2 (red line) rippled glass. The inset shows a sketch of the measurement scheme employed on the thin film devices. (b) The haze in transmission measured on the nano-textured substrate (zone 2) and on the Asahi-U glass sample. Reproduced with permission from Mennucci *et al.*, *Nanotechnology*, **29**, 355301 (2018).¹⁶⁷ Copyright 2018 Institute of Physics.

of ripple patterns, however, the hydrophobicity decreases along the ridge direction, while it remains the same as the fluence increases. It is attributed presumably to both, the anisotropic ripple structure and the distribution of the implanted Ar.

B. Theory and computational studies

We next provide some perspective over the main steps taken in the understanding of surface nanopatterning by IBS from the point of view of theoretical and computational approaches, with a

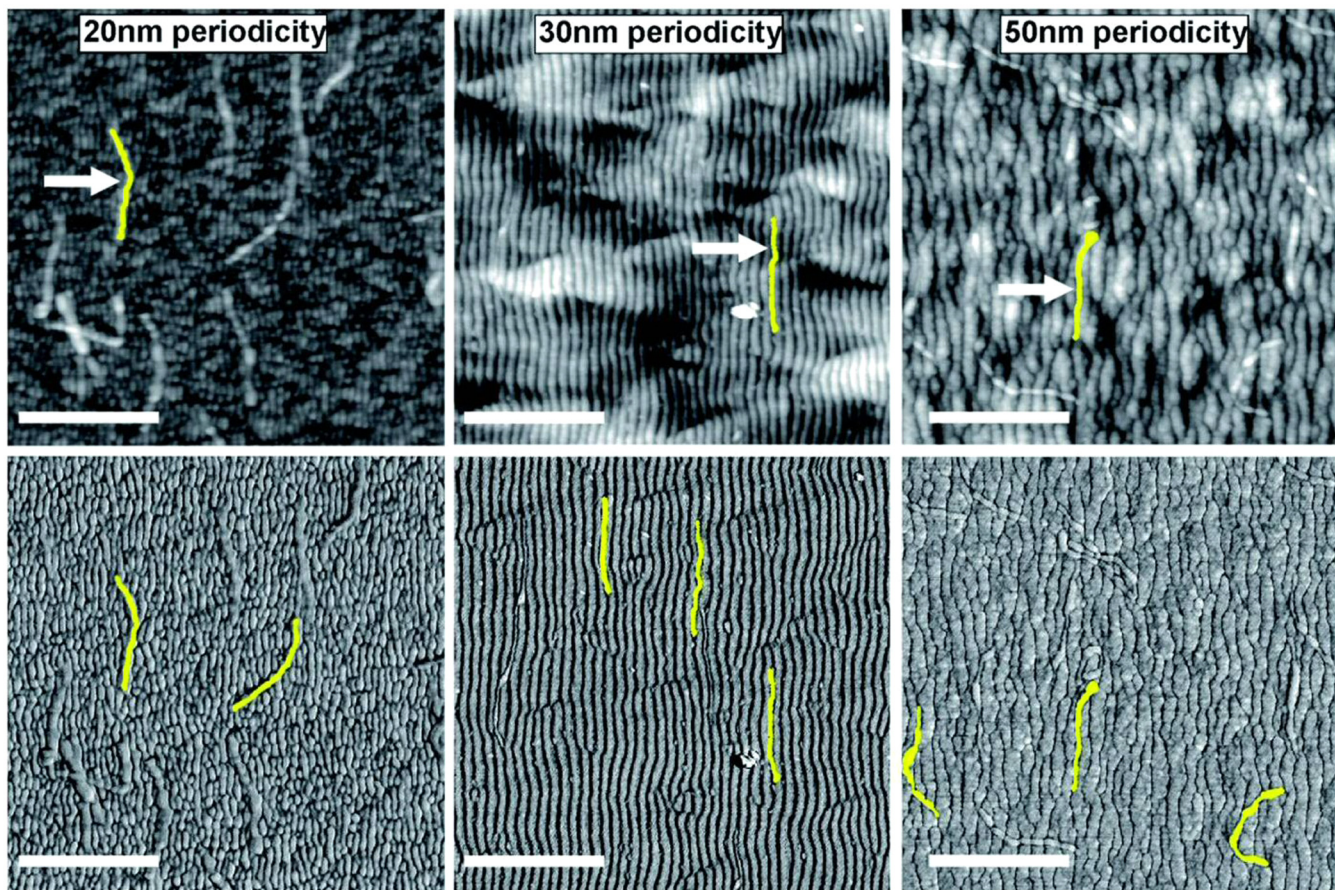


FIG. 14. AFM height (top row) and corresponding phase images (bottom row) of DNA origami nanotubes adsorbed on nanopatterned Si surfaces. Single DNA origami nanotubes have been highlighted. The scale bars are 500 nm long. Reproduced with permission from Tesome *et al.*, *Nanoscale* **6**, 1790 (2014).¹⁷⁴ Copyright 2014 The Royal Society of Chemistry.

view to describe the current consensus on some of the main experimental observations described in the Secs. II A 1–II A 7. Actually, the formation of surface nanostructures by IBS was the focus of theoretical work relatively early on after the initial experimental observations. A number of approaches (surveyed, e.g., in Ref. 177) focused on the kinetic consequences that the known dependencies of the sputtering yield—with incidence angle, ion energy, etc.—may have on the local surface morphology, for instance, inducing front propagation driven by geometry as described, e.g., by Huygens' principle. Analogous geometric effects, such as differential ion reflection by terraces of different sizes, were shown quite early on to induce facet coarsening.¹⁷⁸ Although some of these models have been invoked to account for experimental observations, as for low-energy irradiation of Ge⁹⁴ and Si,⁹⁵ they lack a direct relation to the underlying ion collision processes which are taking place in the near-surface region of the target. Moreover, this class of “geometric” models usually predict ripple wavelengths in the micrometer range, which are much larger than those experimentally observed in low-energy IBS systems.

1. General properties of IBS nanopatterning

As already mentioned in Sec. I, a seminal observation for IBS nanostructuring is due to Sigmund.¹⁰ He had previously developed the classic description of energy deposition by the ion beam within the target, in the linear-collision cascade regime which most frequently holds at the energy range that we are presently considering.⁹ In this regime, energy deposition is dominated by nuclear stopping, with a minor influence of electronic contributions.¹⁷⁹ Shortly after, Sigmund himself noted that local surface minima focus more deposited energy from their surroundings than local surface maxima so that, assuming the local surface erosion velocity to be proportional to the total deposited energy, erosion is faster at minima, making a flat surface unstable to local height perturbations.¹⁰ As established by modern theory of self-organization,⁷ an instability is a key ingredient to pattern formation; however, the characteristic length scale of the pattern emerges as a consequence of the balance between destabilizing and stabilizing forces. It took

15 more years until Bradley and Harper (BH) identified thermally activated surface diffusion, as classically characterized by Mullins,^{11–13} as a possible stabilizing mechanism in the dynamics of the surface.⁸ As has been noted already, the ensuing BH model is a linear evolution equation for the surface height of the bombarded target, whose coefficients depend on physical parameters like the average ion energy, flux, and incidence angle, as well as on temperature. Indeed, as remarked in Sec. II A, the BH equation has the exact same form as Eq. (2), although with a different physical interpretation for the coefficients. At any rate, the BH model predicted for the first time ripple formation with typical wavelengths in the range of tens of nm, and with an orientation with respect to the ion beam that also matched that observed in many experiments.

By the early 1990's, additional experimental features still required explanation. First, the long-time (large-fluence) behavior where target surfaces stabilized into finite-amplitude steady states could not be described by a linear equation like BH, which predicts exponential amplitude growth. Moreover, some dependencies of the ripple wavelength ℓ with physical parameters, like ion energy E_{ion} , did not fit expectations. Specifically, $\ell(E_{\text{ion}})$ was predicted to be a decreasing function, in contrast with some observations. Carrying out the BH approach to lowest nonlinear order in height perturbations led to the so-called anisotropic Kuramoto–Sivashinsky (aKS) equation,²⁰ which, in its simplest version, reads

$$h_t = -Ah_{xx} + A'h_{yy} - B\nabla^4 h + \lambda h_x^2 + \lambda' h_y^2, \quad (3)$$

where A , A' , λ , and λ' likewise depend on experimental parameters.^{20,21} The aKS equation could justify amplitude stabilization and, if enhanced by contributions to surface diffusion originated in the collision cascades via energy deposition *à la* Sigmund,¹⁰⁹ it could additionally predict a non-decreasing $\ell(E_{\text{ion}})$.²¹ Moreover, still higher-order nonlinear generalizations of this equation, devised to account for arbitrarily large surface slopes, were seen to also successfully describe, e.g., the experimental propagation and sharpening of ion-sculpted Si surface features.^{157–159} Generally speaking, the Kuramoto–Sivashinsky equation is a paradigmatic model of spatially extended systems displaying pattern formation and strong (chaotic) fluctuations.⁷ Although the specific $\ell(E_{\text{ion}})$ predictions in Ref. 21 have been superseded by later developments,¹⁸⁰ the aKS equation has been playing a prominent model for IBS. This is possibly related with the occurrence of universality in this type of dynamical processes,¹⁸¹ namely, the fact that the large-scale properties of many spatially extended systems which differ in physical nature is described by the same evolution equation. For instance, the aKS equation is known to also describe the evolution of vicinal surfaces in molecular beam epitaxy,¹⁸² a process which is in principle very different from IBS.

2. Two-field descriptions

By the early 2000s, a full physical model of surface dynamics was available that included nonlinearities and even noise contributions^{20,183,184} reflecting the stochastic nature of the microscopic processes involved in IBS, e.g., energy deposition and material transport at the surface. However, a number of properties remained

to be correctly described. *On the one hand*, some additional nonlinear properties seen in some of the experiments mentioned in Sec. II A could not be reproduced, such as enhanced short- to medium-range order of the patterns, or a time dependent value of the average pattern wavelength (coarsening). Following an insightful analogy by Aste and Valbusa between adatom transport on solid surfaces and grain saltation on aeolian sand dunes,¹⁸⁵ a systematic program originated (so-called *two-field* approach⁴⁵) in which material transport (represented by a density field of transported material, e.g. adatoms and/or vacancies) in the top-most surface layer was explicitly coupled to the time evolution of the surface height field, see Ref. 45 for an overview. Thus, improved short-range order and wavelength coarsening could be described under normal^{25,147} and off-normal^{85,186} incidence conditions, as well as in-plane ripple transport⁴ in a form which has been experimentally verified.⁸³

Mathematically, in the most general case the interface equation obtained by this two-field approach is a nonlinear generalization of the aKS equation, Eq. (3). To fix ideas, we quote it in a simple version,^{45,85,186} which reads

$$h_t = -Ah_{xx} + A'h_{yy} - B\nabla^4 h + \lambda h_x^2 + \lambda' h_y^2 - \nabla^2(\lambda_2 h_x^2 + \lambda'_2 h_y^2), \quad (4)$$

where now all the coefficients depend on parameters characterizing sputtering and surface transport, whether of erosive or of thermal origin.

Such as stated, Eq. (4) generalizes the aKS equation, Eq. (3), by the appearance of the additional nonlinear terms with parameters λ_2 and λ'_2 , and is termed extended KS (eKS) equation.^{25,188} Figure 15 illustrates the comparison of numerical simulations of Eq. (4) with ripple formation experiments on fused silica under oblique-irradiation conditions.⁸⁶ The ripple coarsening that occurs in the experiments is now captured by the continuum model. Possibly related with its universality properties,⁴⁵ the eKS equation has been also shown to account quantitatively for IBS experiments on Pd targets,¹⁸⁹ and on Si targets seeded with metallic impurities^{139,190} under conditions similar to those illustrated in Fig. 8, see Fig. 16 for an explicit comparison.

At this point, it is important to mention that the two-field approach has been also successfully implemented to describe IBS of binary materials, for which differential sputtering rates and diffusivities were shown to play a relevant role, within a linear approximation.¹¹¹ In this case, following earlier developments in epitaxial growth,¹⁹¹ the dynamics of the height field was coupled with that of a *composition* field describing local variations in the target atomic species. We will return to this issue below.

3. Clean amorphizable targets

On the other hand, as seen in Sec. II A, a number of experimental observations on semiconductor targets, especially on Si, suggested the occurrence of a non-zero threshold value θ_c for the incidence angle θ , such that patterns only form provided $\theta > \theta_c$. Based on kinetic arguments, and as also briefly advanced in Sec. II A, Carter and Vishnyakov (CV)²² had shown that momentum transfer from the beam to the substrate, if dominant over energy deposition in the local interface velocity, could account for such a behavior. This contrasts with a surface dynamics purely induced by the Sigmund-like

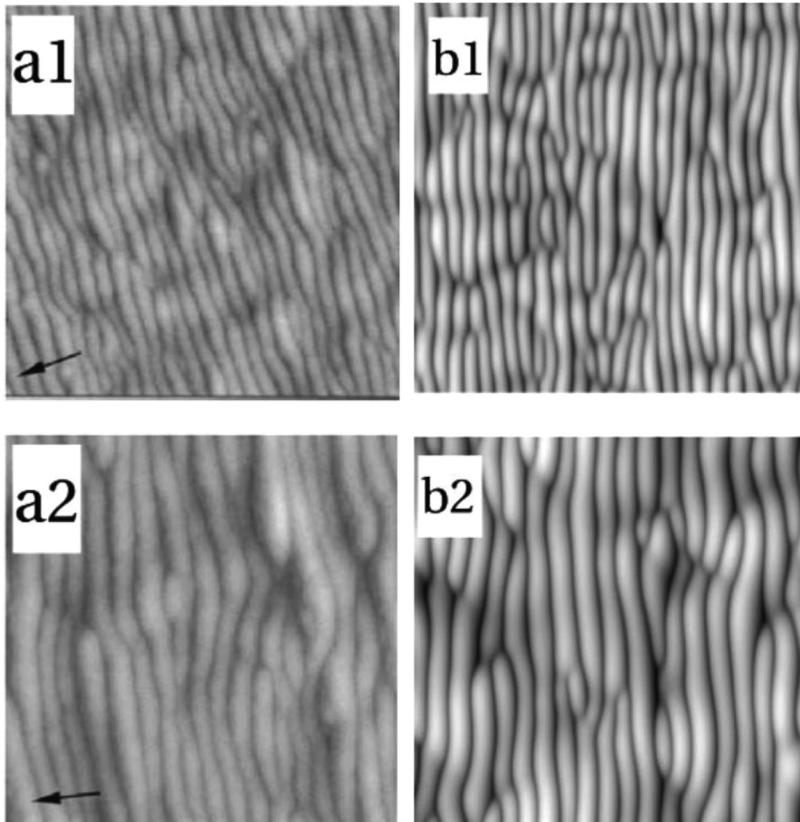


FIG. 15. $1 \times 1 \mu\text{m}^2$ AFM top-views of fused silica after 10 min. (a1) and 60 min. (a2) 800 eV Ar^+ irradiation for $\theta = 60^\circ$ (final ripple amplitude of 15 nm). The black arrow indicates the projection of the ion beam.⁸⁶ (b) Surface morphologies from numerical simulations of Eq. (4) under oblique incidence conditions,¹⁸⁶ for a simulation time in (b1) six times shorter than in (b2). Taken from Ref. 187.

mechanism for the local erosion velocity as induced by energy deposition from collision cascades, which predicts pattern formation for any value of θ including normal incidence ($\theta = 0^\circ$). Although in need of an improved implementation, the so-called CV effect has played an important role in the theoretical understanding of IBS. Analogous kinetic and geometric arguments similarly allowed Carter¹⁹³ to propose a condition for the formation of terraces with a θ -related inclination, which has been particularly fruitful for medium-energy IBS, where ripple amplitudes are larger.^{43,46}

An additional key piece of the puzzle was provided by the $\ell(E_{\text{ion}})$ behavior. Working on experiments on silica, Umbach and collaborators²³ convincingly argued that surface-confined viscous flow (implemented into a continuum model via the classic description by Orchard⁶⁶) induced by irradiation was a natural mechanism that predicted an increasing $\ell(E_{\text{ion}})$ function, as observed. In parallel, surface-confined viscous flow (even if advocated on the basis of thermal spikes, not obvious under low-energy conditions) had also allowed to account for in-plane ripple transport in the experimentally observed direction, for Ga^+ -irradiated targets.⁷⁹

In order to integrate the competition of additional effects of irradiation, beyond sputtering proper, and complex parameter dependencies like those evidenced by the CV effect, a key role has been played by more microscopic, computational approaches. Indeed, along the second half of the 1990s and the 2000s, increasingly detailed information became available from numerical

simulations of discrete/atomistic models of IBS nanopatterning. Some attempts were based on various kinetic Monte Carlo approaches,^{183,194–196} while others explored the dynamics of the surface via a molecular dynamics characterization of the amorphization process which occurs in the near-surface region of the target.^{197–199} Thus, momentum-transfer, CV-like behavior could be demonstrated in simulations of bombarded carbon substrates,¹⁹⁸ while a notion was derived that actual material transport influencing the evolution of the local target surface (e.g., via the formation of craters) could be obtained from the statistics over different MD runs, a so-called crater function approach.^{26,200,201}

In the crater function approach, the moments of a distribution (the so-called crater function) are reconstructed,^{26,200,201} to account for the average change in the surface shape due to single-ion impacts. Such a procedure allows separating the contributions to the interface dynamics due to different physical processes, mostly erosion (sputtering) and local redistribution of target atoms (crater formation). For example, in clean Si targets,^{27,32,200} mass redistribution is thus seen to dominate over sputtering, as discussed above in relation with Fig. 3. While the moments of the crater function describe the topography at small scales, they can be incorporated into continuum models, which are better adapted to large-scale and long-time predictions on the surface dynamics.^{27,47} Thus, parameter values for the various terms in the height equation can be extracted from the microscopic simulations, although in

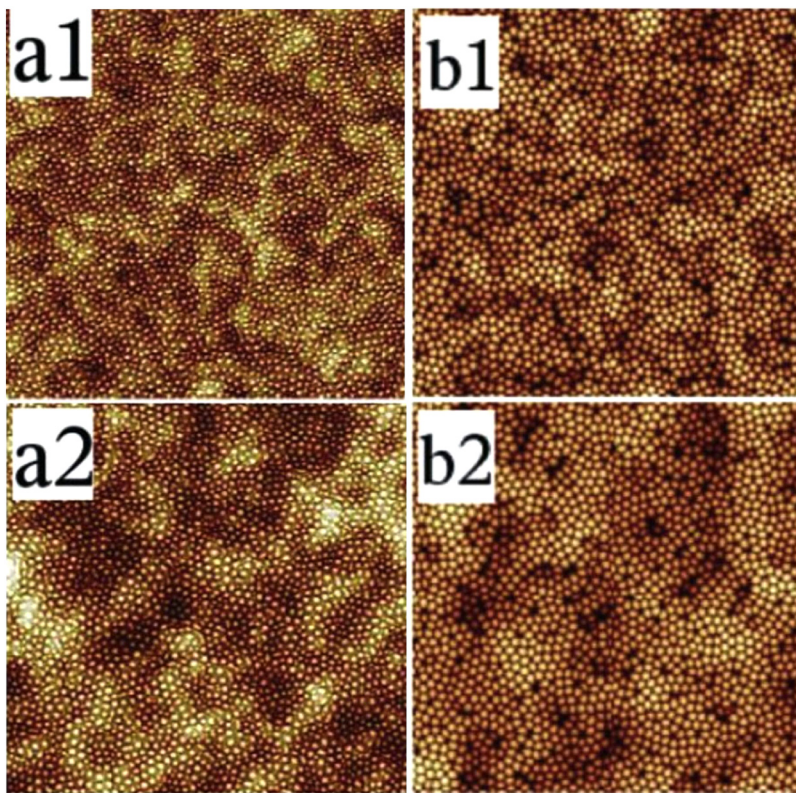


FIG. 16. $3 \times 3 \mu\text{m}^2$ AFM top-views of Si targets irradiated as in Ref. 192 for $\theta = 0^\circ$, after 60 min. (a1) and 960 min. (a2). (b) Surface morphologies from numerical simulations of Eq. (4) under normal incidence conditions,²⁵ for a simulation time in (b1) 16 times shorter than in (b2). Taken from Ref. 187.

these analyses the coefficient B quantifying surface-confined viscous flow [recall Eq. (2)] crucially remains a fitting parameter. Indeed, fully microscopic simulation of viscous flow for the present context remains a computational challenge as of today. Notwithstanding, hybrid MD-kMC simulations^{32,149} also conclude that mass redistribution is the main mechanism for pattern formation on clean Si targets. Thus, crater function approaches have allowed to account for several experimental properties of IBS on Si, like a non-zero θ_c value, the behavior of the ripple wavelength with incidence angle,²⁷ or the rotation of the ripple pattern for glancing incidence angles.²⁰²

Early implementations of the crater function approach^{27,201} assumed a flat surface morphology, which led to inconsistencies^{63,71,203} that have required later refinements of the approach, in which the curvature dependence of crater functions is taken into account.^{63,203,204} These improvements do lead to more consistent predictions, albeit with the conclusion^{71,205} that accurate estimates via crater functions of the parameters entering height equations are computationally expensive. Nevertheless, improved simulations are becoming available,^{29,206,207} while the combination of the crater function approach with additional contributions to the local height velocity also improves the explanatory power which can be reached.⁷⁷

Generally speaking, the mass rearrangement involved in crater formation occurs at distances which are of the order of the ion penetration depth, a few nm for ion energies close to 1 keV,¹⁷⁹

while all associated characteristic lengths remain in that range. Hence, based on such a process alone it is not possible to predict a ripple wavelength which is at least ten times larger. Basically, this fact had motivated BH to consider thermally activated surface diffusion as a competing mechanism, as a result of which realistic ripple wavelengths could seminally be predicted.⁸ Currently, and based on the discussion in this section, consensus has developed that surface-confined viscous flow is a more accurate choice, provided temperature is not close to recrystallization conditions.¹⁰⁸ Notwithstanding and as indicated above, to date the treatment of relaxation by viscous flow remains phenomenological in virtually all crater function approaches, contrasting with the microscopic description of crater formation, see Ref. 47 for an overview. Analogous considerations can be made on detailed Monte Carlo simulations performed with the SDTrim-SP package.^{31,208,209} In this case, the detailed predictions from the atomistic simulations have been phenomenologically rationalized via a continuum model which extends CV's approach^{62,210} by incorporating additional effects like the dependence of the thickness of the amorphized layer with incidence angle, etc. See Ref. 48 for a recent overview.

A program to systematically investigate the role of surface-confined viscous flow via a (mesoscopic) continuum framework was initiated 10 years ago.⁶⁴ The goal is to fully explore the morphological consequences of the assumption that the main mechanism controlling pattern formation is the relaxation, via Newtonian viscous flow,^{24,58} of the residual stress built up by irradiation

throughout the amorphized layer, which had been already assessed earlier.^{211,212} While more complex (e.g., viscoelastic) constitutive laws for relaxation have been seen not to substantially improve predictive power,²¹³ a number of significant refinements have still been incorporated, like an improved description of surface vs body forces,^{24,65} or the corrugation of the amorphous/crystalline interface.⁵⁹ Moreover, the model has been enhanced by incorporating results on ion-induced stress distributions as calculated from MD simulations, leading to a satisfactory comparison with experimental observations on the ion/target species dependence of the critical angle for ripple formation and (finally) a roughly linearly

increasing behavior for $\ell(E_{\text{ion}})$,⁵⁹ as well as predictions on the non-trivial behavior of in-plane ripple motion⁸⁴ and the independence of the morphological behavior with respect to the initial degree of structural order in the topmost surface layer.⁷² Naturally, quantitative agreement with experiments improves when the main mechanisms at play (say, sputtering, mass rearrangement, and viscous flow) are all put together,⁷⁷ but viscous flow does seem to be responsible for the main linear and nonlinear⁷³ features of the nanostructuring process sufficiently close to pattern onset and/or under conditions of negligible sputtering yield.^{206,207} For instance, Fig. 17 shows morphologies obtained from numerical simulations

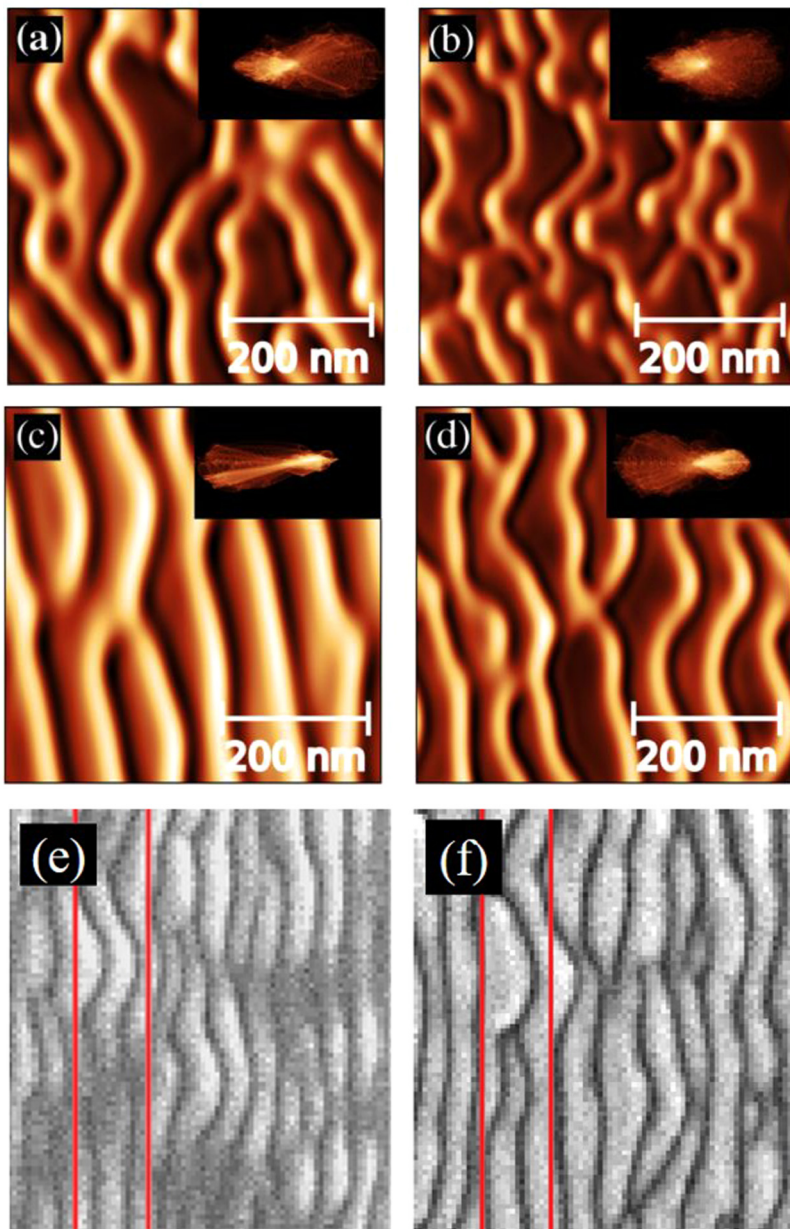


FIG. 17. (a)–(d) Surface morphologies obtained from numerical simulations of the strongly nonlinear equation, Eq. (5), at $t = 425$ min. The insets display the corresponding slope distributions. Different ion-induced stress distributions and incidence angles are considered in each panel: Stress becomes less compressive along the ion-beam direction for (a) $\theta = 50^\circ$ and (b) $\theta = 60^\circ$, while stress becomes increasingly compressive along the ion-beam direction for (c) $\theta = 60^\circ$ and (d) $\theta = 70^\circ$. Parameter values employed are order-of-magnitude estimates for 1 keV Ar⁺ IBS of Si. Reproduced with permission from Muoz-Garcia *et al.*, Phys. Rev. B **100**, 205421 (2019).⁷³ Copyright 2019 American Physical Society. (e)–(f) Top-view SEM images of a glass surface during 30 keV Ga⁺ oblique bombardment at $\theta = 45^\circ$, for fluence values of 21×10^{20} ions m⁻² (e) and 73×10^{20} ions m⁻² (f). The beam enters from the left; the vertical lines are reference lines 0.6 μm away from each other. Reproduced with permission from P. F. Alkemade, Phys. Rev. Lett. **96**, 107602 (2006).⁷⁹ Copyright 2006 American Physical Society.

of the following strongly nonlinear equation, derived in Ref. 73 for the thickness h of the irradiated layer:

$$h_t = -a_1 h h_x - a_2 h^2 h_x + \nabla \cdot (h^2 \mathbf{B} \cdot \nabla h) + c \nabla \cdot (h^3 \nabla h) - \gamma \nabla \cdot (h^3 \nabla \nabla^2 h). \quad (5)$$

In Eq. (5), the parameters $a_{1,2}$, c , and γ , and the tensor \mathbf{B} depend on experimental conditions like the ion incidence angle, θ and the space distribution of residual stress induced by IBS. Figures 17(a)–17(d) show results of numerical simulation of Eq. (5) for the same fixed fluence and different distributions of ion-induced stress and angles of incidence. The detailed properties of the surface ripple pattern are thus seen to depend on those. As further discussed in Ref. 73, a number of general properties (like the behavior of the ripple wavelength and transport velocity, the dynamic behavior of the roughness, and other) of the nonlinear Eq. (5) compare well with many experimental observations on ripple formation dominated by material redistribution, agreeing with established parameter trends. Panels (e) and (f) in Fig. 17 allow for visual comparison of the model morphologies with SEM top-views from experiments on oblique-incidence Ga^+ bombardment of a glass surface,⁷⁹ the two panels corresponding to different stages of the experiment. In spite of the different ion/target combinations considered in the numerical simulations and in this particular experiment, qualitative and even semi-quantitative agreement occurs between the model and experimental dynamics. In this regard, as derived in Ref. 73, the continuum equation features a versatile parameter dependence, enabling modeling of systems which can differ significantly with respect to the value of the critical angle, from $\theta_c \approx 50^\circ - 60^\circ$ as noble-gas IBS of Si or Ge,⁵⁹ to cases with e.g. $\theta_c \approx 30^\circ$ like IBS of pyrochlore targets.^{73,80}

In addition to the above, recent refinements of Sigmund's classic model of sputtering, based on MD simulations²¹⁴ and on MC simulations and continuum models,²¹⁵ and insights on concomitant higher-order nonlinear effects,^{216,217} do seem to improve in turn the sputtering-based description of IBS experiments on amorphous targets.²¹⁸ Hence, the program to describe IBS surface nanopatterning via the interplay between sputtering and surface-confined viscous flow holds promise to provide a fully consistent description of the process.

4. Additional effects

The program just mentioned, albeit promising to this day remains to be fully completed. Moreover, one can readily think of additional physical effects which may also bear importance to the surface dynamics. As examples, we can mention material redeposition and ion implantation. Specifically, redeposition being an intrinsically nonlinear process,²¹⁹ it has been shown to improve ordering of the surface nanopatterns,^{220–222} within a sputtering-dominated dynamics. In turn, according to continuum and MC-based simulations,^{223,224} the morphological effect of ion (self) implantation seems to oppose that of material rearrangement or surface viscous flow, as it is destabilizing for small angles of incidence and becomes stabilizing for incidence angles larger than a non-universal critical value. Nevertheless, see e.g. Ref. 225 for a complementary discussion on the effects of implantation, as derived from MD simulations. The predictive power of theoretical

descriptions of IBS nanopatterning will no doubt improve once such type of contributions to the surface dynamics are suitably taken into account.

5. Relevant crystallinity

Further, we need to stress that the theoretical picture just described applies as such to materials, typically semiconductors,⁵⁰ which either are or become amorphous by ion bombardment in the range of ion energies which we are discussing. As discussed in Sec. II A, this is notably *not* the case for metallic substrates. Indeed, provided experimental conditions are not in the so-called erosive regime⁴ of very small ion fluxes and/or low temperatures, recrystallization is highly effective in metals, which implies dominance of anisotropic surface diffusion as the main relaxation mechanism. In such a so-called diffusive regime,⁴ which occurs at intermediate to high temperatures and intermediate ion fluxes, as seen in Sec. II A it is not the ion beam which controls the orientation of the ripple structure; rather, the pattern features are dictated by the anisotropies in surface diffusion,³ specifically by the well-known instabilities associated with the Ehrlich–Schwoebel barriers to adatom and advacancy diffusion.^{51–53}

Modeling of IBS of metallic targets has been largely addressed via MD simulations, as e.g. for grazing incidence 5 keV Ar^+ ion bombardment of Pt(111) surfaces,²²⁶ see some overviews in Refs. 4 and 43. From the point of view of continuum descriptions, better suited in principle to describe large-scale behavior, polycrystalline metals have been studied e.g. in the context of generalizations of BH theory.²²⁷ In the erosive regime for metals, some of the continuum models discussed above have also demonstrated predictive power. Such is the case, for instance, of the eKS equation, Eq. (4), quite successfully employed to describe quantitatively the nanobead formation process by SIBS of Au targets already discussed in Fig. 10, see Fig. 18.¹³⁷

Actually, taking into account crystallinity-induced anisotropies in surface tension and surface diffusion, like those relevant for epitaxial growth systems,⁵³ leads to generalizations of the eKS equation; for the case of normal-incidence IBS, the resulting equation reads²²⁸

$$h_t = -A \nabla^2 h + \lambda(\nabla h)^2 - \nabla \cdot [\mathcal{K} \nabla(\nabla^2 h)] - \nabla \cdot [\Lambda_2 \nabla(\nabla h)^2], \quad (6)$$

where \mathcal{K} and Λ_2 are constant 2×2 tensors implementing the mentioned crystalline anisotropies. Figure 18(d") shows the result of a numerical simulation of Eq. (6), which improves over the eKS model with respect to the local ordering of the nanobead pattern, as compared with the experimental results.²²⁸

Interestingly, the continuum description of IBS surface nanostructuring of metals may similarly benefit from recent advances in the description of semiconductors at high temperatures. Again as seen in Sec. II A, sufficiently close to their recrystallization temperature, semiconductor targets behave similarly to metals in the diffusive regime, with ES barriers to advacancy diffusion dominating the dynamics.¹⁰⁷ In contrast, IBS of metals does not reduce to a “negative homoepitaxial deposition” of vacancies.²²⁹ At any rate, the strong nonequilibrium nature of the process¹⁰⁸ and the concomitant universality properties enable

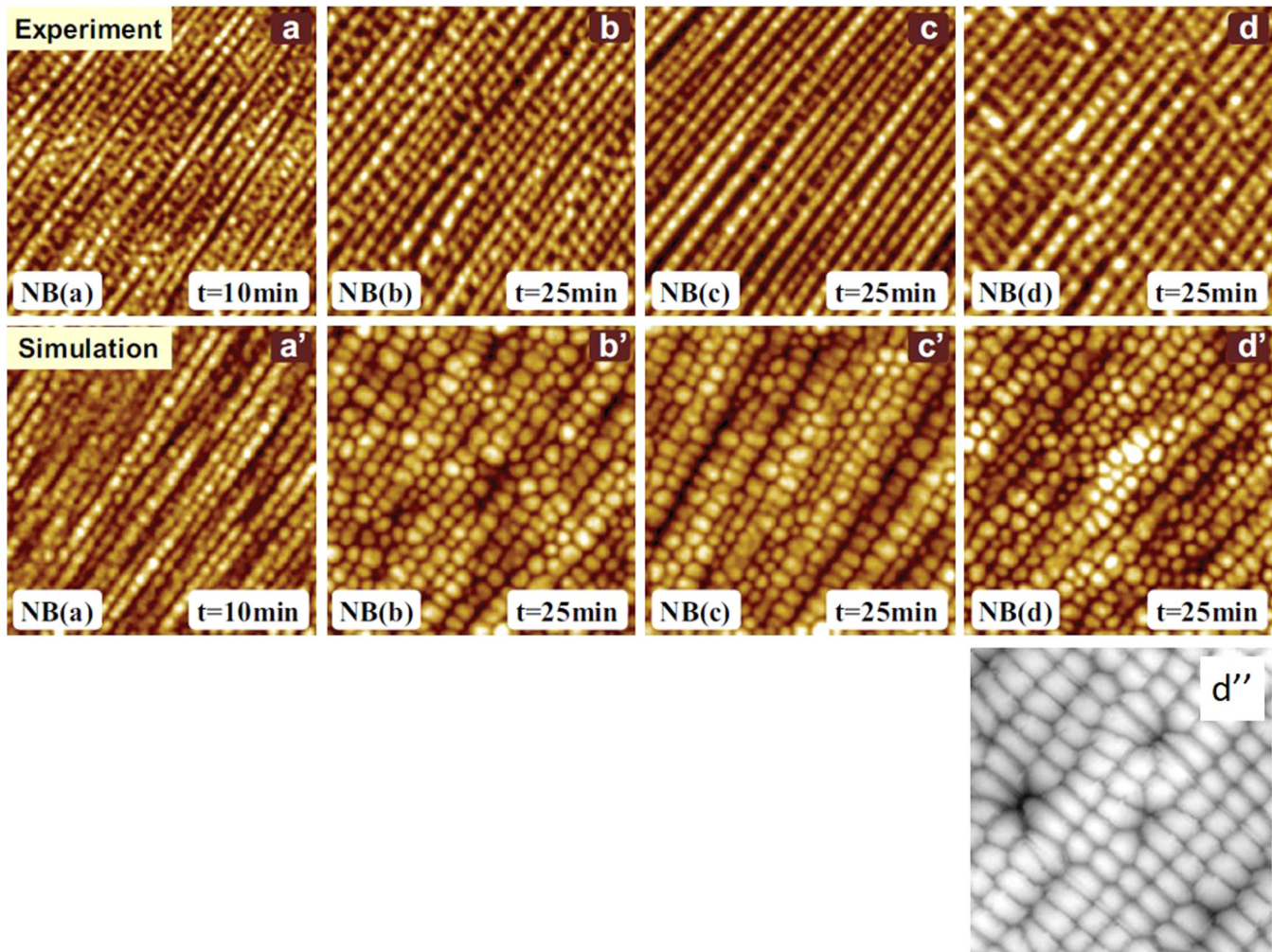


FIG. 18. Comparison of experimental nanobead patterns [(a)–(d)] formed by SIBS of Au targets in the erosive regime on different initial prepatterns [cf. Figs. 10(b)–10(b')], with morphologies predicted by the eKS equation, Eq. (4), using the corresponding experimental prepatterns as initial conditions [(a') to (d')]. Reproduced with permission from Kim *et al.*, Phys. Rev. B **87**, 085438 (2013).¹³⁷ Copyright 2013 American Physical Society. Panel (d'') shows the result of a numerical simulation of Eq. (6), for which the (square) symmetry of the local nanobead order is closer to the experimental one. Reproduced with permission from Renedo *et al.*, Phys. Rev. B **93**, 155424 (2016).²²⁸ Copyright 2016 American Physical Society.

kinetic modeling via continuum height equations,^{107,108} in close parallel to homoepitaxial growth, but with vacancies as the main transported species. As an example, numerical simulations of the continuum model^{107,108}

$$h_t = -A \nabla^2 h - B \nabla^4 h - \lambda_2 \nabla^2 (\nabla h)^2 + \epsilon \sum_{i=x,y} \partial_i (\partial_i h - \delta (\partial_i h)^3), \quad (7)$$

reproduce quite closely experimental results (cf. Fig. 5) on reverse epitaxy of Ge surfaces, see Fig. 19. Here, the nonlinear term with parameter ϵ accounts for the irreversible surface transport of advacancies, in strong analogy with adatom currents in epitaxial growth.⁵³

Let us finally remark that, as in the case of semiconductor targets, again a two-field approach can formulate in a natural way the coupling between surface transport and additional processes like sputtering and step-edge barriers, even under fully anisotropic conditions.²²⁸ Indeed, the standard assumption behind two-field models on a (negligibly) thin surface layer subject to material transport seems to be most suitably satisfied by metals in the diffusive regime, and/or for semiconductors at high temperatures in which amorphization is negligible.

6. Heterogeneous composition

Another instance in which the two-field approach has also been rather fruitful is that of IBS surface nanopatterning processes

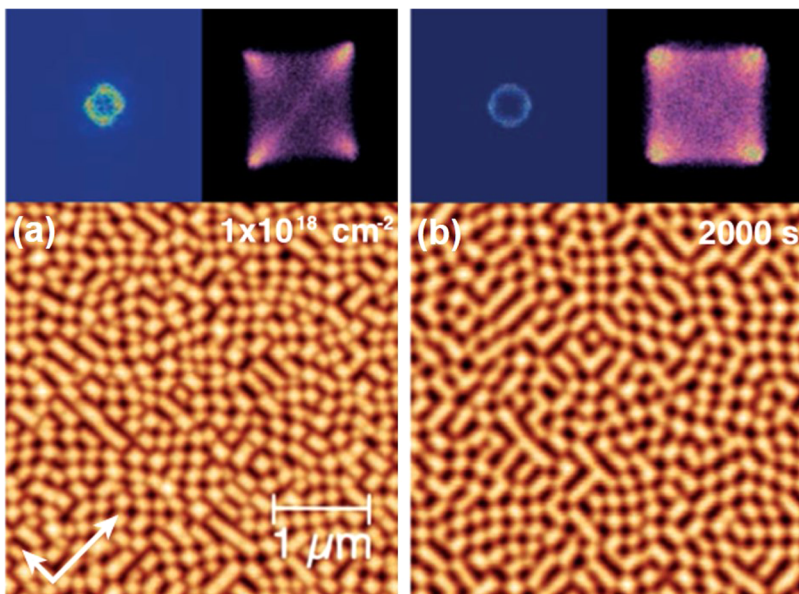


FIG. 19. (a) AFM image of Ge(100) surface irradiated at 350° under normal incidence. (b) Result of a numerical integration of Eq. (7). Above each morphology, the 2D FFT (left) and the two-dimensional angle distribution (right) are shown. Reproduced with permission from Ou et al., Phys. Rev. Lett. **111**, 016101 (2013).¹⁰⁷ Copyright 2013 American Physical Society.

in which a third atomic species plays a relevant role: either because the target is a binary material, or else because an additional atomic species is being concurrently deposited, inadvertently (e.g., deposition of impurities) or on purpose. A key step was taken in 2007,¹¹¹ when the dynamics of a scalar field describing the composition of the topmost surface layer of a binary target undergoing IBS was coupled, within linear approximation, to the time evolution of the surface height. The interplay between differential sputtering and diffusion rates for the two target atomic species was thus elucidated as an origin for the pattern forming behavior, and this was confirmed by nonlinear generalizations of the model.^{112,113,230} Although detailed quantitative comparisons are difficult, a notable theoretical result in this context is the possibility to thus account for the short-to-medium-order of the patterns produced in many experiments with binary materials,^{43,46} first demonstrated in Ref. 2. Figure 20 illustrates the capabilities of different two-field models from this point of view.

Panels (a) and (b) in the figure show simulations of a two-field model of binary targets undergoing IBS.^{112,113,233} Indeed, parameter conditions exist for which the model supports the formation of highly ordered dot patterns, akin to those shown in Fig. 1, or ordered hole patterns, visually very similar to those produced by a focused ion beam on Ge.²³⁴ On the other hand, panels (c) and (d) in Fig. 20 compare experiments of Au⁺ implantation of Ge targets, leading to the formation of virtually defect-free ripple patterns, with simulations of a two-field model tailored for such an experimental setting,²³² which again is seen to capture the long-range order of the experimental nanopatterns.

In the process to further improve the predictive power of the two-field theoretical approach, and trying to identify the key physical mechanism for pattern formation with strong space ordering, a number of physico-chemical processes have been considered, notably the competition between thermodynamic/

kinetic phase separation and differential sputtering for the two atomic species of the target,^{116,235} which has also been assessed via MD simulations within crater function approaches.^{117,236} Such a competition is at the basis of the discrepancy between the theoretical prediction,^{112,113,230} that composition segregation will lead the high-yield species to remain at the top of the nanostructures produced, and diverse experimental observations.^{114,115,235} Incidentally, crater-function approaches for binary materials like GaSb again conclude that, as in the case of clean Si, mass redistribution dominates over sputtering contributions to the local height velocity.²³⁶

The nontrivial effect of the existence of a third atomic species, beyond those of the ion and the target, is also demonstrated in experiments where metallic impurities become deposited concurrently with the IBS process. In this context, two-field models have also allowed to rationalize experimental observations, by coupling the evolution of the surface height to that of a scalar field which measures the composition of the top-most surface layer of the substrate, which is dynamically altered by the flux of impurities. A model in which BH-type sputtering competes with CV-like mass transport and impurity motion^{233,237} predicts deactivation of CV currents by the immobilization of the impurities, provided the impurity concentration is above a certain threshold, leading to pattern formation. The existence of such a threshold agrees qualitatively with many experimental observations, see Sec. II A. Beyond this, compound formation (e.g. silicide formation in the case of Si targets being seeded with metallic impurities) has been shown to be generally required for pattern formation.²³⁸ Admittedly, exceptions exist (e.g., nanoripple formation in Si irradiation under codeposition of Au, non-silicide forming impurities²³⁹), but they can still be accounted for by suitably adapting Sigmund's model of sputtering to the case of two different atomic species in the target.¹³⁴

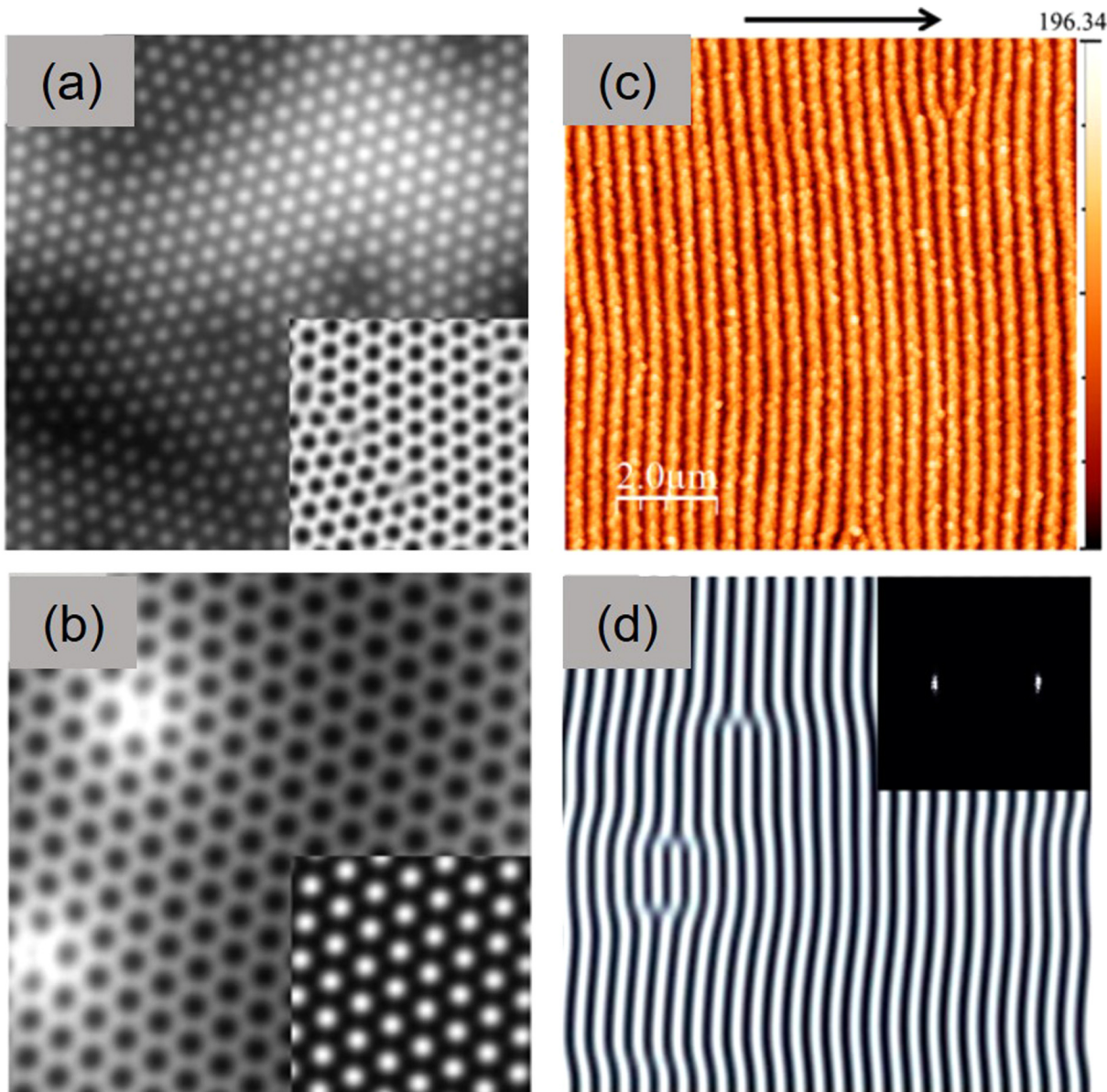


FIG. 20. Improved description of short-range order by two-field models of IBS systems with heterogeneous composition: Large fluence nanodot (a) and nanohole (b) patterns obtained from numerical simulations a two-field model of IBS of binary targets. In each case the inset shows the map of the composition field, in registry with the topographical pattern shown on the main panel. Reproduced with permission from Bradley *et al.*, Appl. Surf. Sci. **258**, 4161 (2012).²³¹ Copyright 2012 Elsevier. (c) AFM image of a defect-free Ge (100) surface bombarded with 26 keV Au⁺ ions. The vertical scale is in nm. (d) Topography from the numerical simulation proposed to describe the experimental process of (c). The inset shows the 2D FFT. Both panels are reproduced with permission from Mollick *et al.*, Appl. Phys. Lett. **104**, 043103 (2014).²³² Copyright 2014 AIP Publishing LLC.

III. SOME OPEN ISSUES

This section is devoted to a discussion, not meant as fully comprehensive, of some of the issues which to date remain open in the context of IBS surface nanostructuring, and which is again organized into two main parts: one involved with experiments and applications and a final one devoted to theory and computational approaches.

A. Experiments and applications

The surface patterning induced by IBS results from the self-assembly of the adspecies subject to transport, and most frequently suffers from a common problem for self-assembled systems,²⁴¹ namely, the limited quality and the range of spatial order in the structure. A number of proposals have been made to remedy this

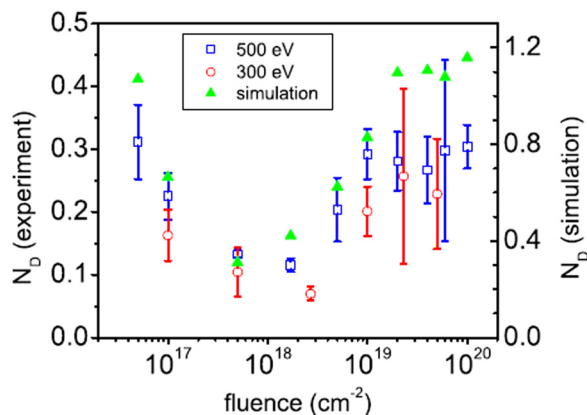


FIG. 21. Normalized defect density for experimental (open symbols, left vertical scale) and simulated (full triangles, right vertical scale) ripple morphologies vs fluence. The error bars represent statistical averages over several samples. Reproduced with permission from Keller *et al.*, New J. Phys. **10**, 063004 (2008).²⁴⁰ Copyright 2008 Institute of Physics.

limitation. For low-energy IBS ripple patterns on Si, Keller *et al.*²⁴⁰ find experimentally the existence of a fluence value for which a minimal defect density is obtained, see Fig. 21. Qualitatively, a similar result is obtained from numerical simulations of a damped generalization of the KS equation,²⁴² suggesting that the existence of a fluence with minimal defect density can be a generic property of IBS nanopatterns.²⁴⁰ Further studies are necessary to establish the generality of this property and to correlate the optimal fluence value with other experimental parameters, so that IBS experiments can be performed minimizing defect density.

Recently, reverse epitaxy can produce ripple patterns with surprisingly high order on compound semiconductors, proving this method as a promising avenue for IBS. However, for elemental semiconductors such as Ge,¹⁰⁷ analogous highly ordered ripple patterns have been never reported. Instead, the compound semiconductors patterned by reverse epitaxy have been used as templates for the growth of highly ordered thin films via transfer of their pattern topographies to the films.⁴⁰ Considering the importance of elemental semiconductors in microelectronics, sensors, and solar cells, further efforts would be quite desirable to further exploit reverse epitaxy to directly pattern elemental semiconductor surfaces with uniaxial surface anisotropy.

Another recent proposal to produce defect-free ripple patterns is due to Harrison and Bradley,²⁴³ who suggest to suitably rock (i.e., change the incidence angle θ periodically in time) the substrate during IBS, based on numerical simulations of the anisotropic KS equation, Eq. (3). Given the fact that the parameters in the equation depend on θ , they find that a defect-free ripple pattern eventually ensues provided that the rocking range is such that the coefficients of the nonlinear terms, λ, λ' , go through zero along the rocking cycle, and provided that the rocking frequency is comparable to the growth rate of the most unstable mode in the linear regime. Indeed, a notable improvement of the order has been observed experimentally in ripple patterns obtained by 0.5 keV Kr⁺

IBS of Si(100) at room temperature,²³⁹ see Fig. 22. Such an improvement in the order in the ripple pattern is further observed for Si(100) and amorphous carbon (a-C) sputtered by 2 keV Kr⁺ ions, even under rocking conditions that do not necessarily imply that λ, λ' go through zero during the rocking cycle.^{41,239} These experimental observations can be elucidated by generalizing the KS equation, Eq. (3), into the eKS equation, Eq. (4), due to the occurrence of the additional nonlinear terms in the latter,²³⁹ which possibly become more important for increased ion energies reflecting enhanced surface viscous flow. These observations suggest moreover that suitable rocking of the substrate may be widely applicable to enhance (if not fully perfect) the order of ripple patterns.

The aforementioned three approaches for the improvement of the order in the IBS pattern can operate without negatively interfering with one another. Thus, an optimal experimental setup for the best ordered pattern could consist in the simultaneous application of the three proposed improvements: A compound semiconductor at a temperature above its recrystallization temperature would be subject to IBS (possibly concurrent with codeposition of selected impurities) while rocking the target, and carrying the experiment up to its optimal fluence value. Still, prior to seeking the synergy among the three approaches, one needs to first find the optimal conditions for each one of them separately. For instance, Ziberi *et al.*³⁹ produced almost perfectly ordered patterns as shown in Fig. 6(a), as well as salient patterns via surfactant sputtering. However, those IBS patterns were made under inadvertent impurity deposition. Thus, no information about the impurity atoms, impurity fluxes, and their deposition directions is known, and reproduction of the pattern is hampered. Considering the high quality of the ordered patterns that have been reported, further systematic studies on surfactant sputtering are awaited in which impurity codeposition is performed in a controlled manner, and promise to be highly rewarding. In such type of studies, which can also be performed in the medium energy range,²⁴⁴ thus accessing novel motifs and typical scales, simultaneous codeposition of more than one atomic species could be attempted trying to otherwise mimic the experimental conditions leading to the remarkable surface nanostructures achieved in Ref. 39.

Beyond its capability to improve the order in the induced ripple patterns, surfactant sputtering also produces chemical modifications of the surface. The impurity atoms or their derivatives arrange themselves below the surface with the same wavelength as that of the ripple pattern, being usually confined near the protruding parts of the pattern, e.g. near the ridge of the ripples as shown in Figs. 7(c) and 7(d). Such chemical modifications should periodically modulate additional physical behaviors also, such as electronic, magnetic, and optical properties. This periodically modified surface could thus serve as a lateral superlattice, a modulated doped surface, or an optical grating. Moreover, the embedded impurities are in the form of nanoclusters whose mean sizes are around or below 10 nm, and should show strong quantum confinement effects. The synergy between the periodic modulation and quantum confinement could provide the electrically, optically, and chemically modulated surface with novel properties and functionalities. This capability to periodically modulate surface properties in the 10 nm range can prove as a unique and quite useful output of

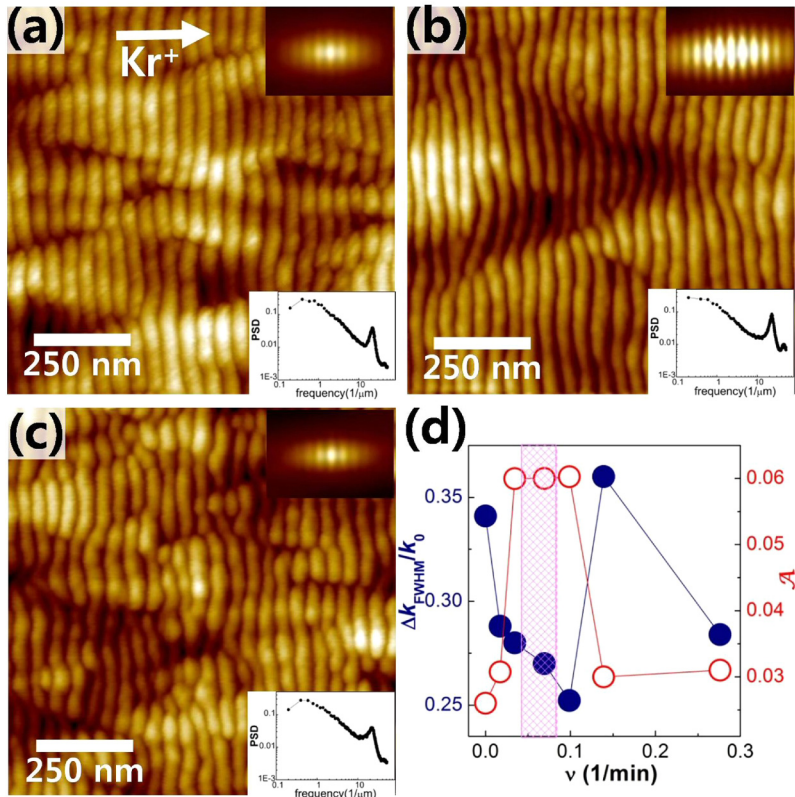


FIG. 22. Ripple patterns on Si substrates rocked for incidence angles in the $65^\circ < \theta < 73^\circ$ interval. The rocking frequency employed in each case is (a) $v = 1.73 \times 10^{-2} \text{ min}^{-1}$, (b) $v = 9.87 \times 10^{-2} \text{ min}^{-1}$, and (c) $v = 1.39 \times 10^{-2} \text{ min}^{-1}$, while $E_{\text{ion}} = 2 \text{ keV}$ and the fluence is $2182 \text{ ions nm}^{-2}$. Insets: height-height correlation map (top right) obtained after normalizing the height by the surface roughness. 1D power spectral density (PSD) (bottom right) obtained from the corresponding $5 \times 5 \mu\text{m}^2$ AFM image. (d) v -dependence of the amplitude (empty symbols, right vertical scale) and full width at half maximum of the peak in the PSD curve (filled symbols, left vertical scale). Reproduced with permission from Kim *et al.*, J. Phys.: Condens. Matter **30**, 274004 (2018).⁴¹ Copyright 2018 Institute of Physics.

surfactant sputtering that is not easily achievable by other means. Such an aspect of the surfactant sputtering approach has not been much explored yet, partly due to the lack of easily accessible nanoprobe with capabilities for chemical analysis. TEM with electronic energy loss spectroscopy provides the spatial resolution required for such type of chemical analysis, but it is a destructive tool and not easy to use. Nowadays, scanning Auger electron microscopy and state-of-the-art scanning photoelectron microscope using synchrotron radiation provide the requested spatial resolution, smaller than 5 nm, so that we expect chemically modulated nanopatterns to soon become better understood, and more widely applied.

Surface nanopatterning by IBS has been employed to study radiation damage and repair of 2D materials²⁴⁵ and also for the modification of their properties via ion trapping.^{246,247} Further, IBS has also been employed to functionalize 2D materials, especially via strain engineering, since these materials can stand large lateral strain. In general, strain engineering has been proposed to locally alter their band structures,^{248,249} and thus their electronic, optoelectronic, and magnetic properties.²⁵⁰ However, most previous strain engineering of 2D materials had been performed either by lithographic patterning²⁵¹ or by uniaxially straining exfoliated flakes on elastomeric substrates.²⁵² These approaches are good test beds, but not for practical applications due to their limited surface coverage. In contrast, e.g. Martella *et al.*^{249,253} have grown a MoS₂ layer on SiO₂ films which had been previously ripple-patterned by IBS. The MoS₂ overlayer grown by chemical vapor deposition conforms to

the substrate pattern, thus featuring a strain which changes along the direction of the ripple periodicity, with the same period as that of the ripple pattern, while strain remains negligible along the ripple ridges, thus inducing anisotropies in the physical properties of the MoS₂ layer. Perpendicular to the ripple ridges, the strain varies from compressive to tensile, making valleys electron-doped while ripple crests are hole-doped. This modulated doping influences physical properties, e.g., by inducing an alternating shift of the optical phonon frequencies along the direction of the ripple periodicity. Observations like these demonstrate the potential of IBS to functionalize 2D materials for practical applications, via substrate nanopatterning, and further developments can be expected.

Further, from the extensive practice of surfactant sputtering, we are aware of the significant role of the metallic impurities on the pattern formation. However, impurities among the projectile ions may also make notable differences in surface pattern formation by IBS.²⁵⁴ Figure 23(a) shows a Si(100) surface sputtered by 8 keV Ar⁺, when impurity ions carried by the beam are filtered out by a dipole magnet mass analyzer. No structure is observed on the surface. In contrast, a similarly sputtered surface, produced without ion-impurity filtering, shows the well-defined ripple pattern seen in Fig. 23(b). In the experiments of Ref. 254, significant amounts of silicon carbide and nitride are found to form on the surface, as revealed by x-ray photoelectron spectrum (XPS) [see Fig. 23(c)], induced by the impurity ions as shown in the mass spectrum provided in Fig. 23(d). Silicon nitride and carbide both have a lower

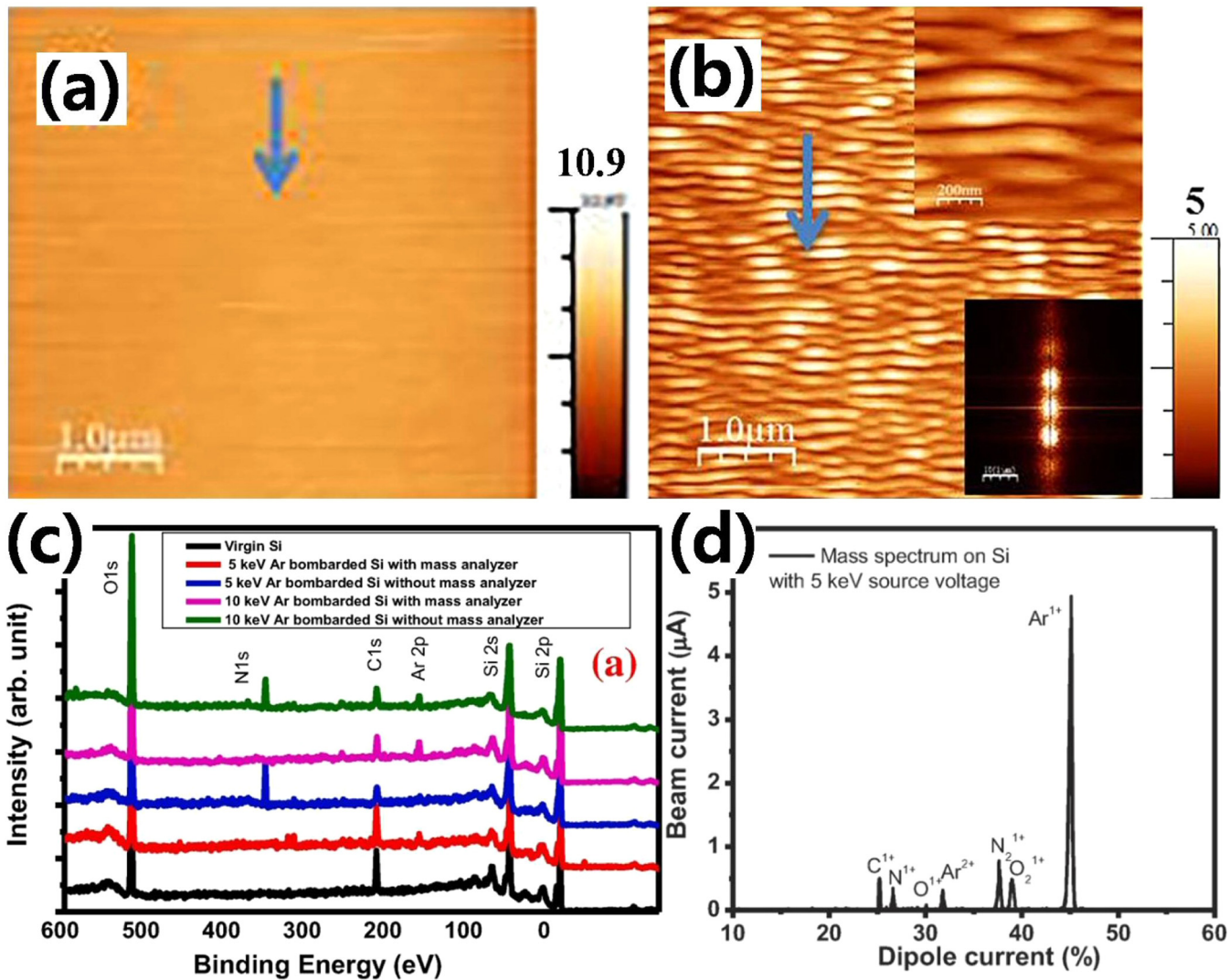


FIG. 23. $5 \times 5 \mu\text{m}^2$ AFM images of mass-analyzed (a) and contaminated (without mass analysis) (b) Si surfaces bombarded with 8 keV Ar⁺ at an oblique angle, $\theta = 60^\circ$, and constant fluence $7 \times 10^{17} \text{ ions cm}^{-2}$. The arrow indicates the ion beam direction, and the Δz scale is shown next to each image. In (b) a $1 \times 1 \mu\text{m}^2$ scan is also shown in the upper corner while the FFT of the main panel appears in the lower right corner, both supporting parallel ripple formation. (c) XPS survey of virgin Si and ion-bombarded Si surfaces with a mass-analyzed beam and without mass analysis. (d) Mass spectrum on Si(100) sample by 5 keV source voltage extracted from an ECR ion source. Reproduced with permission from Bhowmik *et al.*, Nucl. Instrum. Meth. B **444**, 54 (2019).²⁵⁴ Copyright 2019 Elsevier.

sputtering yield than Si itself, causing a surface instability as theoretically described.²³⁸

The previous gas-impurity studies have arguably been performed with a trace amount of the residual impurities. In the other limit, one has reactive ion sputtering, in which ions and molecules of O, C, and N have already proved effective in destabilizing e.g. both, Si and carbon film surfaces.^{255,256} Remaining open questions are whether there is any threshold amount impurity density to ignite the pattern formation, how the impurity density determines the size and shape of the motifs of the patterns, whether there are

any synergistic effects among the various ion species and whether the order of the pattern can be improved by the ion impurities. To answer these questions, the investigation with well controlled experimental conditions need to be performed.

Most of the studies reported on surface patterns formed by IBS deal with periodic structures composed of relatively simple motifs like ripples or dots. However, IBS also produces non-periodic morphologies like, e.g., labyrinthine patterns on polymer surfaces,²⁵⁷ 2D foams on semiconductor surfaces,²⁵⁸ or cauliflower-like structures on HOPG(0001),²⁵⁹ see Fig. 24. For example, Castro

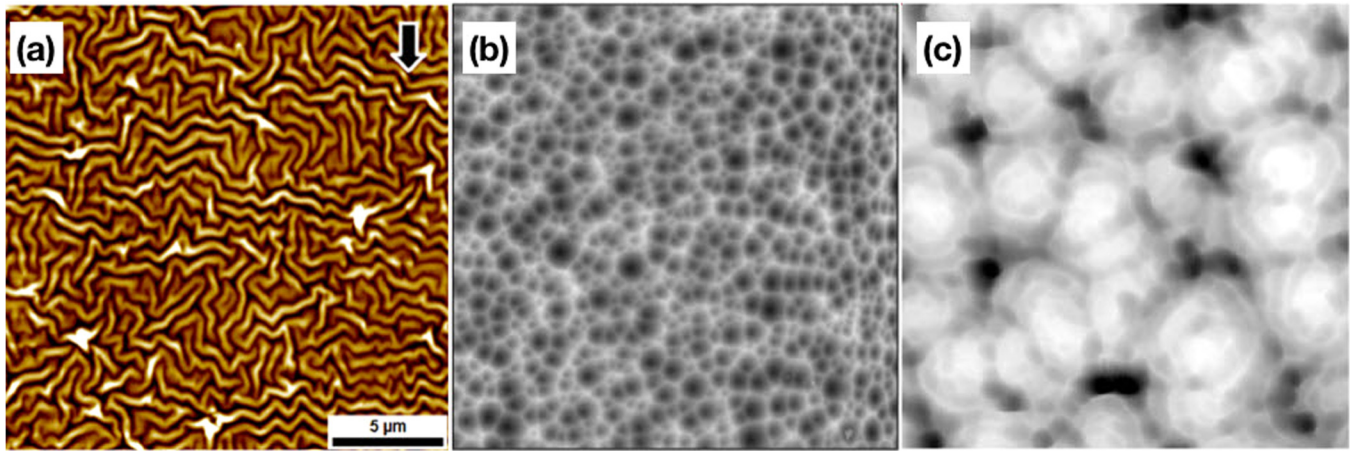


FIG. 24. (a) Labyrinthine surface pattern produced by IBS on PDMS. Reproduced with permission from Yoon *et al.*, J. Appl. Phys. **116**, 024307 (2014).²⁵⁷ Copyright 2014 AIP Publishing LLC. (b) Cellular pattern produced on Si by an Ar^+ ion plasma, reproduced with permission from Castro *et al.*, Phys. Rev. Lett. **112**, 050103 (2014).²⁵⁸ Copyright 2014 American Physical Society. (c) Cauliflower-like morphology that is the inverted image of a pattern induced by IBS on a rotating HOPG target, taken from Ref. 259.

*et al.*²⁵⁸ studied a cellular structure formed on Si(001) by an Ar^+ ion plasma. Remarkably, the analysis of the topological properties of the disordered surface structure produced, like e.g. the distribution of the number of the sides defining each cell,^{260,261} and of their time evolution sheds light on the mechanisms driving, e.g., the coarsening kinetics observed. This topological analysis offers an alternative way to derive the coarsening exponent predicted by the height equation governing the foam evolution, which happens to be the so-called convective Cahn–Hilliard (CCH) equation,^{258,262} a further nonlinear generalization of Eq. (4). In contrast, e.g., the negative cauliflower pattern in Ref. 259 has poorly defined edges, hampering in practice a similar topological analysis. The labyrinthine pattern on PDMS²⁵⁷ has not been analyzed in such a level of detail, either. Actually, many non-periodic patterns produced by IBS have defied conventional analysis using e.g. well-known continuum models like Eqs. (2), (3) or (4), and familiar measures of space ordering properties, which calls for the development of better adapted, novel tools of analysis. For instance, recently, Motta *et al.*²⁶³ have developed innovative topological measures of imperfect hexagonal order. Some of these measures are very sensitive to the existence of defects, which will probably help to find the correlation between these and the appropriate terms in, e.g., a suitable continuum equation describing the corresponding pattern. Since the parameters quantifying the strength of such terms are related to the experimental conditions, suitable measurements which are sensitive to specific defects should help finding the optimal experimental conditions that minimize defect production, thus perfecting the patterns produced.

Generally speaking, the investigation of IBS surface nanopatterns has been undertaken using two different types of probes. The first type corresponds to local probes, such as scanning force microscopies. The second type of probes corresponds to x-ray scattering techniques like GISAXS, which has the advantage over local

probes that it can sample wide areas in real time. However, the coherence of the x-ray beam generated by a synchrotron has not been much exploited, yet. If the surface height is subject to random fluctuations in space and time, then the incident coherent light gains different phase shifts at different positions during IBS, and the scattered light shows a speckle pattern as observed in the scattered laser light. Speckle patterns have been also observed for x-rays by Sutton *et al.*²⁶⁴ In this context, we can mention the work by Bikondoa *et al.*,²⁶⁵ who have measured speckle patterns at different times during IBS. The time-time correlation function (TTCF) has been thus obtained from the experimental patterns. Its analysis provides information on the surface dynamics during IBS at the nano scale that is not available to the phase-averaged x-ray scattering analysis, which only yields averaged kinetic information. The dynamical information is used to discriminate the models elucidating the observed pattern evolution by IBS. This technique, so called x-ray photon correlation spectroscopy (XPCS), has also allowed to recently assess in-plane ripple motion on the irradiated surface during IBS.²¹⁸

Although the potential of XPCS has been long known, it has been applied to very limited cases, partly because the coherence and brightness of the x-rays is not enough to produce a sufficiently well-defined speckle pattern to produce a clear-cut TTCF. In this regard, it is notable that x-ray free electron lasers (XFELs) and the 4th-generation synchrotron employing the novel diffraction-limited storage ring have both become more and more widely available since 2009 and 2016, respectively, greatly enhancing the coherence and brightness of x-ray beams. XPCS can now be performed under better beam conditions and can become accessible to a wider spectrum of users, making it a promising method to study the dynamics of nanopattern formation at surfaces.

Finally, nanopatterned surfaces can still find more bio-inspired applications. For example, cell adhesion is an initial step for cell

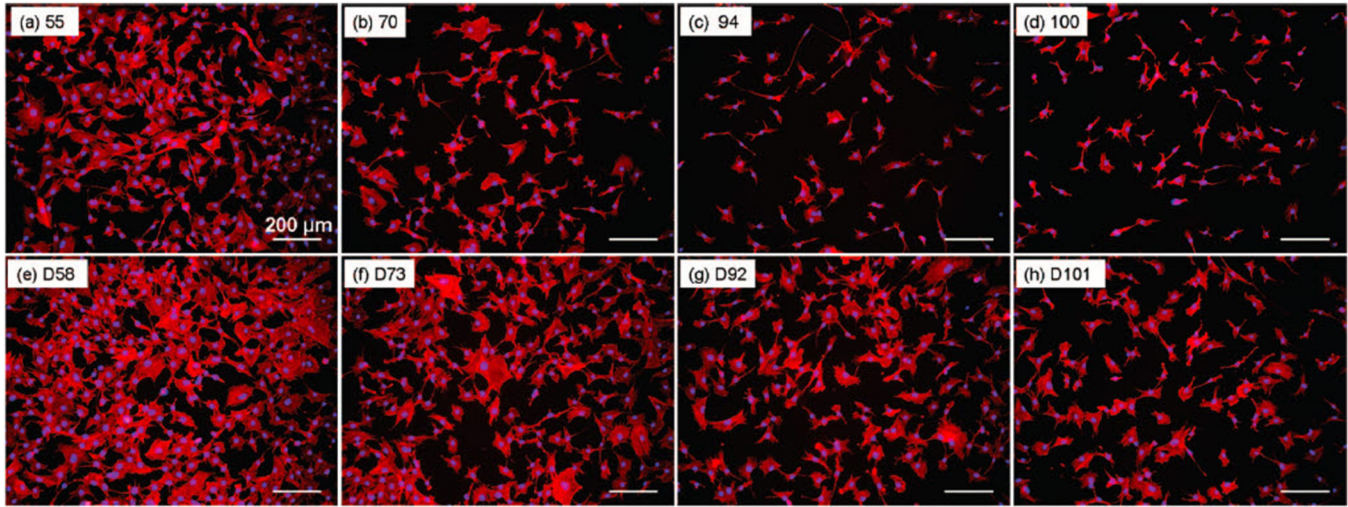


FIG. 25. (a)–(h) Fluorescent micrographs of MC3T3-E1 osteoblast cells labeled for actin (red) and nuclei (blue) after 24 h in culture on ordered (a)–(d) and disordered (e)–(h) IBS nanopatterns. Specific nanopatterns are labeled at the top left of each image, with the numbers representing the average interligand distances. Reproduced with permission from Huang et al., *Nano Lett.* **9**, 1111 (2009).²⁶⁶ Copyright 2009 American Chemical Society.

proliferation and differentiation, both of which are important biological processes.^{267–269} Cell adhesion on surfaces with nanodot patterns has revealed to be sensitively dependent on the spacing among the nanostructures. If the spacing is larger than a critical value in the order of tens of nm, cell adhesion is prohibited.^{266,270} Remarkably, adhesion can depend even on the quality of the space order of the pattern.²⁶⁶ Figure 25 shows fluorescent micrographs of MC3T3-E1 osteoblasts. The images in the upper (lower) row are of cells grown on top of ordered (disordered) Au nanodot patterns coupled with c(RGDfK)-thiol ligands. For each image, the number on the upper left corner is the mean spacing of the dots. Note that the cells do not adhere well on the ordered patterns, as compared with the disordered patterns. Also, observe that, as the mean inter-dot distance increases, the density of adhered cells decreases. In general, biological assays request a very high number of patterned substrates in order to reach statistically significant conclusions. Large patterned areas should readily satisfy such a need. Nanopatterning areas as large as 1 cm² is not feasible by conventional lithography, while IBS is easily scalable, and can readily produce large-area nanopatterns in a single step. IBS can easily adjust the size and spacing of the nanostructures by varying the physical parameters defining IBS, having thus a large potential for many more applications in biomedical studies.

B. Theory and computation

As discussed in Sec. II B above, the quantitative theoretical description of IBS surface nanostructuring is still under progress, even in the simplest context of clean monoatomic targets. This is partly due to the improvement of atomistic simulations methods, which yield detailed information on surface rearrangements at small space and time scales. Thus, different simulation approaches,

like MC and MD, are being contrasted systematically to each other, leading to a better understanding of the capabilities of both.²⁷¹ MD simulations are being used to assess potential limitations of classic models of sputtering, like Sigmund's.²⁷² Also, quantitative estimates on the importance of additional physical effects, like ion implantation,^{225,273} are being extracted from MD. And the same microscopic approach is being taken to describe the surface currents of material rearrangement and the residual stress fields induced by irradiation.²⁰⁷ Actually, general frameworks have been recently developed to tabulate²³⁶ and even automate²⁷⁴ the statistical analysis of MD simulation data for compound and monoatomic targets (specifically, via the crater function approach) so that parameter estimates can be passed on to continuum equations. This provides one way to address the full multiscale nature of IBS nanopatterning and thus improve the matching between theoretical frameworks which in principle operate on different scales. It would be interesting to see analogous tabulations of IBS-induced residual stress distributions and additional properties, like ion-induced diffusivities, under different irradiation conditions (such as different ion/target combinations and different energies), which to date remain affected of large uncertainties. Overall, this type of computational approaches may eventually be able to fully clarify the extent to which pattern formation under IBS is dominated by energy or by momentum transfer between the ion beam and the target.

In turn, progress in the theoretical understanding of IBS nanopatterning is also due to recent results in the (semi)quantitative description of experimental systems by continuum models. Indeed, recent results are available on specific linear²⁷⁵ and nonlinear^{73,217,276} ingredients of continuum interface equations, which can account for various, more detailed, morphological properties of the observed patterns. In particular the latter might be related with previous results for surfaces with arbitrarily large slopes,^{157–159,277} a connection

which seems to warrant further attention. Also worth pursuing seems the understanding of the role of noise in continuum height equations. As already mentioned early in Sec. II A, quantitative fits to experimental data require noise to be incorporated, indeed as expected^{20,183} from the stochastic nature of ion arrival. Indeed, the fact that the KS and related equations generate their own noise via deterministic chaos^{7,43,46} partly compensates for the matter-of-principle limitation of such deterministic continuum models, justifying our presentation in Sec. II B. However, the detailed effect of noise in these nonlinear mesoscopic frameworks needs to be addressed in the process of further validating them against data from experiments and from numerical simulations of more microscopic models. Likewise, an improved understanding on the connection between alternative continuum approaches, like two-field models and hydrodynamics-based formulations, might emerge from a more detailed reflection on the dynamical role of the amorphous-to-crystalline interface.²⁷⁸ This has already led to a practical method to control ripple amplitudes in medium-energy experiments on Si.²⁷⁹ On the other hand, precisely, the existence and role of a topmost surface layer is possibly a key ingredient for the different behavior under IBS of semiconductors at room temperatures and metals or semiconductors at high temperatures. Hence, studies on the conditions for the dynamical relevance of such a layer may facilitate a more comprehensive knowledge of IBS throughout larger classes of targets.

Back to IBS at medium ion energies, actually their systematic study generally seems quite a natural way to improve the theoretical description of surface pattern formation via this technique.²⁸⁰ Indeed, while the microscopic collisional behavior remains basically unchanged (provided nuclear contributions still dominate the stopping power) with respect to low energies,¹⁷⁹ all typical scales—from the thickness of the amorphized layer to the ripple wavelength and amplitude—are amplified approximately by a factor of ten, becoming much more readily accessible to experimental characterization.²⁸¹ This connection has been known and partly exploited, but it probably still remains to show its full potential from the points of view of theory and applications^{131,244} of the IBS technique.

Naturally, once a complete and fully consistent theoretical description is achieved for the case of clean, monoatomic targets, a number of related contexts will benefit from such knowledge, notably those of IBS under concurrent impurity deposition and IBS of binary targets. And, possibly related with these, the case of reactive ions, which, albeit being long known,⁴² has received relatively little attention from the theoretical point of view, in spite of the potentially relevant role of reactive impurities²⁵⁴ for the experimentally observed pattern-forming behavior. Moreover, this context suggests exploring the surface patterning possibilities offered by further changes in the irradiation conditions with respect to the simplest ones discussed in this Perspective article: e.g., by substantially increasing the charge of the ions employed,^{282,283} or via the many-body effects implied by electronic contributions to the stopping power at even higher ion energy,¹⁷⁹ to reach conditions for swift ion irradiation.²⁸⁴ Incidentally, wrinkle formation by IBS of polymeric^{285,286} or soda-lime glass²⁸⁷ surfaces at medium and low energies has been rationalized via strain-mediated instabilities, akin to those classically invoked to describe wrinkle formation under swift heavy ion irradiation of metallic glasses.²⁸⁸ In the last case,

energy deposition within the target differs quite strongly¹⁷⁹ from the picture of binary collision cascades, which naturally impacts the types of mechanisms which are responsible for surface pattern formation. Whether suitably extending the theoretical description to polymeric and glassy low-to-medium-energy systems provides a bridge to still higher energy ranges remains a challenging open issue.

IV. CONCLUSIONS

We have provided an overview on the main aspects of surface nanostructuring by ion-beam irradiation, from experiments and theory to some of its salient and diverse applications. We have adopted a historical point of view that has allowed us to appreciate the difficulties encountered in the understanding of the main physical principles at play in this process. Possibly, the most crucial aspect from this point of view has been the relevant role that can be played by the presence or absence of a third atomic species (besides those of the ion and the target material) with respect to the formation and properties of the surface nanopatterns. Historically, some of these difficulties have actually required a thorough systematic revision of previous experimental and theoretical knowledge, a process that started approximately ten years ago and is still to be fully completed. We have also pointed out a number of issues that remain open in the field, again from the experimental/applied and theoretical/computational points of view. While important challenges seem involved in addressing such issues, the latest achievements in recent works on IBS surface nanopatterning already set the stage to promising forthcoming applications of this versatile surface nanostructuring technique.

ACKNOWLEDGMENTS

We are particularly indebted to M. Castro, R. Gago, B. Kahng, J.-H. Kim, A. Moreno-Barrado, J. Muñoz-García, A. Redondo-Cubero, J. Seo, and L. Vázquez for insightful interactions and collaborations in the topic of this article. This work has been partially supported by Ministerio de Ciencia e Innovación, Agencia Estatal de Investigación, and Fondo Europeo de Desarrollo Regional (Spain and European Union) through Grant No. PGC2018-094763-B-I00 (R.C.) and by Korean Research Foundation through Grant Nos. NRF-2016R1D1A1B03930532 and NRF-2019R1F1A1040955 (J.-S.K.).

DATA AVAILABILITY

The data that support the findings of this study are available within the article.

REFERENCES

- ¹M. Navez, C. Sella, and D. Chaperot, “Étude de l’attaque du verre par bombardement ionique,” *C. R. Acad. Sci.* **254**, 240 (1962).
- ²S. Fácsko, T. Dekorsy, C. Koerdt, C. Trappe, H. Kurz, A. Vogt, and H. L. Hartnagel, “Formation of ordered nanoscale semiconductor dots by ion sputtering,” *Science* **285**, 1551 (1999).
- ³U. Valbusa, C. Boragno, and F. Buaquier de Mongeot, “Nanostructuring surfaces by ion sputtering,” *J. Phys.: Condens. Matter* **14**, 8153 (2002).
- ⁴W. L. Chan and E. Chason, “Making waves: Kinetic processes controlling surface evolution during low energy ion sputtering,” *J. Appl. Phys.* **101**, 121301 (2007).

- ⁵R. Cuerno, L. Vázquez, R. Gago, and M. Castro, "Surface nanopatterns induced by ion-beam sputtering," *J. Phys.: Condens. Matter* **21**, 220301 (2009).
- ⁶N. Taniguchi, "On the basic concept of nanotechnology," in Proceedings of International Conference on Production Engineering Tokyo (1974), Pt. II, pp. 18–23.
- ⁷M. Cross and H. Greenside, *Pattern Formation and Dynamics in Nonequilibrium Systems* (Cambridge University Press, Cambridge, 2009).
- ⁸R. M. Bradley and J. M. E. Harper, "Theory of ripple topography induced by ion bombardment," *J. Vac. Sci. Technol. A* **6**, 2390 (1988).
- ⁹P. Sigmund, "Theory of sputtering. I. Sputtering yield of amorphous and polycrystalline targets," *Phys. Rev.* **184**, 383 (1969).
- ¹⁰P. Sigmund, "A mechanism of surface micro-roughening by ion bombardment," *J. Mater. Sci.* **8**, 1545 (1973).
- ¹¹C. Herring, in *The Physics of Powder Metallurgy*, edited by W. Kingston (McGraw Hill, New York, 1951).
- ¹²W. W. Mullins, "Theory of thermal grooving," *J. Appl. Phys.* **28**, 333 (1957).
- ¹³W. W. Mullins, "Flattening of a nearly plane solid surface due to capillarity," *J. Appl. Phys.* **30**, 77 (1959).
- ¹⁴E. A. Eklund, R. Bruinsma, J. Rudnick, and R. S. Williams, "Submicron-scale surface roughening induced by ion bombardment," *Phys. Rev. Lett.* **67**, 1759 (1991).
- ¹⁵T. Michely and G. Comsa, "Temperature dependence of the sputtering morphology of Pt (111)," *Surf. Sci.* **256**, 217 (1991).
- ¹⁶E. Chason, T. M. Mayer, B. K. Kellerman, D. T. McIlroy, and A. J. Howard, "Roughening instability and evolution of the Ge(001) surface during ion sputtering," *Phys. Rev. Lett.* **72**, 3040 (1994).
- ¹⁷S. Rusponi, C. Boragno, and U. Valbusa, "Ripple structure on Ag(110) surface induced by ion sputtering," *Phys. Rev. Lett.* **78**, 2795 (1997).
- ¹⁸R. Wiesendanger, *Scanning Probe Microscopy and Spectroscopy: Methods and Applications* (Cambridge University Press, 1995).
- ¹⁹D. Carbone, A. Biermanns, B. Ziberi, F. Frost, O. Plantevin, U. Pietsch, and T. H. Metzger, "Ion-induced nanopatterns on semiconductor surfaces investigated by grazing incidence x-ray scattering techniques," *J. Phys.: Condens. Matter* **21**, 224007 (2009).
- ²⁰R. Cuerno and A.-L. Barabási, "Dynamic scaling of ion-sputtered surfaces," *Phys. Rev. Lett.* **74**, 4746 (1995).
- ²¹M. Makeev, R. Cuerno, and A. Barabási, "Morphology of ion-sputtered surfaces," *Nucl. Instrum. Methods B* **197**, 185 (2002).
- ²²G. Carter and V. Vishnyakov, "Roughening and ripple instabilities on ion-bombarded Si," *Phys. Rev. B* **54**, 17647 (1996).
- ²³C. C. Umbach, R. L. Headrick, and K.-C. Chan, "Spontaneous nanoscale corrugation of ion-eroded SO₂: The role of ion-irradiation-enhanced viscous flow," *Phys. Rev. Lett.* **87**, 246104 (2001).
- ²⁴M. Castro and R. Cuerno, "Hydrodynamic approach to surface pattern formation by ion beams," *Appl. Surf. Sci.* **258**, 4171 (2012).
- ²⁵M. Castro, R. Cuerno, L. Vázquez, and R. Gago, "Self-organized ordering of nanostructures produced by ion-beam sputtering," *Phys. Rev. Lett.* **94**, 016102 (2005).
- ²⁶N. Kalyanasundaram, J. Freund, and H. Johnson, "A multiscale crater function model for ion-induced pattern formation in silicon," *J. Phys.: Condens. Matter* **21**, 224018 (2009).
- ²⁷S. A. Norris, J. Samela, L. Bokonte, M. Backman, F. Djurabekova, K. Nordlund, C. S. Madi, M. P. Brenner, and M. J. Aziz, "Molecular dynamics of single-particle impacts predicts phase diagrams for large scale pattern formation," *Nat. Commun.* **2**, 276 (2011).
- ²⁸K. Nordlund, S. J. Zinkle, A. E. Sand, F. Granberg, R. S. Averback, R. Stoller, T. Suzudo, L. Malerba, F. Banhart, W. J. Weber, F. Willaime, S. L. Dudarev, and D. Simeone, "Improving atomic displacement and replacement calculations with physically realistic damage models," *Nat. Commun.* **9**, 1084 (2018).
- ²⁹A. Lopez-Cazalilla, A. Ilinov, K. Nordlund, and F. Djurabekova, "Modeling of high-fluence irradiation of amorphous Si and crystalline Al by linearly focused ion beams," *J. Phys.: Condens. Matter* **31**, 075302 (2019).
- ³⁰E. Chason and W. L. Chan, "Kinetic Monte Carlo simulations compared with continuum models and experimental properties of pattern formation during ion beam sputtering," *J. Phys.: Condens. Matter* **21**, 224016 (2009).
- ³¹O. Bobes, K. Zhang, and H. Hofäss, "Ion beam induced surface patterns due to mass redistribution and curvature-dependent sputtering," *Phys. Rev. B* **86**, 235414 (2012).
- ³²Z. Yang, M. Lively, and J. P. Allain, "Atomistic simulation of ion beam patterning with crater functions," *Nucl. Instrum. Methods B* **307**, 189 (2013).
- ³³R. Gago, L. Vázquez, R. Cuerno, M. Varela, C. Ballesteros, and J. M. Albella, "Production of ordered silicon nanocrystals by low-energy ion sputtering," *Appl. Phys. Lett.* **78**, 3316 (2001).
- ³⁴F. Frost, A. Schindler, and F. Bigl, "Roughness evolution of ion sputtered rotating InP surfaces: Pattern formation and scaling laws," *Phys. Rev. Lett.* **85**, 4116 (2000).
- ³⁵G. Ozaydin, A. S. Özcan, Y. Wang, F. Ludwig, H. Zhou, R. L. Headrick, and D. P. Siddons, "Real-time x-ray studies of Mo-seeded Si nanodot formation during ion bombardment," *Appl. Phys. Lett.* **87**, 163104 (2005).
- ³⁶R. Gago, L. Vázquez, O. Plantevin, J. A. Sánchez-García, M. Varela, M. C. Ballesteros, J. M. Albella, and T. H. Metzger, "Temperature influence on the production of nanodot patterns by ion beam sputtering of Si(001)," *Phys. Rev. B* **73**, 155414 (2006).
- ³⁷H. Hofäss and K. Zhang, "Surfactant sputtering," *Appl. Phys. A* **92**, 517 (2008).
- ³⁸J. A. Sánchez-García, L. Vázquez, R. Gago, A. Redondo-Cubero, J. M. Albella, and Z. Czigány, "Tuning the surface morphology in self-organized ion beam nanopatterning of Si(001) via metal incorporation: From holes to dots," *Nanotechnology* **19**, 355306 (2008).
- ³⁹B. Ziberi, M. Cornejo, F. Frost, and B. Rauschenbach, "Highly ordered nanopatterns on Ge and Si surfaces by ion beam sputtering," *J. Phys.: Condens. Matter* **21**, 224003 (2009).
- ⁴⁰Q. Huang, Q. jia, J. Feng, H. Huang, X. Yang, J. Grenzer, K. Huang, S. Zhang, J. Lin, H. Zhou, T. You, W. Yu, S. Facsko, P. Jonnard, M. Wu, A. Giglia, Z. Zhang, Z. Liu, Z. Wang, X. Wang, and X. Ou, "Realization of wafer-scale nanogratings with sub-50 nm period through vacancy epitaxy," *Nat. Commun.* **10**, 2437 (2019).
- ⁴¹J. Kim, S. Yoon, S. Jo, J. Seo, and J. Kim, "Nanopatterning by ion beam sputtering in unconventional formats," *J. Phys.: Condens. Matter* **30**, 274004 (2018).
- ⁴²M. V. R. Murty, "Sputtering: The material erosion tool," *Surf. Sci.* **500**, 523 (2002).
- ⁴³J. Muñoz-García, L. Vázquez, R. Cuerno, J. A. Sánchez-García, M. Castro, and R. Gago, "Self-organized surface nanopatterning by ion beam sputtering," in *Toward Functional Nanomaterials*, edited by Z. M. Wang (Springer, 2009), pp. 323–398.
- ⁴⁴F. Buatier de Mongeot and U. Valbusa, "Applications of metal surfaces nanostructured by ion beam sputtering," *J. Phys.: Condens. Matter* **21**, 224022 (2009).
- ⁴⁵R. Cuerno, M. Castro, J. Muñoz-García, R. Gago, and L. Vázquez, "Nanoscale pattern formation at surfaces under ion-beam sputtering: A perspective from continuum models," *Nucl. Instrum. Methods B* **269**, 894 (2011).
- ⁴⁶J. Muñoz-García, L. Vázquez, M. Castro, R. Gago, A. Redondo-Cubero, A. Moreno-Barrado, and R. Cuerno, "Self-organized nanopatterning of silicon surfaces by ion beam sputtering," *Mater. Sci. Eng. R: Rep.* **86**, 1 (2014).
- ⁴⁷S. A. Norris and M. J. Aziz, "Ion-induced nanopatterning of silicon: Toward a predictive model," *Appl. Phys. Rev.* **6**, 011311–28 (2019).
- ⁴⁸H. Hofäss and O. Bobes, "Prediction of ion-induced nanopattern formation using Monte Carlo simulations and comparison to experiments," *Appl. Phys. Rev.* **6**, 021307 (2019).
- ⁴⁹J. Muñoz-García, R. Cuerno, M. Castro, L. Vázquez, R. Gago, and A. Redondo-Cubero, "Special issue on surfaces patterned by ion sputtering," *J. Phys.: Condens. Matter* **30**, 450301 (2018).
- ⁵⁰H. Gnaser, *Low Energy Ion Irradiation of Solid Surfaces* (Springer-Verlag, 1999).
- ⁵¹G. Ehrlich and F. Hudha, "Atomic view of surface self-diffusion: Tungsten on tungsten," *J. Chem. Phys.* **44**, 1039 (1966).

- ⁵²R. L. Schwoebel and E. J. Shipsey, "Step motion on crystal surfaces," *J. Appl. Phys.* **37**, 3682 (1966).
- ⁵³T. Michely and J. Krug, *Islands, Mounds and Atoms* (Springer Science & Business Media, 2004).
- ⁵⁴C. S. Madi and M. J. Aziz, "Multiple scattering causes the low energy-low angle constant wavelength topographical instability of argon ion bombarded silicon surfaces," *Appl. Surf. Sci.* **258**, 4112 (2012).
- ⁵⁵C. S. Madi, "Linear stability and instability patterns in ion bombarded silicon surfaces," Ph.D. thesis (Harvard University, 2011).
- ⁵⁶C. Madi, B. Davidovitch, H. George, S. Norris, M. Brenner, and M. Aziz, "Multiple bifurcation types and the linear dynamics of ion sputtered surfaces," *Phys. Rev. Lett.* **101**, 246102 (2008).
- ⁵⁷C. Madi, B. Davidovitch, H. George, S. Norris, M. Brenner, and M. Aziz, "Erratum: Multiple bifurcation types and the linear dynamics of ion sputtered surfaces [Phys. Rev. Lett. 101, 246102 (2008)]," *Phys. Rev. Lett.* **107**, 049902 (2011).
- ⁵⁸M. Castro, R. Gago, L. Vázquez, J. Muñoz-García, and R. Cuerno, "Stress-induced solid flow drives surface nanopatterning of silicon by ion-beam irradiation," *Phys. Rev. B* **86**, 214107 (2012).
- ⁵⁹A. Moreno-Barrado, M. Castro, R. Gago, L. Vázquez, J. Muñoz-García, A. Redondo-Cubero, B. Galiana, C. Ballesteros, and R. Cuerno, "Nonuniversality due to inhomogeneous stress in surface nanopatterning by ion-beam irradiation," *Phys. Rev. B* **91**, 155303 (2015).
- ⁶⁰S. K. Garg, D. P. Datta, M. Kumar, D. Kanjilal, and T. Som, "60 keV Ar+ion induced pattern formation on Si surface: Roles of sputter erosion and atomic redistribution," *Appl. Surf. Sci.* **310**, 147 (2014).
- ⁶¹D. P. Datta, S. K. Garg, T. Basu, B. Satpati, H. Hofsäss, D. Kanjilal, and T. Som, "Temporal evolution of Ge surface topography under keV ion irradiation: Combined effects of curvature-dependent sputter erosion and atomic redistribution," *Appl. Surf. Sci.* **360**, 131 (2016).
- ⁶²H. Hofsäss, "Surface instability and pattern formation by ion-induced erosion and mass redistribution," *Appl. Phys. A* **114**, 401 (2014).
- ⁶³M. P. Harrison and R. M. Bradley, "Crater function approach to ion-induced nanoscale pattern formation: Craters for flat surfaces are insufficient," *Phys. Rev. B* **89**, 245401 (2014).
- ⁶⁴M. Castro and R. Cuerno, "Ion induced solid flow," arXiv:1007.2144 (2010).
- ⁶⁵S. A. Norris, "Stress-induced patterns in ion-irradiated silicon: Model based on anisotropic plastic flow," *Phys. Rev. B* **86**, 235405 (2012).
- ⁶⁶S. E. Orchard, "On surface levelling in viscous liquids and gels," *Appl. Sci. Res.* **11A**, 451 (1962).
- ⁶⁷Y. Yamamura, Y. Itikawa, and N. Itoh, "Angular dependence of sputtering yields of monatomic solids," IPPJ Rep. AM-26 (1983).
- ⁶⁸Y. Yamamura, C. Mössner, and H. Oechsner, "The bombarding-angle dependence of sputtering yields under various surface conditions," *Rad. Eff.* **103**, 25–43 (1987).
- ⁶⁹C. Madi, E. Anzenberg, K. Ludwig, and M. Aziz, "Mass redistribution causes the structural richness of ion-irradiated surfaces," *Phys. Rev. Lett.* **106**, 66101 (2011).
- ⁷⁰E. Anzenberg, C. S. Madi, M. J. Aziz, and K. F. Ludwig, Jr., "Time-resolved measurements of nanoscale surface pattern formation kinetics in two dimensions on ion-irradiated Si," *Phys. Rev. B* **84**, 214108 (2011).
- ⁷¹J. C. Perkinson, E. Anzenberg, M. J. Aziz, and J. K. F. Ludwig, "Model-independent test of the truncated crater function theory of surface morphology evolution during ion bombardment," *Phys. Rev. B* **89**, 115433 (2014).
- ⁷²A. Moreno-Barrado, R. Gago, A. Redondo-Cubero, L. Vázquez, J. Muñoz-García, R. Cuerno, K. Lorenz, and M. Castro, "Ion damage overrides structural disorder in silicon surface nanopatterning by low-energy ion beam sputtering," *Europhys. Lett.* **109**, 48003 (2015).
- ⁷³J. Muñoz-García, R. Cuerno, and M. Castro, "Stress-driven nonlinear dynamics of ion-induced surface nanopatterns," *Phys. Rev. B* **100**, 205421 (2019).
- ⁷⁴A. Metya and D. Ghose, "Investigation of ion beam induced nanopattern formation near the threshold energy," *Appl. Phys. Lett.* **103**, 161602 (2013).
- ⁷⁵D. Chowdhury, D. Ghose, and S. A. Mollick, "Homoepitaxy of germanium by hyperthermal ion irradiation," *Vacuum* **107**, 23 (2014).
- ⁷⁶D. Chowdhury, D. Ghose, S. A. Mollick, B. Satpati, and S. R. Bhattacharyya, "Nanorippling of ion irradiated gas (001) surface near the sputter-threshold energy," *Phys. Stat. Sol. B* **252**, 811 (2015).
- ⁷⁷S. A. Norris, J. C. Perkinson, M. Mokhtarzadeh, E. Anzenberg, M. J. Aziz, and K. F. Ludwig, "Distinguishing physical mechanisms using GISAXS experiments and linear theory: The importance of high wavenumbers," *Sci. Rep.* **7**, 2016 (2017).
- ⁷⁸S. Habenicht, K. P. Lieb, J. Koch, and A. D. Wieck, "Ripple propagation and velocity dispersion on ion-beam-eroded silicon surfaces," *Phys. Rev. B* **65**, 115327 (2002).
- ⁷⁹P. F. Alkemade, "Propulsion of ripples on glass by ion bombardment," *Phys. Rev. Lett.* **96**, 107602 (2006).
- ⁸⁰Q. Wei, J. Lian, L. A. Boatner, L. Wang, and R. C. Ewing, "Propagation of ripples on pyrochlore induced by ion beam bombardment," *Phys. Rev. B* **80**, 085413 (2009).
- ⁸¹H. Gnaser, B. Reuscher, and A. Zeuner, "Propagation of nanoscale ripples on ion-irradiated surfaces," *Nucl. Instrum. Methods B* **285**, 142 (2012).
- ⁸²H. Hofsäss, K. Zhang, H. Gehrke, and C. Brüsewitz, "Propagation of ripple patterns on Si during ion bombardment," *Phys. Rev. B* **88**, 075426 (2013).
- ⁸³D. Kramczynski, B. Reuscher, and H. Gnaser, "Wavelength-dependent ripple propagation on ion-irradiated prepatterned surfaces driven by viscous flow corroborates two-field continuum model," *Phys. Rev. B* **89**, 205422 (2014).
- ⁸⁴A. Moreno-Barrado, M. Castro, J. Muñoz-García, and R. Cuerno, "Stress vs sputtering effects in the propagation of surface ripples produced by ion-beam sputtering," *Nucl. Instrum. Methods B* **365**, 15 (2015).
- ⁸⁵J. Muñoz-García, R. Cuerno, and M. Castro, "Coupling of morphology to surface transport in ion-beam irradiated surfaces: Oblique incidence," *Phys. Rev. B* **78**, 205408 (2008).
- ⁸⁶D. Flamm, F. Frost, and D. Hirsch, "Evolution of surface topography of fused silica by ion beam sputtering," *Appl. Surf. Sci.* **179**, 95 (2001).
- ⁸⁷A. Keller, S. Roßbach, S. Facska, and W. Möller, "Simultaneous formation of two ripple modes on ion sputtered silicon," *Nanotechnology* **19**, 135303 (2008).
- ⁸⁸M. Teichmann, J. Lorbeer, F. Frost, and B. Rauschenbach, "Ripple coarsening on ion beam-eroded surfaces," *Nanoscale Res. Lett.* **9**, 439 (2014).
- ⁸⁹D. Datta and T. Chini, "Coarsening of ion-beam-induced surface ripple in Si: Nonlinear effect vs geometrical shadowing," *Phys. Rev. B* **76**, 075323 (2007).
- ⁹⁰D. P. Adams, T. M. Mayer, M. J. Vasile, and K. Archuleta, "Effects of evolving surface morphology on yield during focused ion beam milling of carbon," *Appl. Surf. Sci.* **252**, 2432 (2006).
- ⁹¹J. Völlner, B. Ziberi, F. Frost, and B. Rauschenbach, "Topography evolution mechanism on fused silica during low-energy ion beam sputtering," *J. Appl. Phys.* **109**, 043501 (2011).
- ⁹²T. Basu, D. P. Datta, and T. Som, "Transition from ripples to faceted structures under low-energy argon ion bombardment of silicon: Understanding the role of shadowing and sputtering," *Nanoscale Res. Lett.* **8**, 289 (2013).
- ⁹³M. Teichmann, J. Lorbeer, B. Ziberi, F. Frost, and B. Rauschenbach, "Pattern formation on Ge by low energy ion beam erosion," *New J. Phys.* **15**, 103029 (2013).
- ⁹⁴M. Engler, S. Macko, F. Frost, and T. Michely, "Evolution of ion beam induced patterns on Si (001)," *Phys. Rev. B* **89**, 245412 (2014).
- ⁹⁵D. Datta and T. Chini, "Atomic force microscopy study of 60-keV Ar-ion-induced ripple patterns on Si(100)," *Phys. Rev. B* **69**, 235313 (2004).
- ⁹⁶P. Karmakar and D. Ghose, "Nanoscale periodic and faceted structures formation on Si(1 0 0) by oblique angle oxygen ion sputtering," *Nucl. Instrum. Methods B* **230**, 539 (2005).
- ⁹⁷S. Habenicht, W. Bolse, K. P. Lieb, K. Reimann, and U. Geyer, "Nanometer ripple formation and self-affine roughening of ion-beam-eroded graphite surfaces," *Phys. Rev. B* **60**, 2200 (1999).
- ⁹⁸A. Keller, R. Cuerno, S. Facska, and W. Möller, "Anisotropic scaling of ripple morphologies on high-fluence sputtered silicon," *Phys. Rev. B* **79**, 115437 (2009).

- ¹⁰⁰E. Vivo, M. Nicoli, M. Engler, T. Michely, L. Vázquez, and R. Cuerno, "Strong anisotropy in surface kinetic roughening: Analysis and experiments," *Phys. Rev. B* **86**, 245427 (2012).
- ¹⁰¹D. Chowdhury and D. Ghose, "Super-roughening scaling behaviour of Si surface morphology at grazing incidence low energy ion beam sputtering," *Appl. Surf. Sci.* **324**, 517 (2015).
- ¹⁰²S. K. Garg, D. P. Datta, T. Basu, D. Kanjilal, and T. Som, "Statistical analysis of ripple morphology on Si surfaces due to 60 keV Ar⁺-ions," *Surf. Topogr. Metrol. Prop.* **4**, 015002 (2016).
- ¹⁰³J. Kim, N. Ha, J. Kim, M. Joe, K. Lee, and R. Cuerno, "One-dimensional pattern of au nanodots by ion-beam sputtering: Formation and mechanism," *Nanotechnology* **22**, 285301 (2011).
- ¹⁰⁴J. W. Evans, P. A. Thiel, and M. C. Bartelt, "Morphological evolution during epitaxial thin film growth: Formation of 2D islands and 3D mounds," *Surf. Sci. Rep.* **61**, 1 (2006).
- ¹⁰⁵G. Costantini, S. Rusponi, F. B. de Mongeot, C. Boragno, and U. Valbusa, "Periodic structures induced by normal-incidence sputtering on Ag (110) and Ag (001): Flux and temperature dependence," *J. Phys.: Condens. Matter* **13**, 5875 (2001).
- ¹⁰⁶M. A. Garcia, J. Rickards, R. Cuerno, R. Trejo-Luna, J. Cañetas-Ortega, L. R. De La Vega, and L. Rodriguez-Fernández, "Surface morphologies of Ti and Ti-Al-V bombarded by 1.0-MeV Au⁺ ions," *Phys. Rev. Appl.* **8**, 064027 (2017).
- ¹⁰⁷X. Ou, A. Keller, M. Helm, J. Fassbender, and S. Facsko, "Reverse epitaxy of Ge: Ordered and faceted surface patterns," *Phys. Rev. Lett.* **111**, 016101 (2013).
- ¹⁰⁸X. Ou, K. H. Heinig, R. Hübner, J. Grenzer, X. Wang, M. Helm, J. Fassbender, and S. Facsko, "Faceted nanostructure arrays with extreme regularity by self-assembly of vacancies," *Nanoscale* **7**, 18928 (2015).
- ¹⁰⁹M. Makeev and A.-L. Barabási, "Ion-induced effective surface diffusion in ion sputtering," *Appl. Phys. Lett.* **71**, 2800 (1997).
- ¹¹⁰S. Facsko, H. Kurz, and T. Dekorsy, "Energy dependence of quantum dot formation by ion sputtering," *Phys. Rev. B* **63**, 165329 (2001).
- ¹¹¹V. Shenoy, W. Chan, and E. Chason, "Composititionally modulated ripples induced by sputtering of alloy surfaces," *Phys. Rev. Lett.* **98**, 256101 (2007).
- ¹¹²R. M. Bradley and P. D. Shipman, "Spontaneous pattern formation induced by ion bombardment of binary compounds," *Phys. Rev. Lett.* **105**, 145501 (2010).
- ¹¹³P. D. Shipman and R. M. Bradley, "Theory of nanoscale pattern formation induced by normal-incidence ion bombardment of binary compounds," *Phys. Rev. B* **84**, 085420 (2011).
- ¹¹⁴S. Le Roy, E. Barthel, N. Brun, A. Lelarge, and E. Søndergaard, "Self-sustained etch masking: A general concept to initiate the formation of nanopatterns during ion erosion," *J. Appl. Phys.* **106**, 094308 (2009).
- ¹¹⁵S. Le Roy, E. Søndergaard, I. Nerbo, M. Kildemo, and M. Plapp, "Diffuse-interface model for nanopatterning induced by self-sustained ion-etch masking," *Phys. Rev. B* **81**, 161401 (2010).
- ¹¹⁶S. A. Norris, "Ion-assisted phase separation in compound films: An alternate route to ordered nanostructures," *J. Appl. Phys.* **114**, 204303 (2013).
- ¹¹⁷O. El-Atwani, S. A. Norris, K. Ludwig, S. Gonderman, and J. P. Allain, "Ion beam nanopatterning of III-V semiconductors: Consistency of experimental and simulation trends within a chemistry-driven theory," *Sci. Rep.* **5**, 18207 (2015).
- ¹¹⁸F. Frost, B. Ziberi, T. Höche, and B. Rauschenbach, "The shape and ordering of self-organized nanostructures by ion sputtering," *Nucl. Instrum. Methods B* **216**, 9 (2004).
- ¹¹⁹T. Som, T. K. Chini, Y. S. Katharia, S. Tripathy, and D. Kanjilal, "Formation of nanodots on oblique ion sputtered InP surfaces," *Appl. Surf. Sci.* **256**, 562–566 (2009).
- ¹²⁰E. Tryniewicz, B. R. Jany, A. Janas, and F. Krok, "Recent developments in ion beam-induced nanostructures on AlII-BV compound semiconductors," *J. Phys.: Condens. Matter* **30**, 304005 (2018).
- ¹²¹J. Zhou, S. Facsko, M. Lu, and W. Moller, "Nanopatterning of Si surfaces by normal incident ion erosion: Influence of iron incorporation on surface morphology evolution," *J. Appl. Phys.* **109**, 104315 (2011).
- ¹²²M. Engler, F. Frost, S. Müller, S. Macko, M. Will, R. Feder, D. Spermann, R. Hübner, S. Facsko, and T. Michely, "Silicide induced ion beam patterning of Si(001)," *Nanotechnology* **25**, 115303 (2014).
- ¹²³S. Macko, F. Frost, M. Engler, D. Hirsch, T. Höche, J. Grenzer, and T. Michely, "Phenomenology of iron-assisted ion beam pattern formation on Si (001)," *New J. Phys.* **13**, 073017 (2011).
- ¹²⁴K. Zhang, M. Brötzmann, and H. Hofäss, "Surfactant-driven self-organized surface patterns by ion beam erosion," *New J. Phys.* **13**, 013033 (2011).
- ¹²⁵S. Macko, J. Grenzer, F. Frost, M. Engler, D. Hirsch, M. Fritzsche, A. Mücklich, and T. Michely, "Iron-assisted ion beam patterning of Si (001) in the crystalline regime," *New J. Phys.* **14**, 073003 (2012).
- ¹²⁶H. Hofäss, O. Bobes, and K. Zhang, "Is sputtering relevant for ion-induced self-organized pattern formation?," *AIP Conf. Proc.* **1525**, 386 (2013).
- ¹²⁷K. Zhang, O. Bobes, and H. Hofäss, "Designing self-organized nanopatterns on Si by ion irradiation and metal co-deposition," *Nanotechnology* **25**, 085301 (2014).
- ¹²⁸R. Gago, A. Redondo-Cubero, F. J. Palomares, and L. Vázquez, "Influence of metal co-deposition on silicon nanodot patterning dynamics during ion-beam sputtering," *Nanotechnology* **25**, 415301 (2014).
- ¹²⁹J. A. Sánchez-García, R. Gago, R. Caillard, A. Redondo-Cubero, J. A. Martín-Gago, F. J. Palomares, M. Fernández, and L. Vázquez, "Production of nanohole/nanodot patterns on Si(001) by ion beam sputtering with simultaneous metal incorporation," *J. Phys.: Condens. Matter* **21**, 224009 (2009).
- ¹³⁰A. Redondo-Cubero, R. Gago, F. Palomares, A. Mücklich, M. Vinnichenko, and L. Vázquez, "Nanopatterning dynamics on Si (100) during oblique 40-keV Ar⁺ erosion with metal codeposition: Morphological and compositional correlation," *Phys. Rev. B* **86**, 085436 (2012).
- ¹³¹A. Redondo-Cubero, B. Galiana, K. Lorenz, F. Palomares, D. Bahena, C. Ballesteros, I. Hernández-Calderón, and L. Vázquez, "Self-organised silicide nanodot patterning by medium-energy ion beam sputtering of Si(100): Local correlation between the morphology and metal content," *Nanotechnology* **27**, 444001 (2016).
- ¹³²B. Moon, S. Yoo, J. S. Kim, S. J. Kang, J. Muñoz-García, and R. Cuerno, "Ion-beam nanopatterning of silicon surfaces under codeposition of non-silicide-forming impurities," *Phys. Rev. B* **93**, 115430 (2016).
- ¹³³H. Hofäss, K. Zhang, A. Pape, O. Bobes, and M. Brötzmann, "The role of phase separation for self-organized surface pattern formation by ion beam erosion and metal atom co-deposition," *Appl. Phys. A* **111**, 653 (2013).
- ¹³⁴R. M. Bradley, "Morphological transitions in nanoscale patterns produced by concurrent ion sputtering and impurity co-deposition," *J. Appl. Phys.* **119**, 134305 (2016).
- ¹³⁵A. Cuenat, H. B. George, K. C. Chang, J. M. Blakely, and M. J. Aziz, "Lateral templating for guided self-organization of sputter morphologies," *Adv. Mater.* **17**, 2845 (2005).
- ¹³⁶A. Keller and S. Facsko, "Tuning the quality of nanoscale ripple patterns by sequential ion-beam sputtering," *Phys. Rev. B* **82**, 155444 (2010).
- ¹³⁷J.-H. Kim, J.-S. Kim, J. Muñoz-García, and R. Cuerno, "Role of nonlinearities and initial prepatterned surfaces in nanobead formation by ion-beam bombardment of au (001): Experiments and theory," *Phys. Rev. B* **87**, 085438 (2013).
- ¹³⁸J. H. Kim and J. S. Kim, "Pattern evolution during ion beam sputtering: Reductionistic view," *Nucl. Instrum. Methods B* **383**, 59–64 (2016).
- ¹³⁹J. Muñoz-García, R. Gago, R. Cuerno, J. Sánchez-García, A. Redondo-Cubero, M. Castro, and L. Vázquez, "Independence of interrupted coarsening on initial system order: Ion-beam nanopatterning of amorphous versus crystalline silicon targets," *J. Phys.: Condens. Matter* **24**, 375302 (2012).
- ¹⁴⁰S. Garg, R. Cuerno, D. Kanjilal, and T. Som, "Anomalous behavior in temporal evolution of ripple wavelength under medium energy Ar⁺-ion bombardment on Si: A case of initial wavelength selection," *J. Appl. Phys.* **119**, 225301 (2016).
- ¹⁴¹A. Zalar, "Improved depth resolution by sample rotation during auger electron spectroscopy depth profiling," *Thin Solid Films* **124**, 223 (1985).
- ¹⁴²D. Chowdhury, D. Ghose, and B. Satpati, "Production of ordered and pure Si nanodots at grazing ion beam sputtering under concurrent substrate rotation," *Mater. Sci. Eng.: B* **179**, 1 (2014).

- ¹⁴³T. Basu, D. A. Pearson, R. M. Bradley, and T. Som, "Temporal evolution of a silicon surface subject to low energy ion irradiation and concurrent sample rotation," *Appl. Surf. Sci.* **379**, 480 (2016).
- ¹⁴⁴S. M. Yoon and J. S. Kim, "Nanopatterning of swinging substrates by ion-beam sputtering," *J. Appl. Phys.* **119**, 205301 (2016).
- ¹⁴⁵R. M. Bradley and E.-H. Cirlin, "Theory of improved resolution in depth profiling with sample rotation," *Appl. Phys. Lett.* **68**, 3722 (1996).
- ¹⁴⁶R. M. Bradley, "Dynamic scaling of ion-sputtered rotating surfaces," *Phys. Rev. E* **54**, 6149 (1996).
- ¹⁴⁷J. Muñoz-García, R. Cuerno, and M. Castro, "Coupling of morphology to surface transport in ion-beam-irradiated surfaces: Normal incidence and rotating targets," *J. Phys.: Condens. Matter* **21**, 224020 (2009).
- ¹⁴⁸T. Yasseri and R. Kree, "A Monte Carlo study of surface sputtering by dual and rotated ion beams," *Nucl. Instrum. Methods B* **268**, 2496 (2010).
- ¹⁴⁹Z. Yang, M. A. Lively, and J. P. Allain, "Kinetic Monte Carlo simulation of self-organized pattern formation induced by ion beam sputtering using crater functions," *Phys. Rev. B* **91**, 075427 (2015).
- ¹⁵⁰M. Joe, J. H. Kim, C. Choi, B. Kahng, and J. S. Kim, "Nanopatterning by multiple-ion-beam sputtering," *J. Phys.: Condens. Matter* **21**, 224011 (2009).
- ¹⁵¹G. Carter, "Proposals for producing novel periodic structures by ion bombardment sputtering," *Vacuum* **77**, 97 (2004).
- ¹⁵²S. Vogel and S. J. Linz, "Surface structuring by multiple ion beams," *Phys. Rev. B* **75**, 085425 (2007).
- ¹⁵³M. Joe, C. Choi, B. Kahng, and J. S. Kim, "Nanopatterning by dual-ion-beam sputtering," *Appl. Phys. Lett.* **91**, 233115 (2007).
- ¹⁵⁴B. Ziberi, F. Frost, M. Tartz, H. Neumann, and B. Rauschenbach, *Appl. Phys. Lett.* **92**, 063102 (2008).
- ¹⁵⁵R. Kree, T. Yasseri, and A. K. Hartmann, "The influence of beam divergence on ion-beam induced surface patterns," *Nuclear Inst. Methods Phys. Res. B* **267**, 1407–1411 (2009).
- ¹⁵⁶J. Li, D. Stein, C. McMullan, D. Branton, M. J. Aziz, and J. A. Golovchenko, "Ion-beam sculpting at nanometre length scales," *Nature* **412**, 166 (2001).
- ¹⁵⁷H. H. Chen, O. A. Urquidez, S. Ichim, L. H. Rodriguez, M. P. Brenner, and M. J. Aziz, "Shocks in ion sputtering sharpen steep surface features," *Science* **310**, 294 (2005).
- ¹⁵⁸M. Holmes-Cerfon, M. J. Aziz, and M. P. Brenner, "Creating sharp features by colliding shocks on uniformly irradiated surfaces," *Phys. Rev. B* **85**, 165441 (2012).
- ¹⁵⁹J. C. Perkinson, M. J. Aziz, M. P. Brenner, and M. C. Holmes-Cerfon, "Designing steep, sharp patterns on uniformly ion-bombarded surfaces," *Proc. Natl. Acad. Sci. U.S.A.* **113**, 11425 (2016).
- ¹⁶⁰F. Everts, H. Wormeester, and B. Poelsema, "Optical anisotropy induced by ion bombardment of Ag(001)," *Phys. Rev. B* **78**, 155419 (2008).
- ¹⁶¹T. W. Oates, A. Keller, S. Facko, and A. Mücklich, "Aligned silver nanoparticles on rippled silicon templates exhibiting anisotropic plasmon absorption," *Plasmonics* **2**, 47 (2007).
- ¹⁶²M. Saini, R. Singh, S. K. Srivastava, and T. Som, "Broadband antireflection property of conformally grown zinc tin oxide thin films on nanorippled- and nanofaceted-Si substrates," *J. Phys. D: Appl. Phys.* **51**, 275305 (2018).
- ¹⁶³F. Siewert, B. Löchel, J. Buchheim, F. Eggenstein, A. Firsov, G. Gwalt, O. Kutz, S. Lemke, B. Nelles, I. Rudolph, F. Schäfers, T. Seliger, F. Senf, A. Sokolov, C. Waberski, J. Wolf, T. Zeschke, I. Zizak, R. Follath, T. Arnold, F. Frost, F. Pietag, and A. Erko, "Gratings for synchrotron and FEL beamlines: A project for the manufacture of ultra-precise gratings at Helmholtz Zentrum Berlin," *J. Synchrotron Radiat.* **25**, 91–99 (2018).
- ¹⁶⁴A. Toma, D. Chiappe, C. Boragno, and F. Bautier de Mongeot, "Self-organized ion-beam synthesis of nanowires with broadband plasmonic functionality," *Phys. Rev. B* **81**, 165436 (2010).
- ¹⁶⁵M. Ranjan, T. W. H. Oates, S. Facko, and W. Möller, "Optical properties of silver nanowire arrays with 35 nm periodicity," *Opt. Lett.* **35**, 2576 (2010).
- ¹⁶⁶M. Barelli, D. Repetto, and F. B. de Mongeot, "Infrared plasmonics via self-organized anisotropic wrinkling of Au/PDMS nanoarrays," *ACS Appl. Polym. Mater.* **1**, 1334 (2019).
- ¹⁶⁷C. Mennucci, S. D. Sorbo, S. Pirotta, M. Galli, L. C. Andreani, C. Martella, M. C. Giordano, and F. B. de Mongeot, "Light scattering properties of self-organized nanostructured substrates for thin-film solar cells," *Nanotechnology* **29**, 355301 (2018).
- ¹⁶⁸C. Martella, D. Chiappe, P. D. Veneri, L. V. Mercaldo, I. Usatii, and F. B. de Mongeot, "Self-organized broadband light trapping in thin film amorphous silicon solar cells," *Nanotechnology* **24**, 225201 (2013).
- ¹⁶⁹R. Moroni, D. Sekiba, F. Bautier de Mongeot, G. Gonella, C. Boragno, L. Mattera, and U. Valbusa, "Uniaxial magnetic anisotropy in nanostructured Co/Cu(001): From surface ripples to nanowires," *Phys. Rev. Lett.* **91**, 8153 (2003).
- ¹⁷⁰R. Moroni, F. Bisio, F. Bautier de Mongeot, C. Boragno, and L. Mattera, "Kink contribution to the magnetic anisotropy of nanostructured ultrathin Co/Cu(001) and Fe/Ag(001) films," *Phys. Rev. B* **76**, 214423 (2007).
- ¹⁷¹C. Quirós, L. Peverini, L. Zrate, A. Alija, J. Díaz, M. Vélez, G. Rodríguez-Rodríguez, F. Fauth, E. Ziegler, and J. M. Alameda, "Enhancement of antiferromagnetic coupling in magnetic multilayers by low energy ion beam substrate nanopatterning," *J. Phys.: Condens. Matter* **21**, 224024 (2009).
- ¹⁷²G. Costantini, F. Bautier de Mongeot, S. Rusponi, C. Boragno, U. Valbusa, L. Vattuone, U. Burghaus, L. Savio, and M. Rocca, "Tuning surface reactivity by in situ surface nanostructuring," *J. Chem. Phys.* **112**, 6840 (2000).
- ¹⁷³L. Vattuone, U. Burghaus, L. Savio, M. Rocca, G. Costantini, F. Bautier de Mongeot, C. Boragno, S. Rusponi, and U. Valbusa, "Oxygen interaction with disordered and nanostructured Ag(001) surfaces," *J. Chem. Phys.* **115**, 3346 (2001).
- ¹⁷⁴B. Teshome, S. Facko, and A. Keller, "Topography-controlled alignment of DNA origami nanotubes on nanopatterned surfaces," *Nanoscale* **6**, 1790 (2014).
- ¹⁷⁵I. Wittenbrink, A. Hausmann, K. Schickle, I. Lauria, R. Davtalab, M. Foss, A. Keller, and H. Fischer, "Low-aspect ratio nanopatterns on bioinert alumina influence the response and morphology of osteoblast-like cells," *Biomaterials* **62**, 58 (2015).
- ¹⁷⁶S. K. Garg, D. P. Datta, J. Ghatak, I. Thakur, K. Khare, D. Kanjilal, and T. Som, "Tunable wettability of Si through surface energy engineering by nanopatterning," *RSC Adv.* **6**, 48550 (2016).
- ¹⁷⁷G. Carter, "The physics and applications of ion beam erosion," *J. Phys. D: Appl. Phys.* **34**, R1 (2001).
- ¹⁷⁸W. Hauffe, "Faceting mechanism in the sputtering process," *Phys. Stat. Sol. A* **35**, K93 (1976).
- ¹⁷⁹M. A. Nastasi, J. W. Mayer, and J. K. Hirvonen, *Ion-Solid Interactions: Fundamentals and Applications* (Cambridge University Press, New York, 1996).
- ¹⁸⁰In particular, the morphological instability of Sigmund's mechanism has been shown to hold independently of perturbative approximations, which is relevant to predictions in Ref. 21 for the KS equation, see R. M. Bradley, "Exact linear dispersion relation for the Sigmund model of ion sputtering," *Phys. Rev. B* **84**, 075413 (2011).
- ¹⁸¹R. Cuerno, M. Castro, J. Muñoz-García, R. Gago, and L. Vázquez, "Universal non-equilibrium phenomena at submicrometric surfaces and interfaces," *Eur. Phys. J. Spec. Top.* **146**, 427 (2007).
- ¹⁸²C. Misbah, O. Pierre-Louis, and Y. Saito, "Crystal surfaces in and out of equilibrium: A modern view," *Rev. Mod. Phys.* **82**, 981 (2010).
- ¹⁸³R. Cuerno, H. A. Makse, S. Tomassone, S. T. Harrington, and H. E. Stanley, "Stochastic model for surface erosion via ion sputtering: Dynamical evolution from ripple morphology to rough morphology," *Phys. Rev. Lett.* **75**, 4464 (1995).
- ¹⁸⁴K. B. Lauritsen, R. Cuerno, and H. A. Makse, "Noisy Kuramoto-Sivashinsky equation for an erosion model," *Phys. Rev. E* **54**, 3577 (1996).
- ¹⁸⁵T. Aste and U. Valbusa, "Surface instabilities in granular matter and ion-sputtered surfaces," *Physica A* **332**, 548 (2004).
- ¹⁸⁶J. Muñoz-García, M. Castro, and R. Cuerno, "Nonlinear ripple dynamics on amorphous surfaces patterned by ion beam sputtering," *Phys. Rev. Lett.* **96**, 086101 (2006).
- ¹⁸⁷R. Cuerno, J. Muñoz-García, M. Castro, R. Gago, and L. Vázquez, "Modelos de la dinámica de las ondulaciones en la nanoarena," *Rev. Esp. Fca.* **21**, 65 (2007).
- ¹⁸⁸T. C. Kim, C.-M. Ghim, H. J. Kim, D. H. Kim, D. Y. Noh, N. D. Kim, J. W. Chung, J. S. Yang, Y. J. Chang, T. W. Noh, B. Kahng, and J.-S. Kim, "Reply

- to comment on ‘kinetic roughening of ion-sputtered Pd(001) surface: Beyond the Kuramoto-Sivashinsky model,’ *Phys. Rev. Lett.* **94**, 139602 (2005).
- ¹⁸⁹T. C. Kim, C.-M. Ghim, H. J. Kim, D. H. Kim, D. Y. Noh, N. D. Kim, J. W. Chung, J. S. Yang, Y. J. Chang, T. W. Noh, B. Kahng, and J.-S. Kim, ‘Kinetic roughening of ion-sputtered Pd(001) surface: Beyond the Kuramoto-Sivashinsky model,’ *Phys. Rev. Lett.* **92**, 246104 (2004).
- ¹⁹⁰J. Muñoz-García, R. Gago, L. Vázquez, J. A. Sánchez-García, and R. Cuerno, ‘Observation and modeling of interrupted pattern coarsening: Surface nanostructuring by ion erosion,’ *Phys. Rev. Lett.* **104**, 026101 (2010).
- ¹⁹¹B. Spencer, P. Voorhees, and J. Tersoff, ‘Morphological instability theory for strained alloy film growth: The effect of compositional stresses and species-dependent surface mobilities on ripple formation during epitaxial film deposition,’ *Phys. Rev. B* **64**, 235318 (2001).
- ¹⁹²R. Gago, L. Vázquez, O. Plantévin, T. H. Metzger, J. M. noz García, R. Cuerno, and M. Castro, ‘Order enhancement and coarsening of self-organized silicon nanodot patterns induced by ion-beam sputtering,’ *Appl. Phys. Lett.* **89**, 233101 (2006).
- ¹⁹³G. Carter, ‘The effects of surface ripples on sputtering erosion rates and secondary ion emission yields,’ *J. Appl. Phys.* **85**, 455 (1999).
- ¹⁹⁴I. Koponen, M. Hautala, and O.-P. Sievänen, ‘Simulations of ripple formation on ion-bombarded solid surfaces,’ *Phys. Rev. Lett.* **78**, 2612 (1997).
- ¹⁹⁵A. K. Hartmann, R. Kree, U. Geyer, and M. Kölbel, ‘Long-time effects in a simulation model of sputter erosion,’ *Phys. Rev. B* **65**, 193403 (2002).
- ¹⁹⁶E. O. Yewande, R. Kree, and A. K. Hartmann, ‘Propagation of ripples in Monte Carlo models of sputter-induced surface morphology,’ *Phys. Rev. B* **71**, 195405 (2005).
- ¹⁹⁷M. C. Moore, N. Kalyanasundaram, J. B. Freund, and H. T. Johnson, ‘Structural and sputtering effects of medium energy ion bombardment of silicon,’ *Nucl. Instrum. Methods B* **225**, 241 (2004).
- ¹⁹⁸M. Moseler, P. Gumbsch, C. Casiraghi, A. C. Ferrari, and J. Robertson, ‘The ultrasmoothness of diamond-like carbon surfaces,’ *Science* **309**, 1545 (2005).
- ¹⁹⁹N. Kalyanasundaram, M. C. Moore, J. B. Freund, and H. T. Johnson, ‘Stress evolution due to medium-energy ion bombardment of silicon,’ *Acta Mater.* **54**, 483 (2006).
- ²⁰⁰N. Kalyanasundaram, M. Ghazisaeidi, J. Freund, and H. Johnson, ‘Single impact crater functions for ion bombardment of silicon,’ *Appl. Phys. Lett.* **92**, 131909 (2008).
- ²⁰¹S. A. Norris, M. P. Brenner, and M. J. Aziz, ‘From crater functions to partial differential equations: A new approach to ion bombardment induced nonequilibrium pattern formation,’ *J. Phys.: Condens. Matter* **21**, 224017 (2009).
- ²⁰²M. Z. Hossain, K. Das, J. B. Freund, and H. T. Johnson, ‘Ion impact crater asymmetry determines surface ripple orientation,’ *Appl. Phys. Lett.* **99**, 151913 (2011).
- ²⁰³M. L. Nietiadi and H. M. Urbassek, ‘Influence of local curvature on sputtering,’ *Appl. Phys. Lett.* **103**, 113108 (2013).
- ²⁰⁴H. M. Urbassek, R. M. Bradley, M. L. Nietiadi, and M. Wolfhard, ‘Sputter yield of curved surfaces,’ *Phys. Rev. B* **91**, 165418 (2015).
- ²⁰⁵M. L. Nietiadi and H. M. Urbassek, ‘Influence of local curvature on sputtering,’ *Appl. Phys. Lett.* **103**, 113108 (2013).
- ²⁰⁶A. Lopez-Cazalilla, D. Chowdhury, A. Ilinov, S. Mondal, P. Barman, S. Bhattacharyya, D. Ghose, F. Djurabekova, K. Nordlund, and S. Norris, ‘Pattern formation on ion-irradiated Si surface at energies where sputtering is negligible,’ *J. Appl. Phys.* **123**, 235108 (2018).
- ²⁰⁷A. Lopez-Cazalilla, F. Djurabekova, A. Ilinov, C. Fridlund, and K. Nordlund, ‘Direct observation of ion-induced self-organization and ripple propagation processes in atomistic simulations,’ *Mater. Res. Lett.* **8**, 110 (2020).
- ²⁰⁸H. Hofäss, K. Zhang, and A. Mutzke, ‘Simulation of ion beam sputtering with SDTrimSP, TRIDYN and SRIM,’ *Appl. Surf. Sci.* **310**, 134 (2014).
- ²⁰⁹H. Hofäss, O. Bobes, and K. Zhang, ‘Argon ion beam induced surface pattern formation on Si,’ *J. Appl. Phys.* **119**, 035302 (2016).
- ²¹⁰H. Hofäss, ‘Model for roughening and ripple instability due to ion-induced mass redistribution [Addendum to H. Hofäss, *Appl. Phys. A* 114 (2014) 401: ‘Surface instability and pattern formation by ion-induced erosion and mass redistribution’],’ *Appl. Phys. A* **119**, 687 (2015).
- ²¹¹H. Windischmann, ‘An intrinsic stress scaling law for polycrystalline thin films prepared by ion beam sputtering,’ *J. Appl. Phys.* **62**, 1800 (1987).
- ²¹²C. A. Davis, ‘A simple model for the formation of compressive stress in thin films by ion bombardment,’ *Thin Solid Films* **226**, 30 (1993).
- ²¹³S. A. Norris, ‘Stability analysis of a viscoelastic model for ion-irradiated silicon,’ *Phys. Rev. B* **85**, 155325 (2012).
- ²¹⁴M. Z. Hossain, J. B. Freund, and H. T. Johnson, ‘Ion impact energy distribution and sputtering of Si and Ge,’ *J. Appl. Phys.* **111**, 103513 (2012).
- ²¹⁵R. M. Bradley and H. Hofäss, ‘A modification to the Sigmund model of ion sputtering,’ *J. Appl. Phys.* **116**, 234304 (2014).
- ²¹⁶D. A. Pearson and R. M. Bradley, ‘Theory of terraced topographies produced by oblique-incidence ion bombardment of solid surfaces,’ *J. Phys.: Condens. Matter* **27**, 015010 (2015).
- ²¹⁷M. P. Harrison, D. A. Pearson, and R. M. Bradley, ‘Emergence and detailed structure of terraced surfaces produced by oblique-incidence ion sputtering,’ *Phys. Rev. E* **96**, 032804 (2017).
- ²¹⁸M. Mokhtarzadeh, J. G. Ulbrandt, P. Myint, S. Narayanan, R. L. Headrick, and K. F. Ludwig, ‘Nanoscale kinetics and dynamics during Ar⁺ patterning of SiO₂,’ *Phys. Rev. B* **99**, 165429 (2019).
- ²¹⁹R. M. Bradley, ‘Redeposition of sputtered material is a nonlinear effect,’ *Phys. Rev. B* **83**, 75404 (2011).
- ²²⁰C. Diddens and S. Linz, ‘Redeposition during ion-beam erosion can stabilize well-ordered nanostructures,’ *Europhys. Lett.* **104**, 17010 (2013).
- ²²¹C. Diddens and S. J. Linz, ‘Continuum modeling of particle redeposition during ion-beam erosion,’ *Eur. Phys. J. B* **86**, 397 (2013).
- ²²²C. Diddens and S. J. Linz, ‘Continuum modeling of particle redeposition during ion-beam erosion: Laterally two-dimensional case,’ *Eur. Phys. J. B* **88**, 190 (2015).
- ²²³R. M. Bradley and H. Hofäss, ‘Nanoscale patterns produced by self-sputtering of solid surfaces: The effect of ion implantation,’ *J. Appl. Phys.* **120**, 074302 (2016).
- ²²⁴H. Hofäss, K. Zhang, and O. Bobes, ‘Self-organized surface ripple pattern formation by ion implantation,’ *J. Appl. Phys.* **120**, 074302 (2016).
- ²²⁵M. A. Lively, S. X. Bennett, and J. P. Allain, ‘Molecular dynamics studies of ion beam implantation and patterning of silicon: Effect of noble gas cluster formation,’ *Phys. Rev. B* **97**, 235443 (2018).
- ²²⁶A. Redinger, H. Hansen, U. Linke, Y. Rosandi, H. Urbassek, and T. Michely, ‘Superior regularity in erosion patterns by planar subsurface channeling,’ *Phys. Rev. Lett.* **96**, 106103 (2006).
- ²²⁷T. Škereň, K. Temst, W. Vandervorst, and A. Vantomme, ‘Ion-induced roughening and ripple formation on polycrystalline metallic films,’ *New J. Phys.* **15**, 093047 (2013).
- ²²⁸J. Renedo, R. Cuerno, M. Castro, and J. Muñoz-García, ‘Symmetry of surface nanopatterns induced by ion-beam sputtering: Role of anisotropic surface diffusion,’ *Phys. Rev. B* **93**, 155424 (2016).
- ²²⁹G. Costantini, F. B. de Mongeot, C. Boragno, and U. Valbusa, ‘Is ion sputtering always a ‘negative homoepitaxial deposition?’,’ *Phys. Rev. Lett.* **86**, 838 (2001).
- ²³⁰F. C. Motta, P. D. Shipman, and R. M. Bradley, ‘Highly ordered nanoscale surface ripples produced by ion bombardment of binary compounds,’ *J. Phys. D: Appl. Phys.* **45**, 122001 (2012).
- ²³¹R. M. Bradley and P. D. Shipman, ‘A surface layer of altered composition can play a key role in nanoscale pattern formation induced by ion bombardment,’ *Appl. Surf. Sci.* **258**, 4161 (2012).
- ²³²S. A. Mollick, D. Ghose, P. D. Shipman, and R. M. Bradley, ‘Anomalous patterns and nearly defect-free ripples produced by bombarding silicon and germanium with a beam of gold ions,’ *Appl. Phys. Lett.* **104**, 043103 (2014).
- ²³³R. M. Bradley, ‘Theory of nanodot and sputter cone arrays produced by ion sputtering with concurrent deposition of impurities,’ *Phys. Rev. B* **83**, 195410 (2011).

- ²³⁴Q. Wei, X. Zhou, B. Joshi, Y. Chen, K.-D. Li, Q. Wei, K. Sun, and L. Wang, "Self-assembly of ordered semiconductor nanoholes by ion beam sputtering," *Adv. Mater.* **21**, 2865–2869 (2009).
- ²³⁵O. El-Atwani, J. Allain, A. Cimaroli, and S. Ortoleva, "The significance of *in situ* conditions in the characterization of GaSb nanopatterned surfaces via ion beam sputtering," *J. Appl. Phys.* **110**, 074301 (2011).
- ²³⁶S. A. Norris, J. Samela, M. Vestberg, K. Nordlund, and M. J. Aziz, "Crater functions for compound materials: A route to parameter estimation in coupled-PDE models of ion bombardment," *Nucl. Instrum. Methods B* **318**, 245 (2014).
- ²³⁷J. Zhou and M. Lu, "Mechanism of Fe impurity motivated ion-nanopatterning of Si (100) surfaces," *Phys. Rev. B* **82**, 125404 (2010).
- ²³⁸R. M. Bradley, "Nanoscale patterns produced by ion erosion of a solid with codeposition of impurities: The crucial effect of compound formation," *Phys. Rev. B* **87**, 205408 (2013).
- ²³⁹S. Jo, J. Jun, E. Lee, S. M. Yoon, J. Seo, J. Muñoz-García, R. Cuerno, and J.-S. Kim, "Order improvement of surface nanopatterns via substrate rocking under ion bombardment: Experiments and nonlinear models," *Phys. Rev. B* **102**, 045421 (2020).
- ²⁴⁰A. Keller, S. Facska, and W. Möller, "Minimization of topological defects in ion-induced ripple patterns on silicon," *New J. Phys.* **10**, 063004 (2008).
- ²⁴¹N. Ghoniem and D. Walgraef, *Instabilities and Self-organization in Materials* (Oxford University Press, 2008).
- ²⁴²M. Paniconi and K. R. Elder, "Stationary, dynamical, and chaotic states of the two-dimensional damped Kuramoto-Sivashinsky equation," *Phys. Rev. E* **56**, 2713 (1997).
- ²⁴³M. P. Harrison and R. M. Bradley, "Producing virtually defect-free nanoscale ripples by ion bombardment of rocked solid surfaces," *Phys. Rev. E* **93**, 040802 (2016).
- ²⁴⁴A. Redondo-Cubero, K. Lorenz, F. J. P. Simon, Á. Muñoz, M. Castro, J. Muñoz-García, R. Cuerno, and L. V. Burgos, "Concurrent segregation and erosion effects in medium-energy iron beam patterning of silicon surfaces," *J. Phys.: Condens. Matter* **30**, 274001 (2018).
- ²⁴⁵C. Herbig and T. Michely, "Graphene: The ultimately thin sputtering shield," *2D Materials* **3**, 025032 (2016).
- ²⁴⁶C. Herbig, E. H. Åhlgren, U. A. Schröder, A. J. Martínez-Galera, M. A. Arman, J. Kotakoski, J. Knudsen, A. V. Krasheninnikov, and T. Michely, "Xe irradiation of graphene on ir(111): From trapping to blistering," *Phys. Rev. B* **92**, 085429 (2015).
- ²⁴⁷S. Yoo, E. H. Åhlgren, J. Seo, W. Kim, S. Chiang, and J. S. Kim, "Growth kinetics of Kr nano structures encapsulated by graphene," *Nanotechnology* **29**, 385601 (2018).
- ²⁴⁸A. Castellanos-Gomez, "Black phosphorus: Narrow gap, wide applications," *J. Phys. Chem. Lett.* **6**, 4280–4291 (2015).
- ²⁴⁹C. Martella, C. Mennucci, A. Lamperti, E. Cappelluti, F. B. de Mongeot, and A. Molle, "Designer shape anisotropy on transition-metal-dichalcogenide nanosheets," *Adv. Mater.* **30**, 1705615 (2018).
- ²⁵⁰L. Kou, T. Frauenheim, and C. Chen, "Nanoscale multilayer transition-metal-dichalcogenide heterostructures: Band gap modulation by interfacial strain and spontaneous polarization," *J. Phys. Chem. Lett.* **4**, 1730–1736 (2013).
- ²⁵¹J. Bai, X. Zhong, S. Jiang, Y. Huang, and X. Duan, "Graphene nanomesh," *Nat. Nanotechnol.* **5**, 190–194 (2010).
- ²⁵²J. Quereda, P. San-Jose, V. Parente, L. Vaquero-Garzon, A. J. Molina-Mendoza, N. Agrait, G. Rubio-Bollinger, F. Guinea, R. Roldn, and A. Castellanos-Gomez, "Strong modulation of optical properties in black phosphorus through strain-engineered rippling," *Nano Lett.* **16**, 2931–2937 (2016).
- ²⁵³C. Martella, C. Mennucci, E. Cinquanta, A. Lamperti, E. Cappelluti, F. Buatier de Mongeot, and A. Molle, "Anisotropic MoS₂ nanosheets grown on self-organized nanopatterned substrates," *Adv. Mater.* **29**, 1605785 (2016).
- ²⁵⁴D. Bhowmik, M. Mukherjee, and P. Karmakar, "Presence of reactive impurities in Ar+ ion beam plays a key role for Si ripple formation," *Nucl. Instrum. Methods B* **444**, 54 (2019).
- ²⁵⁵S. Bhattacharjee, P. Karmakar, and A. Chakrabarti, "Key factors of ion induced nanopatterning," *Nucl. Instrum. Methods B* **278**, 58 (2012).
- ²⁵⁶S. Bhattacharjee, P. Karmakar, V. Naik, A. Sinha, and A. Chakrabarti, "The role of carbon in ion beam nano-patterning of silicon," *Appl. Phys. Lett.* **103**, 181601 (2013).
- ²⁵⁷S. M. Yoon, J.-S. Kim, D. Yoon, H. Cheong, Y. Kim, and H. H. Lee, "Effects of polycrystallinity in nano patterning by ion-beam sputtering," *J. Appl. Phys.* **116**, 024307 (2014).
- ²⁵⁸M. Castro, R. Cuerno, M. M. García-Hernández, and L. Vázquez, "Pattern-wavelength coarsening from topological dynamics in silicon nanofoams," *Phys. Rev. Lett.* **112**, 050103 (2014).
- ²⁵⁹E. Lee, J. Seo, J.-S. Kim, M. Castro, and R. Cuerno, "Nanopatterning on rotating HOPG(0001) by the ion beam sputtering" (unpublished).
- ²⁶⁰F. Ratto, T. Johnston, S. Heun, and F. Rosei, "A numerical approach to quantify self-ordering among self-organized nanostructures," *Surf. Sci.* **602**, 249 (2008).
- ²⁶¹I. Levchenko, S. Kumar, M. M. A. Yajadda, Z. J. Han, S. Furman, and K. Ostrikov, "Self-organization in arrays of surface-grown nanoparticles: Characterization, control, driving forces," *J. Phys. D: Appl. Phys.* **44**, 174020 (2011).
- ²⁶²A. A. Golovin, A. A. Nepomnyashchy, S. H. Davis, and M. A. Zaks, "Convective Cahn-Hilliard models: From coarsening to roughening," *Phys. Rev. Lett.* **86**, 1550 (2001).
- ²⁶³F. C. Motta, R. Neville, P. D. Shipman, D. A. Pearson, and R. M. Bradley, "Measures of order for nearly hexagonal lattices," *Physica D* **380**, 17 (2018).
- ²⁶⁴M. Sutton, S. G. J. Mochrie, T. Greylak, S. E. Nagler, L. E. Berman, G. A. Held, and G. B. Stephenson, "Observation of speckle by diffraction with coherent x-rays," *Nature* **352**, 608 (1991).
- ²⁶⁵O. Bikondoa, D. Carbone, V. Chamard, and T. H. Metzger, "Ion beam sputtered surface dynamics investigated with two-time correlation functions: A model study," *J. Phys.: Condens. Matter* **24**, 445006 (2012).
- ²⁶⁶J. Huang, S. V. Grater, F. Corbellini, S. Rinck, E. Bock, R. Kemkemer, H. Kessler, J. Ding, and J. P. Spatz, "Impact of order and disorder in RGD nanopatterns on cell adhesion," *Nano Lett.* **9**, 1111 (2009).
- ²⁶⁷J. W. Costerton, Z. Lewandowski, D. E. Caldwell, D. R. Korber, and H. M. Lappin-Scott, "Microbial biofilms," *Ann. Rev. Microbiol.* **49**, 711 (1995).
- ²⁶⁸J. N. Wilking, T. E. Angelini, A. Seminara, M. P. Brenner, and D. A. Weitz, "Biofilms as complex fluids," *MRS Bull.* **36**, 385 (2011).
- ²⁶⁹K. Grandfield, "Bone, implants, and their interfaces," *Phys. Today* **68**, 40 (2015).
- ²⁷⁰M. Arnold, V. C. Hirschfeld-Warneken, T. Lohmüller, P. Heil, J. Blümmel, E. A. Cavalcanti-Adam, M. López-García, P. Walther, H. Kessler, B. Geiger, and J. P. Spatz, "Induction of cell polarization and migration by a gradient of nanoscale variations in adhesive ligand spacing," *Nano Lett.* **8**, 2063 (2008).
- ²⁷¹G. Hobler, D. Maciążek, and Z. Postawa, "Ion bombardment induced atom redistribution in amorphous targets: MD versus BCA," *Nucl. Instrum. Methods B* **447**, 30 (2019).
- ²⁷²G. Hobler, R. M. Bradley, and H. M. Urbassek, "Probing the limitations of Sigmund's model of spatially resolved sputtering using Monte Carlo simulations," *Phys. Rev. B* **93**, 205443 (2016).
- ²⁷³G. Hobler, D. Maciążek, and Z. Postawa, "Crater function moments: Role of implanted noble gas atoms," *Phys. Rev. B* **97**, 155307 (2018).
- ²⁷⁴S. A. Norris, "Pycraters: A python framework for crater function analysis," *arXiv:1410.8489* (2014).
- ²⁷⁵K. M. Loew and R. M. Bradley, "Effect of dispersion on the nanoscale patterns produced by ion sputtering," *Phys. Rev. E* **100**, 012801 (2019).
- ²⁷⁶D. A. Pearson, R. M. Bradley, F. C. Motta, and P. D. Shipman, "Producing nanodot arrays with improved hexagonal order by patterning surfaces before ion sputtering," *Phys. Rev. E* **92**, 062401 (2015).
- ²⁷⁷M. Holmes-Cerfon, W. Zhou, A. L. Bertozzi, M. P. Brenner, and M. J. Aziz, "Development of knife-edge ridges on ion-bombarded surfaces," *Appl. Phys. Lett.* **101**, 143109 (2012).
- ²⁷⁸T. Kumar, A. Kumar, D. C. Agarwal, N. P. Lalla, and D. Kanjilal, "Ion beam-generated surface ripples: New insight in the underlying mechanism," *Nanoscale Res. Lett.* **8**, 336 (2013).

- ²⁷⁹T. Kumar, A. Kumar, and D. Kanjilal, "An approach to tune the amplitude of surface ripple patterns," *Appl. Phys. Lett.* **103**, 131604 (2013).
- ²⁸⁰T. Chini, D. Datta, and S. Bhattacharyya, "Ripple formation on silicon by medium energy ion bombardment," *J. Phys.: Condens. Matter* **21**, 224004 (2009).
- ²⁸¹T. K. Chini, F. Okuyama, M. Tanemura, and K. Nordlund, "Energy-dependent wavelength of the ion-induced nanoscale ripple," *Phys. Rev. B* **67**, 205403 (2003).
- ²⁸²S. Facsko, R. Heller, A. S. El-Said, W. Meissl, and F. Aumayr, "Surface nanostructures by single highly charged ions," *J. Phys. Condens. Matter* **21**, 224012 (2009).
- ²⁸³R. A. Wilhelm, A. S. El-Said, F. Krok, R. Heller, E. Gruber, F. Aumayr, and S. Facsko, "Highly charged ion induced nanostructures at surfaces by strong electronic excitations," *Prog. Surf. Sci.* **90**, 377 (2015).
- ²⁸⁴F. Aumayr, S. Facsko, A. S. El-Said, C. Trautmann, and M. Schleberger, "Single ion induced surface nanostructures: A comparison between slow highly charged and swift heavy ions," *J. Phys. Condens. Matter* **23**, 393001 (2011).
- ²⁸⁵M.-W. Moon, S. H. Lee, J.-Y. Sun, K. H. Oh, A. Vaziri, and J. W. Hutchinson, "Wrinkled hard skins on polymers created by focused ion beam," *Proc. Nat. Acad. Sci. U.S.A.* **104**, 1130–3 (2007).
- ²⁸⁶Q. Wei, J. Lian, S. Zhu, W. Li, K. Sun, and L. Wang, "Ordered nanocrystals on argon ion sputtered polymer film," *Chem. Phys. Lett.* **452**, 124–128 (2008).
- ²⁸⁷M. C. Giordano and F. B. de Mongeot, "Anisotropic nanoscale wrinkling in solid-state substrates," *Adv. Mater.* **30**, 1801840 (2018).
- ²⁸⁸A. Gutzmann, S. Klaumünzer, and P. Meier, "Ion-beam-induced surface instability of glassy Fe₄₀Ni₄₀B₂₀," *Phys. Rev. Lett.* **74**, 2256–2260 (1995).